TECHNICAL UNIVERSITY OF LIBEREC
Faculty of Mechanical Engineering

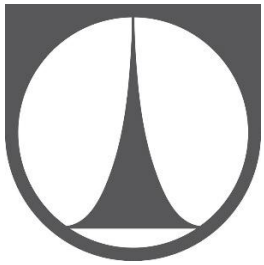

MODELLING OF DYNAMICAL AND STATICAL PROPERTIES OF A CAR SEAT WITH ADJUSTABLE PRESSURE PROFILE

Dissertation Thesis

Liberec 2019 **MsC. Tien Tran Xuan**

TECHNICAL UNIVERSITY OF LIBEREC
Faculty of Mechanical Engineering

Modelling of Dynamical and Statical Properties of a Car Seat with Adjustable Pressure Profile

Dissertation Thesis

Study programme: P2301 Mechanical Engineering
Study branch: Applied Mechanics

Author: **Ing. Tien Tran Xuan**
Thesis Supervisor: doc. Ing. David Cirkl, Ph.D.
Department of Engineering Mechanics

Liberec 2019

Declaration

I hereby certify I have been informed that my dissertation is fully governed by Act No. 121/2000 Coll., the Copyright Act, in particular Article 60 – School Work.

I acknowledge that the Technical University of Liberec does not infringe my copyrights by using my dissertation for internal purposes of the Technical University of Liberec.

I am aware of my obligation to inform the Technical University of Liberec on having used or granted license to use the results of my dissertation; in such a case the Technical University of Liberec may require reimbursement of the costs incurred for creating the result up to their actual amount.

I, myself, have written my dissertation as an original and primary work using the literature listed below and consulting it with my thesis supervisor and my thesis counsellor.

At the same time, I honestly declare that the texts of the printed version of my dissertation and of the electronic version uploaded into the IS/STAG are identical.

December 17, 2019 Ing. Tien Tran Xuan

Acknowledgements

I would like to express my deep gratitude to doc.Ing. David Cirkl Ph.D, my research supervisor, for his patient guidance, enthusiastic encouragement and useful critiques of this research work.

I would also like to thank all the professors from the Department of Applied Mechanics for their advice which helped me to keep my progress on schedule.

I would also like to say thanks to Ing. Lubomir Sivcak, the technician of the laboratory of the Department of Applied Mechanics, for his help in doing experiments.

Finally I want to express my gratitude to my family for their support and encouragement throughout my study.

Abstract

This work is aimed to the field of increasing of passenger's comfort in vehicles by using mechanical devices. There have been many such devices known through patents and used in specific applications. One of those devices is called pneumatic spring. It was created in a previous project at the Department of Applied Mechanics (TUL) which resulted in a patented solution. It can be inserted inside a car seat to adjust contact pressure distribution between a seat and a human body. This thesis presents a continuation of the study on this device. The aims of my study include improvement of the regulation of pressure inside the pneumatic spring and investigation of effect of this device. It is assessed through its influence on the regulation of pressure on the transmission of acceleration and on the change of contact pressure distribution.

In this thesis, I present a variety of methods that are used appropriately for each specific study purpose. The methods include the analytic calculation method, and FEM method, in combination with experimental measurements for verification. An improved version of this device was designed and made experimentally.

The device is considered as a multidisciplinary system (mechanical, electrical, and fluid). The mathematical model of the system was created. The numerical calculation method was used for determination of behavior of the system characteristics by using Matlab software. In this way the influence of device on the regulation of pressure and on the transmission of acceleration was evaluated.

The finite element method was used for simulation of deformation of mechanical parts of the device in the working process and the pressure distribution in the contact zone between the seat with the device inserted inside and the human body. The simulations were carried out by MSC. Marc software.

The calculation and simulation results were compared with the corresponding experimental results for verification. The results show that the system improvement brings positive influences.

Keywords:

pneumatic spring, mathematical model, finite element method, constitutive model of material, contact pressure distribution, transmission of acceleration

Abstrakt

Tato práce je zaměřena do oblasti zvýšování pohodlí cestujících ve vozidlech s využitím mechanických systémů. Existuje mnoho takových zařízení známých z publikací, patentů nebo použití v konkrétních aplikačních případech. Jedno z těchto zařízení je pneumatická pružina. Konkrétní aplikace takového pneumatického pružicího prvku byla zrelizována v předchozím projektu na Katedře mechaniky, pružnosti a pevnosti (TUL) a vedla ke vzniku patentu. Tento prvek může být vložen do automobilové sedačky za účelem ovlivnění rozložení kontaktního tlaku mezi sedákem a lidským tělem. Tato práce představuje pokračování studie na tomto zařízení. Cíle mé studie zahrnují sestavení simulačního modelu tohoto zařízení a prozkoumání způsobu zlepšení regulace tlaku v pneumatické pružině a zkoumání vlivu tohoto zařízení na dynamické charakteristiky systému. Funkce tohoto zařízení je hodnocena podle kvality regulace tlaku a přenosu zrychlení. Dalším kriteriem pro posouzení funkce systému je i změna distribuce kontaktního tlaku v případě statického zatížení.

V této práci uvádím různé metody, které jsou vhodně použity pro každý konkrétní účel studie. Je užito analytického počtu s návazným numerickým řešením i metoda konečných prvků v kombinaci s experimentálním měřením. Byla navržena vylepšená verze tohoto zařízení a experimentálně zralizována.

Zařízení je modelováno jako multidisciplinární systém (mechanický, elektrický a tekutinový). Ke stanovení jeho charakteristik byla použita kombinace analytických a numerických výpočetních metod a byl vyhodnocen vliv zařízení na regulaci tlaku a na přenos zrychlení.

Metoda konečných prvků byla použita pro simulaci chování mechanických částí zařízení v zatíženém stavu a bylo vypočteno rozložení tlaku v kontaktní zóně mezi sedadlem s implementovaným pneumatickým prvkem a lidským tělem.

Výsledky simulací byly porovnány s odpovídajícími experimentálními výsledky. Ukázalo se, že provedené úpravy systému přináší zlepšení v regulaci tlaku v pneumatickém prvku.

Klíčová slova:

pneumatická pružina, matematický model, metoda konečných prvků, konstitutivní model materiálu, rozložení kontaktního tlaku, přenos zrychlení

Contents

List of Figures

Notation and symbols

Symbol	Unit	Description
p_d	[kPa]	desired pressure
p_s	[kPa]	instant pressure inside pneumatic spring element
q_{sj}	[l/min]	air flow rate through valve *j* (j=1..4)
p_{inlet}	[kPa]	inlet pressure of a proportional valve
p_{outlet}	[kPa]	outlet pressure of a proportional valve
Δp	[kPa]	pressure difference
C_{dv}	[l/(s.bar)]	sonic conductance of a discrete valve
b_{dv}	[-]	critical pressure ratio of a discrete valve
$p_{downstream}$	[kPa]	downstream pressure of a discrete valve
$p_{upstream}$	[kPa]	upstream pressure of a discrete valve
q_s	[l/min]	total air flow through the pneumatic spring element
$i_{j\ (j=1,2,3,4)}$	[A]	coil current supplied to control a proportional valve V_j
e_t	[kPa]	pressure threshold
Δp_s	[kPa]	value of pressure sensitivity
e	[kPa]	pressure error
C_f		experimental compressed air capacitance
q_c	[l/min]	supplied flowrate from the compressor
p_{cr}	[kPa]	pressure inside the compressed air reservoir
a_1, b_1	[-]	experimental coeficients of compressor model
$V_{\exp}$	[l]	the volume of a rigid container
β	[kPa]	the bulk modulus of air
p_{atm}	[kPa]	atmosphere pressure
x	[m]	displacement
v	[m]	applied excitation
z	[m/s]	velocity
f_f	[-]	the course of friction coefficient in the model of foam
V	[l]	the volume of the latex tube

V_j	[l]	part j of volume of latex tube (j=1..3)
R	[m]	latex tube radius before the deformation
l_1	[m]	l_1 is the length of the tube corresponding to the volume V_1
a	[m]	a dimenssion of elliptical cross-section volume V_1
b	[m]	a dimenssion of elliptical cross-section volume V_1
l_2	[m]	length of the tube corresponding to the volume V_2
l_3	[m]	length of the tube corresponding to the volume V_3
r	[m]	the radius of the volume of a sphere cap V_3
h	[m]	height of volume of a sphere cap V_3
V_{foam}	[l]	the volume of PU foam that occupies the interior of the latex tube
V_{ls}	[l]	total volume of latex spring
$\dot{V}_{ls}$	[l/min]	derivative of V_{ls} with respect to time
$\dot{p}_s$	[kPa/min]	derivative of p_s with respect to time
T	[^{0}K]	the temperature of the air inside the pneumatic spring element
κ	[-]	adiabatic exponent
R_{gas}	[J kg^{-1} K^{-1}]	gas constant
$\dot{V}_1$	[l/min]	derivative of V_1 with respect to time
$\dot{V}_2$	[l/min]	derivative of V_2 with respect to time
$\dot{V}_3$	[l/min]	derivative of V_3 with respect to time
F_p	[N]	force interaction between the pneumatic spring element and mass
S	[m^2]	the contact zone between and pneumatic spring and the mass
m	[kg]	mass
g	[m/s^2]	gravitational acceleration
$\ddot{x}$	[m/s^2]	second derivative of x with respect to time
p_{r2}	[kPa]	pressure inside the reservoir R_2
a_2, b_2	[-]	experimental values of vacuum pump model
q_{vp}	[l/min]	flowrate from vacuum pump
V_{ils}	[l]	total volume of latex air spring in improved system

V_{add}	[l]	volume of the additional latex tube
V_{PSE}	[l]	total volume of latex air spring
$\dot{V}_{PSE}$	[l/min]	a derivative of V_{PSE} with respect to time
$\dot{V}_{add}$	[l/min]	a derivative of V_{add} with respect to time
$\dot{V}_{ils}$	[l/min]	a derivative of V_{ils} with respect to time
p_m	[kPa]	applied pressure in bulge test of a latex membrane
r_m	[m]	bulge radius of curvature
t_m	[m]	membrane thickness
h_m	[m]	height of bulge window
R_m	[m]	Radius of bulge window
σ_m	[kPa]	stress in a spherical membrane
t_{m0}	[m]	initial thickness of the membrane
θ	[rad]	angle property in bulge test of latex membrane
θ_0	[rad]	initial angle property in bulge test of latex membrane
λ	[1]	engineering strain
l_m	[m]	instantaneous length of meridian curve of deformed membrane
l_{m0}	[m]	initial length of meridian curve of deformed membrane
W	[J]	strain energy function
$\lambda_1, \lambda_2, \lambda_3$	[1]	engineering strain components
μ_n, α_n, β_n	[-]	material constants of Ogden and Foam model
J	[-]	volumetric ratio
I_1, I_2, I_3	[-]	three simplest possible even-powered functions (invariants)
$C_{10}, C_{01}, C_{11}, C_{20}$	[-]	material constants of Mooney-Rivlin model

1. Introduction

In various ground vehicles, for example, on-road or off-road vehicles, industrial trucks, agricultural tractors, railway vehicles, etc., the isolation of the seated operator from vibration and shock is of considerable importance. Studies have shown that vibration can be harmful to the human body and, in some cases, may lead to permanent injuries. Published results approve that with long-term exposure of the human body to vibration, the number of errors in work performance is increasing due to impaired perception [1,2]. Also, dynamic stresses are induced in the spine as a result of the whole-body vibrations, producing micro-fractures in the endplates and vertebral bodies [3,4]. Thus, preventing fatigue during driving vehicle has an important role [5,6]. Increasing passenger's comfort is the task inherently connected with using seats in different means of transport. One of the big topics of interest is how to decrease the influence of vibration on the human body.

The passenger seat of a car is one of the essential interfaces between the human body and the vehicle. Seats can be divided into two main categories: conventional foam cushions seats and suspension seats (e.g. [7]). The suspension mechanism generally consists of a spring and damper mounted beneath a relatively firm seat cushion. Conventional seats are typically constructed using a foam cushion on either a rigid or sprung seat pan. Modern automotive seats are constructed from open-cell polyurethane foam supported by an internal metal structure and covered with trim material [8]. A standard in the automotive seating industry is the implementation of full-depth open-cell polyurethane foam seat, which means the foam is placed on a metal pan rigidly mounted to the vehicle floor pan [9]. Seat design using foam is influenced by cost and weight reduction of the assembled seat and green considerations (disassembly for recycling). In a full foam seat, there are no springs to adjust, and the foam is the main means of reduction of vibration transmitted to the occupant. Foam is the primary provider of static comfort (posture and pressure distribution at the interfaces of the human body and seat) and dynamic comfort (vibration isolation). The former generally refers to the occupant's comfort feeling without vibration load, and the main factors that should be considered are the seat geometry, foam material properties, etc. The latter refers to comfort feeling under vibration, which is transmitted to the driver via seat [10]. Seat comfort evaluation is complicated since it is related to the human body, which is a kind of soft tissue with complex physiological characteristics. Objective evaluation of seat comfort has not been solved well yet, particularly in the aspect of seat foam properties. The stiffness of the seat affecting the level of seat comfort depends on foam material properties such as indentation hardness, thickness, damping, and density. There are some different concepts in production companies regarding the hardness of the seat. Variable stiffness is a way to personalize the seat. It is another level of seat

personalization. Special elements with variable stiffness can be added to the car, train or aeroplane seat, sanitary lounger, hospital bed or other equipment.

Following a patented solution [11], a seat which is possible to change its stiffness was created already as a functional prototype. It contains an active vibration isolation element called the pneumatic spring element (the PSE). The modified seat causes an improvement in the comfort of a sitting person.

Objectives of the thesis are:

- ❖ Derivation of the analytical model of the pneumatic spring system with lumped parameters
  - ✓ Analysis of the system using a multidisciplinary approach.
  - ✓ Numerical simulation of the model for different working conditions (constant stiffness and constant pressure mode, quasi-static load, dynamic load).
  - ✓ Investigation of the dynamical behavior of the system. Numerical simulation of transmission of acceleration.
- ❖ Finding a solution to improve the system from the point of view of faster regulation of pressure inside the PSE
  - ✓ Providing a theoretical basis for the idea of improvement and solution.
  - ✓ Carrying out the numerical simulation of the improved system.
- ❖ Investigation the influence of the PSE on transmission of acceleration.
  - ✓ Comparison of simulation results between original and improved systems.
  - ✓ Comparison of experimental results between original and improved systems.
  - ✓ Assessment of quality of the system improvement.
- ❖ Creation of FEM model of the seat with adjustable pressure profile in interaction with a simplified model of the human body
  - ✓ Determination of suitable constitutive models for materials of seat's parts.
  - ✓ Modelling of interaction between a foam block with a PSE inserted and a mass to simulate the deformation of PSE and foam under static conditions.
  - ✓ Modelling of interaction between the car seat cushion with a PSE inserted and a simplified human body.
  - ✓ Calculation of the pressure profile in the contact zone between the seat and simplified human body. Comparison with the experimental results.

2. Seat with adjustable pressure profile

The seat with adjustable pressure profile (see Fig 2.1a) was created within the project "New technologies and special components of machines" (CZ.1.05/3.1.00/13.0291) in section "Practical application of pneumatic spring element" by team of doc. Cirkl in years 2011-2013. The project was supported by endowement from Ministry of Education, youth and sports. The presented solution is based on patent [11] which introduces another way of seat personalization. The purpose of the solution is to change the pressure distribution in the contact zone between seat cushion and human body. The seat is able to change continuously its stiffness and make cushion harder or softer. This change is made by a PSE inserted inside seat cushion. Change of the pressure inside the PSE affects locally the force balance in the contact zone and therefore changes the distribution of the contact pressure. One of the ways how the influence of pressure change can be evaluated as a change of value of pressure peaks in contact zone for soft or hard seat setup (see Fig.2.2) and this change can be even in the range of tenth of percent. This illustrates good system performance under static conditions.

a) The seat in reality b) A simplified scheme

Figure 2.1. Seat with adjustable pressure profile

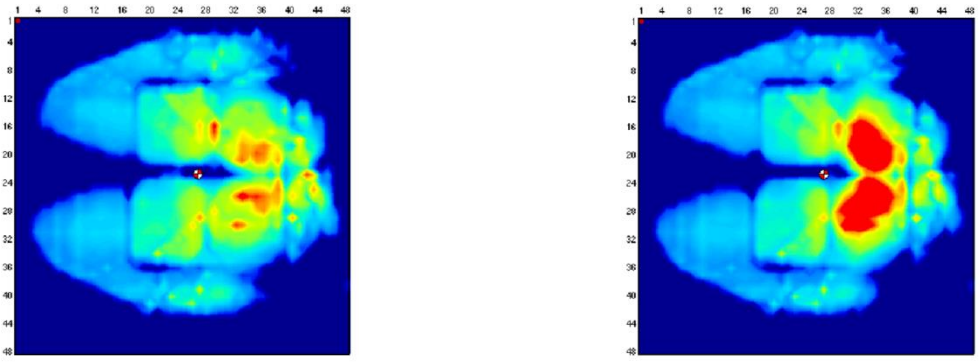

a) Low (softer cushion setup) b) High (harder cushion setup)

Figure 2.2. Pressure profile

The purpose of this work is to investigate the dynamical behavior of the system and identify the ability of the PSE system to work under dynamic conditions regarding the response time of the system. This leads to identification of frequency range where the feedback loop circuit is able to keep desired values of pressure inside PSE. As the frequency limit may be expected quite low for the original version of the system design another purpose of this work is to suggest, realize and quantify the system improvement. This improvement should lead to increasing the frequency limit for satisfactory time response of the system. The analysis of the system lies in solution of a multidisciplinary problem as the system consists of mechanical subsystem, electro-pneumatic circuit, electronic controller and control software.

2.1. Mechanical subsystem

The basic part of mechanical subsystem is an pneumatic spring element (PSE) which is inserted inside the car seat cushion (shown in Fig 2.1b). The PSE (shown in Fig 2.3) consists of a latex tube filled in with foam while the tube is partially covered by fabric adhesive tape. The part of the tube which is covered by tape keeps the original shape and its deformation is constrained. When the PSE is supplied with compressed air both ends of latex tube which are not covered by tape stretch and bulge.

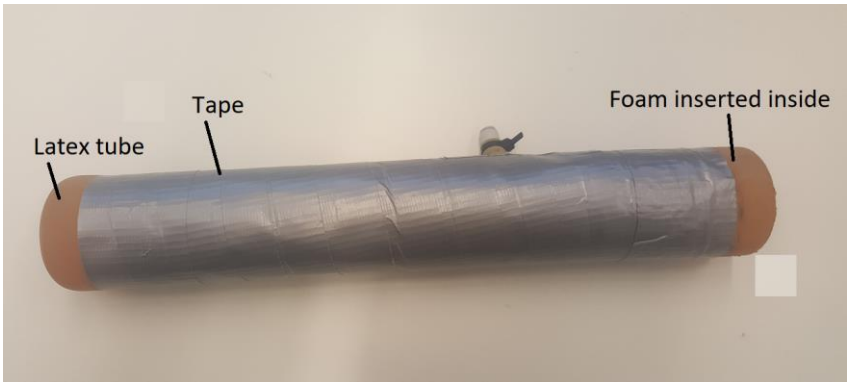

Figure 2.3. Pneumatic spring element

2.2. Electro-pneumatic control subsystem

The pressure inside the PSE is controlled and regulated by a control system consisting of pneumatic actuators and a controller. A simplified scheme of electro-pneumatic control circuit is in Fig 2.4.

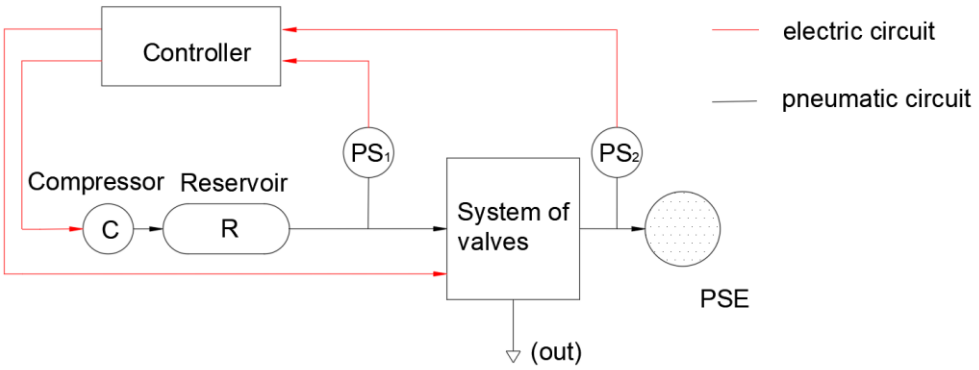

Figure 2.4. Scheme of the control system

The compressor C supplies compressed air into the reservoir R. Compressed air from the reservoir R flows to the pneumatic spring element S through the valve system. The system of valves consists of a couple of proportional valves (V_1, V_2) and a couple of discrete solenoid valves (V_3, V_4). Two pressure sensors (PS_1, PS_2) are used for measuring the pressure in the reservoir R and the pressure inside PSE. The signal from the sensors is sent to the Controller. The controller controls the operation of the compressor and the system of valves. The pressure value inside the PSE is varied in the range [0,25] kPa according to user-defined values or modes set in the control software, e.g., value of desired pressure.

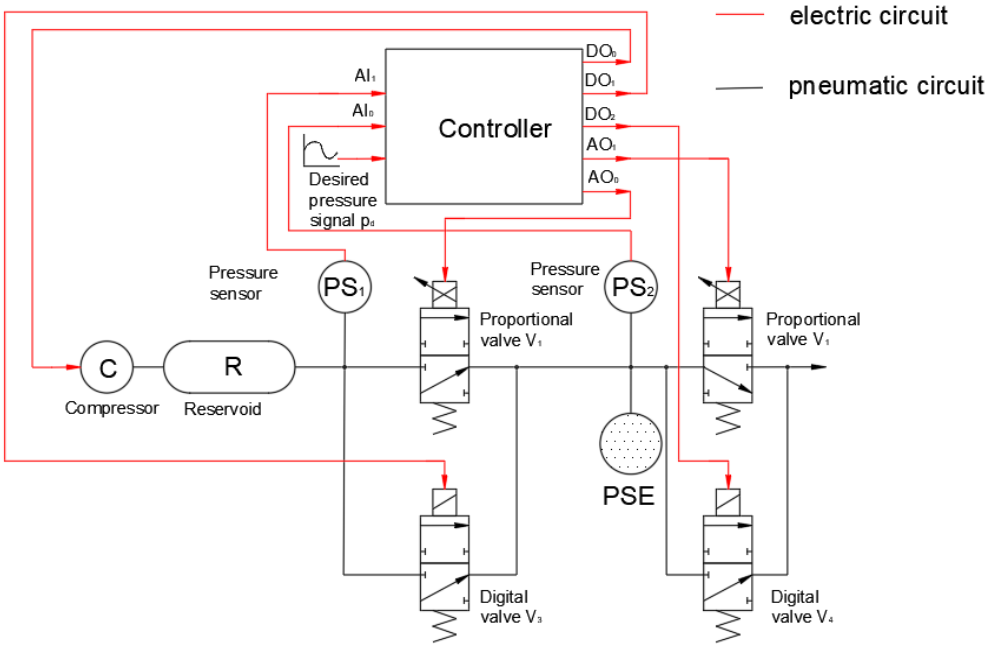

Figure 2.5. Scheme of the electro-pneumatic system in detail

The detailed scheme of the system is described in Fig 2.5. For the distribution of compressed air in and out of the PSE, the system of valves is divided into two pairs. Each pair (input and output) consisting of one proportional valve and one discrete valve. The first pair of input valves (V_1, V_3) is used to distribute the compressed air supplied from the reservoir into the PSE, the second pair of output valves (V_2, V_4) is to distribute the air from the PSE to the outlet. The proportional valves V_1, V_2 are intended for small airflow in case of small control error (the difference between desired and instant value) which is less than the threshold value set in the control software. The discrete valves V_3, V_4 for faster airflow are opened when the difference between the desired and the instant pressure value is bigger than the threshold value. Sensor PS_1 measures pressure in the reservoir (denoted p_{cr}) and sensor PS_2 measures pressure inside the PSE (denoted p_s). The sensor transforms physical quantity – pressure to electric quantity – voltage. The voltage signal sent from the sensors to the controller is in analog form.

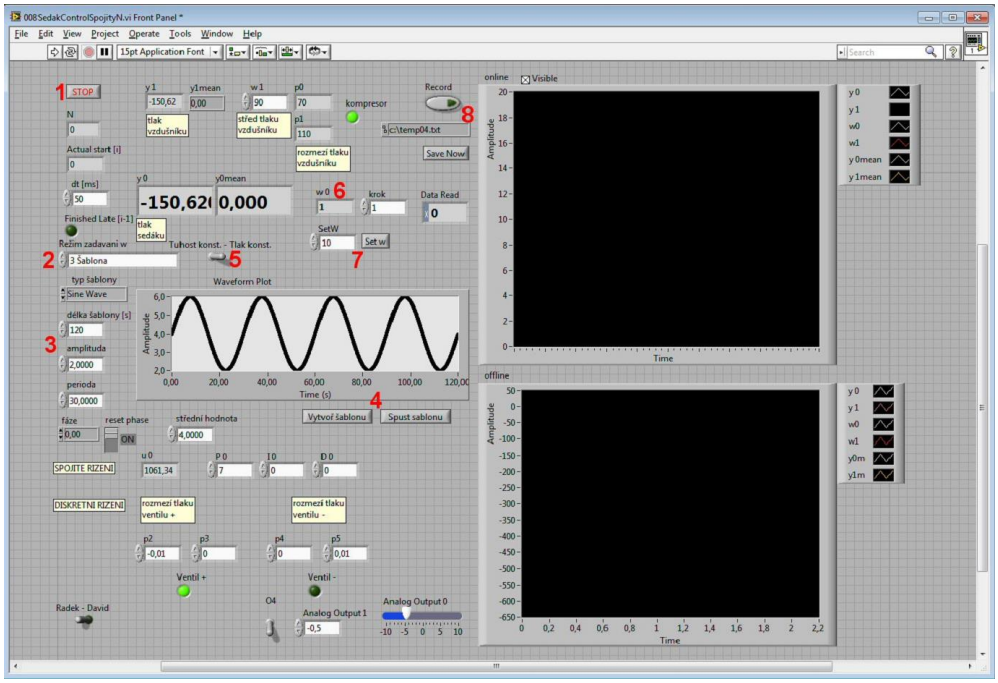

Figure 2.6. The control software in Labview

For the control of compressor and discrete valves (V_2, V_4) the on/off control method is used while the magnitude of orifices of valves (V_1, V_3) is controlled proportionally. The signal sent from the controller to the compressor and the discrete valves is in digital form. The signal sent to proportional valves is in analog form. The control software was created in Labview environment (shown in Fig 2.6). It enables to display the courses of system values in time as desired pressure in PSE, measured unfiltered and filtered pressure in PSE, value of control error, etc. The control

software is also used for setting of system parameters as upper and lower limit value of pressure in the reservoir, constants of PID controller, selection of working mode (there are 2 modes: constant pressure and constant stiffness), the selection of function of desired pressure in case of automated operation (constant, harmonic or triangular with amplitude and frequency).

Principally two different modes of system operation are possible: constant stiffness mode and constant pressure one. In the constant stiffness mode, the pressure inside the PSE (p_s) is set to chosen desired pressure value p_d at the initial time. After that, the inlet and outlet valves are closed even if the seat is mechanically loaded or not. In this mode, the control system allows setting fixed stiffness characteristics of the seat cushion. In the constant pressure mode, the control system tries to keep the value of pressure p_s inside PSE equal to desired value p_d.

3. Mathematical model

This chapter deals with derivation of mathematical models of the PSE system used for subsequent analysis. The model is considered as a mixed model which is a combination of single-discipline subsystems as mechanical, electrical, fluid and control ones. The mathematical models of the original system and the improved one are presented. The simulations are carried out for varied input parameters and both the system parameters and system characteristics are calculated. For model excitation, the kinematic excitation or predefined function of desired pressure is used. The behavior of models is assessed by means of system characteristics as system time response, frequency transmission response, value of control error etc. In this way, the influences of the original and improved systems are analyzed and compared.

3.1. Mathematical model of the original system

This section deals with the description of a mathematical model of the original system. For convenience of modeling, the original system is divided into two parts: electro-pneumatic control subsystem and mechanical subsystem. The model of electro-pneumatic control part is considered first.

3.1.1. Model of the electro-pneumatic control subsystem

The components of this part are proportional and discrete valves, compressor and PID controller. The relationship between the characteristic quantities of electro-pneumatic elements is presented by the equations.

3.1.1.1. Mathematical model of the valves

The proportional valves denoted V_1 and V_2 are of type SMC-PVQ13-6M-08-M5-A. They are characterized by dependence of flow rate q_{sj} (j=1,2) on pressure difference Δp ($\Delta p = p_{inlet} - p_{outlet}$) between inlet pressure p_{inlet} and outlet pressure p_{outlet} and coil current i_j (which is supplied to control the proportional valve j). The course of these characteristics (Fig 3.1a) is taken from the datasheet [12] and it is transformed by means of data-fit algorythm into a two-parametric function (3.1).

$$q_{sj} = q_{pv}\left(i_j, \Delta p\right) = k_{00} + k_{10}.i_j.\Delta p + k_{01}.\Delta p + k_{20}.i_j^{\,2} + k_{11}.i_j.\Delta p + k_{02}\Delta p^2 + k_{30}.i_j^{\,3} + k_{21}.i_j^{\,2}.\Delta p + k_{12}.i_j.\Delta p^2 + k_{03}.\Delta p^3 \tag{3.1}$$

The set of coefficients obtained by calculation in Matlab is:

k_{00} = 8.467173667721427e-05 k_{02} = 1.802838160958181e-15
k_{10} = -0.002744641178498 k_{30} = -0.074855751145469
k_{01} = -1.176858765765336e-09 k_{12} = -3.308168372719213e-08
k_{20} = 0.026466971305911 k_{21} = -2.307680895852796e-14
k_{11} = 1.753880923939311 k_{03} = 5.555058587281294e-21

in case of the process of the increasing the flow rate through a valve, and

k_{00} = 8.467173667721427e-05 k_{02} = 1.802838160958181e-15
k_{10} = -0.002744641178498 k_{30} = -0.074855751145469
k_{01} = -1.176858765765336e-09 k_{12} = -3.308168372719213e-08
k_{20} = 0.026466971305911 k_{21} = -2.307680895852796e-14
k_{11} = 1.753880923939311 k_{03} = 5.555058587281294e-21

in case of the process of decreasing the flow rate through a valve

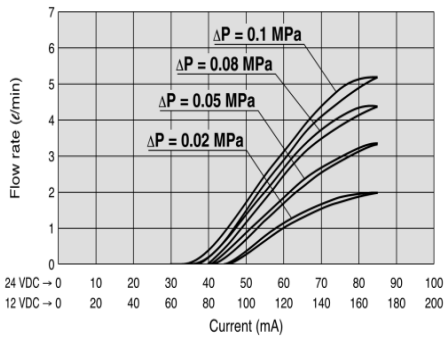

a) From the datasheet

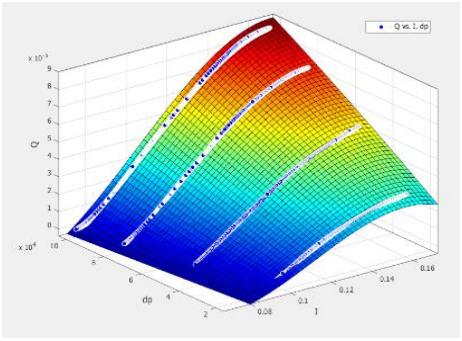

b) By a fitting algorithm

Figure 3.1. Characteristics of the proportional valve

From Fig 2.5, we have $p_{inlet} = p_{cr}$, $p_{outlet} = p_s$ for valve V_1 and $p_{inlet} = p_s$, $p_{outlet} = p_{atm}$ for valve V_2

where p_{atm} is the atmospheric pressure (p_{atm}=0.1 MPa).

For the purpose of controlling the system we define a pressure error e as a difference between desired pressure p_d inside the PSE and instant internal pressure p_s (3.5). Beside that we define a threshold e_t which addresses an insensitivity of control system. If absolute value of control error is less than e_t the control system does not apply control procedure to the proportional valves V_1, V_2. In other cases, the flow rate through valve V_1 is calculated by the formula (3.1) if $e < -e_t$ and is set to 0 if $e \geq -e_t$. The flow rate through valve V_2 is calculated by the formula (3.1) too but for case of $e > e_t$ and it is set to 0 if $e \leq e_t$.

So we have:

$$q_{s1} = \begin{cases} q_{pv}\left(i_1, p_{cr} - p_s\right) \text{ if } e < -e_t \\ 0 \qquad\qquad\quad \text{if } e \geq -e_t \end{cases} \tag{3.2}$$

$$q_{s2} = \begin{cases} q_{pv}\left(i_2, p_s - p_{atm}\right) \text{ if } e > e_t \\ 0 \qquad\qquad\quad \text{if } e \leq e_t \end{cases} \tag{3.3}$$

The PID controller is used for control of the coil current which is supplied to proportional valves V_1, V_2. Using the equation of PID controller the coil current is a function of the pressure error e and it is presented in the form:

$$i_j = K_P.e + K_I.\int_0^t e(\tau)\,d\tau + K_D.\frac{de}{dt}, \tag{3.4}$$

where:

$i_j(t)$ is the current supplied for controlling the proportional valve j $(j=1,2)$,

e is the pressure error given by the expression:

$$e = p_s - p_d\,. \tag{3.5}$$

The proportional valves V_1, V_2 are able to realize only relatively small flow rates an in some cases it would not be enough. For cases when we need to realize considerably higher flow rates to make system work faster we need to use the pair of discrete valves V_3, V_4 (in the type of SMC-S070B-6A) which increase the flow rate in step-change.

According to [13] flow characteristics of the discrete valve include sonic conductance C_{dv}=0.083 l/(s.bar) and critical pressure ratio b_{dv}=0.28. The formula for the flow rate calculation of discrete valve is:

$$\frac{p_{downstream}}{p_{upstream}} \leq b_{dv} \rightarrow q_{sj} = q_{dv1}\left(p_{upstream}\right) = 600.C_{dv}.p_{upstream}.\sqrt{\frac{293}{273+T}} \quad \text{l/min} \tag{3.6}$$

in case of choked flow, and

$$\frac{p_{downstream}}{p_{upstream}} \geq b_{dv} \rightarrow q_{sj} = q_{dv2}\left(p_{downstream}, p_{upstream}\right)$$

$$= 600.C_{dv}.p_{upstream}.\sqrt{1-\left(\frac{\frac{p_{downstream}}{p_{upstream}}-b_{dv}}{1-b}\right)^2}\sqrt{\frac{293}{273+T}} \quad \text{l/min} \tag{3.7}$$

in case of subsonic flow where

j=3,4,

$p_{upstream}$, $p_{downstream}$ represents upstream pressure and downstream pressure of the valve respectively,

in case of valve V_3, $p_{upstream} = p_{cr}$ and $p_{downstream}=p_s$, in case of valve V_4, $p_{upstream} = p_s$ and $p_{downstream}=p_{atm}$,

and T is the temperature inside the PSE which is assumed to be constant (297^0K).

The discrete valves V_3, V_4 are used for increasing of airflow when control error is recognized as high which is beyond the sum of the threshold (e_t) and another parameter (denoted Δp_s) which is set in the control software and called the value of pressure sensitivity. The discrete valve V_3 is switched on if $e < -e_t - \Delta p_s$ and switched off if $e \geq -e_t - \Delta p_s$. The discrete valve V_4 is switched on if $e > e_t + \Delta p_s$ and switched off if $e \leq e_t + \Delta p_s$.

So we have:

$$q_{s3} = \begin{cases} q_{dv1}\left(p_{cr}\right) & \text{if } \frac{p_{cr}}{p_s} \leq b_{dv} \text{ and } e < -e_t - \Delta p_s \\ q_{dv2}\left(p_{cr}, p_s\right) & \text{if } \frac{p_{cr}}{p_s} \geq b_{dv} \text{ and } e < -e_t - \Delta p_s \\ 0 & \text{if } e \geq -e_t - \Delta p_s \end{cases} \tag{3.8}$$

$$q_{s4} = \begin{cases} q_{dv1}(p_s) \text{ if } \dfrac{p_s}{p_{atm}} \le b_{dv} \text{ and } e > e_t + \Delta p_s \\ q_{dv2}(p_s) \text{ if } \dfrac{p_s}{p_{atm}} \ge b_{dv} \text{ and } e > e_t + \Delta p_s \\ 0 \qquad\qquad\qquad\qquad if\ e \le e_t + \Delta p_s \end{cases} \tag{3.9}$$

The total flow rate q_s is then given by the addition of flowrates of all individual valves q_{sj} as it is expressed by:

$$q_s = q_{s1} - q_{s2} + q_{s3} - q_{s4}. \tag{3.10}$$

3.1.1.2. Mathematical model of the compressed air supply

Compressed air is generated by the compressor C and is stored in the reservoir R. The pressure inside the reservoir p_r is a factor influencing the flow rate from the reservoir to the PSE. The process of transporting air from the compressor to the reservoir and distributing compressed air from the reservoir through inlet valves (V_1 and V_3) to the PSE is shown in Fig 3.2.

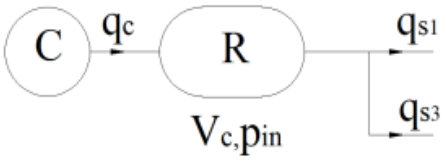

Figure 3.2. The scheme of the process of transmitting compressed air to PSE

According to [14] the elementary equation for an ideal compressed air reservoir is

$$q_c = C_f \cdot \frac{dp_{cr}}{dt}, \tag{3.11}$$

where :

q_c is the flow rate from the compressor to the reservoir,

C_f is the compressed air capacitance found experimentally. The capacity of a given volume of fluid in a rigid container is given by:

$$C_f = \frac{V_{\exp}}{\beta}, \tag{3.12}$$

where

V_{exp} is the volume of the rigid container ($V_{exp} = 0.63\ l$),

β is the bulk modulus of air (β=142 kPa).

The compressor characteristics in time and pressure domain are calculated on the experimental basis. They are a dependence of pressure of compressed air on time during filling of a rigid container and a dependence of flow rate on pressure (see Fig. 3.3).

Based on the scheme (Fig 3.2) the total air flowrate q_{cr} through the reservoir is then given by:

$$q_{cr} = q_c - q_{s1} - q_{s3}\,, \tag{3.13}$$

where

q_{s1}, q_{s3} are flow rates of both valves V_1, V_3,

q_c is supplied flow rate from the compressor.

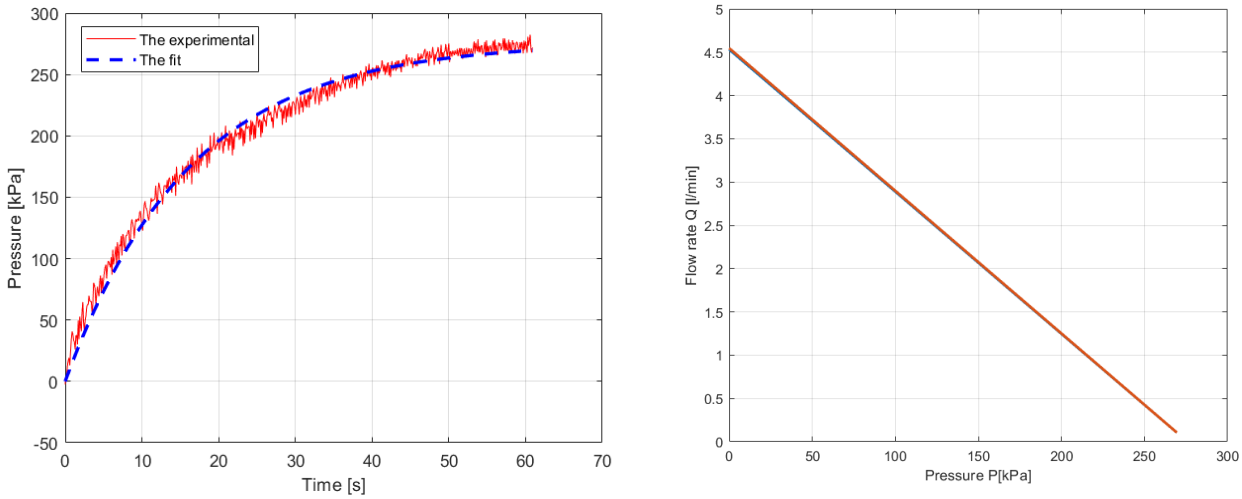

a) Dependence of pressure of compressed air on time

b) Dependence of flowrate air on pressure

Figure 3.3.The characteristics of the compressor

When the compressor is working, the flow rate q_c can be expressed in form of a linear function of the pressure inside the reservoir p_{cr}:

$$q_c = a_1\left(\frac{p_{cr} - p_{atm}}{b_1}\right), \tag{3.14}$$

The constants $a_1 = 0.062$, $b_1 = 275.92$ are experimentally determined to correspond to the results in Fig 3.3b.

Pressure p_r is measured by sensor PS_1 and it is kept in the interval [p_{cr1}, p_{cr2}] by the control system. Values p_{cr1}, p_{cr2} are set in control software as user-defined system parameters. The compressor is switched on in case $p_{cr} < p_{cr1}$ (*State*=ON) and switched off in case of $p_{cr} > p_{cr2}$ (*State*=OFF). The "*State*" is an internal variable which is automatically set by the controller. Normally, the values of p_{cr1} and p_{cr2} are set to 90 kPa and 110 kPa respectively.

The function describing the flow from the compressor to the reservoir is presented as follows:

$$\begin{cases} q_c = a_1\left(\frac{p_{cr} - p_{atm}}{b_1}\right) \text{ and } State = ON \text{ if } p_{cr} < p_{cr1} \\ q_c = 0 \text{ and } State = OFF \text{ if } p_{cr} > p_{cr2} \\ q_c = a_1\left(\frac{p_{cr} - p_{atm}}{b_1}\right) \text{ if } State = ON \text{ and } p_{cr1} < p_r < p_{cr2} \\ q_c = 0 \text{ if } State = OFF \text{ and } p_{cr1} < p_{cr} < p_{cr2} \end{cases} \tag{3.15}$$

3.1.2. Model of the mechanical subsystem

Practically it is possible to assume that the PSE changes pressure distributions in all contact zone between the human body and the seat cushion. But for the purpose of creation of my model, I take into account a much smaller area where we expect maximum pressure change influence. Regarding also to the compatibility with our laboratory equipment we set the contact area of our model to value (100x100) mm^2 (see Fig 3.4a). This subsystem is considered as a mechanical model with lumped parameters.

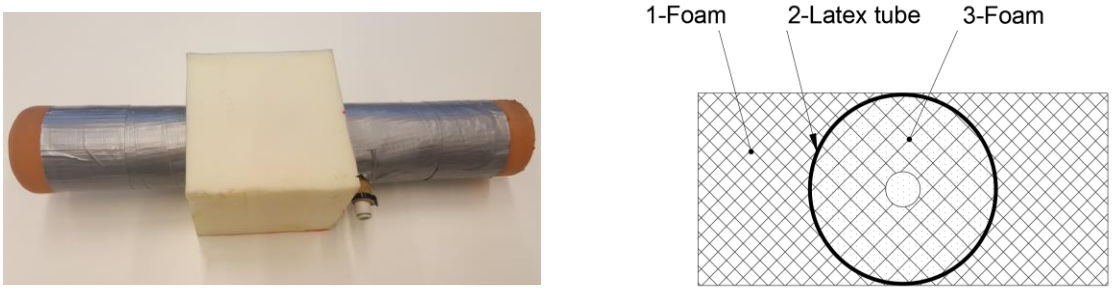

a) In reality b) Cross-section

Figure 3.4.The foam block with area (100x100) mm^2 and a PSE inserted inside

The model is built with the assumption that the mechanical subsystem represents a combination of foam block 100x100x50 mm^3 and a PSE. The scheme of cross-section of this part is in Fig 3.4b. For the model simplification we consider that foam part (1) and foam part (3) can be represented by 1 cuboidal foam block in parallel arrangement with the latex tube (2) filled by compressed air

(4). For the purpose of better correspondence with the real mechanical subsystem (see Fig 3.4a), the internal volume of latex tube is decreased about the volume of foam solid material originally inserted inside. We assume that the hole in the center of the foam part (3) is negligible, so we consider that the mechanical subsystem is applicable to the system equivalence presented in Fig 3.5. In this equivalent subsystem, the model is divided into 2 parts: foam block 100x100x50 mm^3 and a latex air spring. Forces acting on the mass are illustrated in the free-body diagram (see Fig 3.5c) where $x, \dot{x}, \ddot{x}$ represent the kinematic displacement excitation, velocity excitation and acceleration excitation, $\vec{F}_{foam}, \vec{F}_p$ represent the contact forces between the foam block, the latex air spring and the mass sequentially.

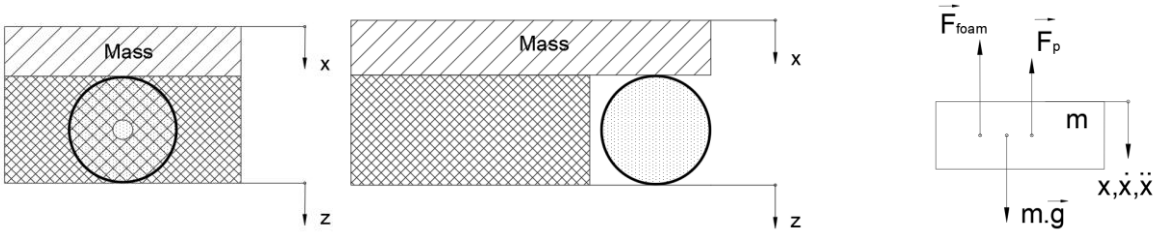

a) Mechanical subsystem

b) Equivalent mechanical subsystem

c) Free-body diagram

Figure 3.5. Simplified scheme of the mechanical subsystem

and it is possible to set up the equation of motion of mass *m* in the form:

$$m.g - F_{foam} - F_p = m.\ddot{x} \tag{3.16}$$

For further model derivation, we used this simplified approach. So the model structure is considered as presented in Fig 3.6 where *z* represents the kinematic displacement excitation and *x* represents the model displacement response.

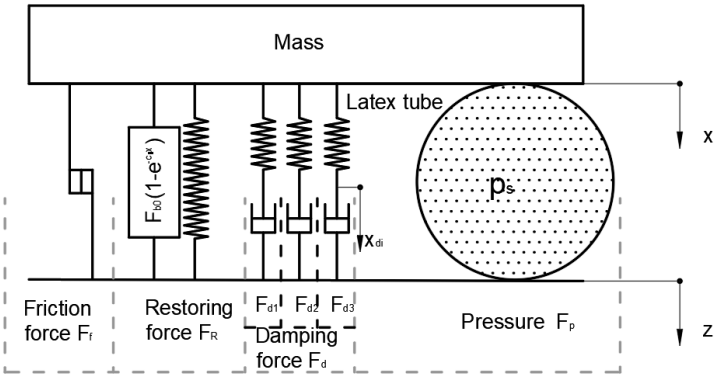

Figure 3.6. Detailed scheme of the mechanical subsystem

3.1.2.1. Model of polyurethane foam

Computational scheme of the rheological model the PU foam block is depicted in the left part of Fig 3.6. It is the result of research taken from the article [15]. The concept of this lumped parameter model follows from the phenomenological approach. It comprises nonlinear restoring force F_R, damping force F_d and frictional force F_f in general force response F_{foam}. The model definition of PU foam is described in detail in Appendix A:

$$\begin{aligned} F_{foam} &= F_{foam}\left(x, \dot{x}, x_{di}, \dot{x}_{di}\right) \\ &= F_R\left(x\right) + F_d\left(x, \dot{x}, x_{di}, \dot{x}_{di}\right) + F_f\left(x, \dot{x}, x_{di}, \dot{x}_{di}\right) \end{aligned} \tag{3.17}$$

$$F_R = F_b + F_{dp} \tag{3.18}$$

3.1.2.2. Model of the latex air spring

Basically the latex air spring is considered as a latex tube covered with fabric adhesive tape. The contact force F_p between the latex air spring and the mass (see Fig 3.5c) depends on the contact area (S) and the internal pressure (p_s). The theoretical formula of the contact force F_p is given by:

$$F_p = S.\left(p_s - p_{atm}\right) \tag{3.19}$$

where

p_{atm} is the atmospheric pressure (p_{atm}=0.1 MPa),

From empirical observation the contact area S varies in dependence on the deformation of the latex air spring and the internal pressure. Because the foam and the latex air spring are arranged in parallel (see Fig 3.5), the deformation of air spring is equal to the deformation of the foam block (x-z).

In short, the contact force F_p can be considered as a function depending on the deformation (x-z) and pressure p_s. The change of pressure, deformation and change of contact area is a complex phenomenon, therefore, the dependence of contact force on the deformation and the pressure is determined experimentally. In this way an experiment was performed on the Instron E3000 machine as shown in Fig 3.7. A latex air spring was compressed by an indentor. The vertical force was measured by the force cell and the deformation of latex air spring was considered equal to the displacement of indentor. The pressure inside the latex air spring was set to initial value (0, 5, 10, 15, 20, 25) kPa at the beginning of the experiment and this value was kept constant during compression by means of electro-pneumatic control subsystem. The dependency of contact force

on displacement of indentor was measured. For measurement of internal pressure the pressure sensor PSE543A – R06 was used.

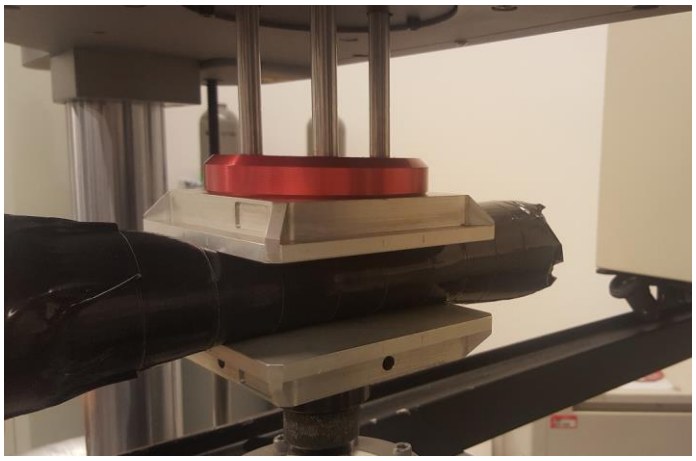

Figure 3.7.Setup of the experiment

The contact force F_p is possible to consider in the form of polynomial function:

$$F_p = F_p(\mathrm{x}, p_s) = k_{00} + k_{10}.(\mathrm{x}-\mathrm{z}) + k_{01}.(p_s - p_{atm}) + k_{20}.(\mathrm{x}-\mathrm{z})^2 + k_{11}.(\mathrm{x}-\mathrm{z}).(p_s - p_{atm}) + k_{02}(p_s - p_{atm})^2 + k_{30}.(\mathrm{x}-\mathrm{z})^3 + k_{21}.(\mathrm{x}-\mathrm{z})^2.(p_s - p_{atm}) + k_{12}.(\mathrm{x}-\mathrm{z}).(p_s - p_{atm})^2 + k_{03}.(p_s - p_{atm})^3 \quad 3.20)$$

and the 3D graph of interaction force F_p is shown in Fig 3.8.

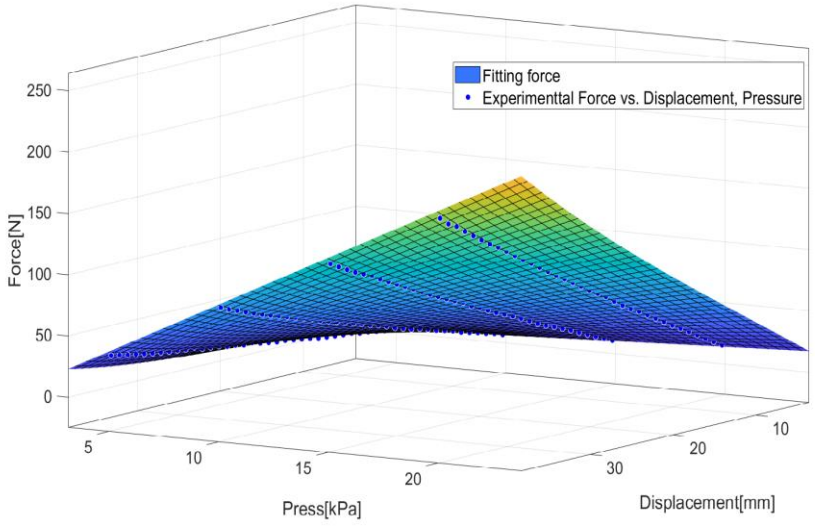

Figure 3.8. Relationship between contact force, displacement and pressure

According to [16] the internal pressure (p_s) depends on its the volume (V_b) and the flow rate of supplied air (q_s) and is expressed in the form of the differential equation:

$$\dot{p}_s = \frac{\kappa.q_s.R_{gas}.T}{V_{ls}} - \kappa.p_s.\frac{\dot{V}_{ls}}{V_{ls}} \tag{3.21}$$

where

T is the temperature of the air inside the PSE which is assumed to be constant (T=297 ^{0}K),

κ=1.4 is adiabatic exponent,

R_{gas}=287 J kg^{-1} K^{-1}is the gas constant.

In fact the volume V_{ls} must be the volume of compressed air inside the PSE. So it is easy to realize that this volume is the rest of the volume of PSE which is not occupied by the structure of foam material (see Fig 3.9a). For simplified calculation, the total volume of the PSE is separated into three parts. Part one, with volume V_1, is deformed because of the interaction with the loading mass. After being covered with tape this part is not deformed by pressure. Part two, with volume V_2, is covered with tape too but it is not in contact with the mass so it is considered as non-deformable. Part three consists of two free ends (volume V_3). These two ends are not covered by tape therefore they are deformed by pressure inside the PSE (see Fig 3.9b).

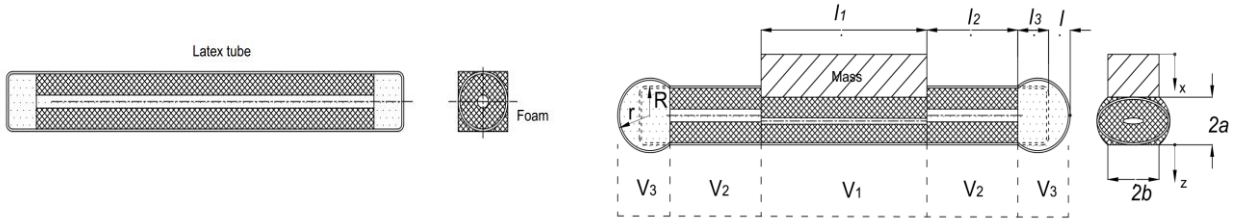

a) Undeformed shape b) Deformed shape

Figure 3.9.Scheme of the latex tube with foam inserted inside

For calculation of volume V_1, the elliptical cross-section is considered so the volume is given by :

$$V_1 = V_1(x) = \pi.a.b.l_1 \tag{3.22}$$

where

$a = R - \frac{x-z}{2}$, $b \approx \sqrt{2R^2 - a^2}$,

l_1 is the length of the tube corresponding to the volume V_1 (l_1 =0.2 m), R is the latex tube radius before the deformation (R=0.025 m).

Volume V_2 with a circular cross-section is given by the formula:

$$V_2 = \pi.R^2.l_2 \tag{3.23}$$

where l_2 is the length corresponding to the volume V_2 (l_2 =0.1 m).

To determine the dependence of volume V_3 on the internal pressure of the PSE, an experiment was carried out. The setup of the experiment is shown in Fig 3.10. In this experiment, the PSE is kept fixed vertically. The compressed air is pumped into the PSE and the internal pressure p_s is measured by the pressure sensor PSE543A – R06. A distance sensor OptoNCDT 1402 fixed above the PSE is used for measuring the displacement l of the center point C of the end of the PSE (see Fig 3.11).

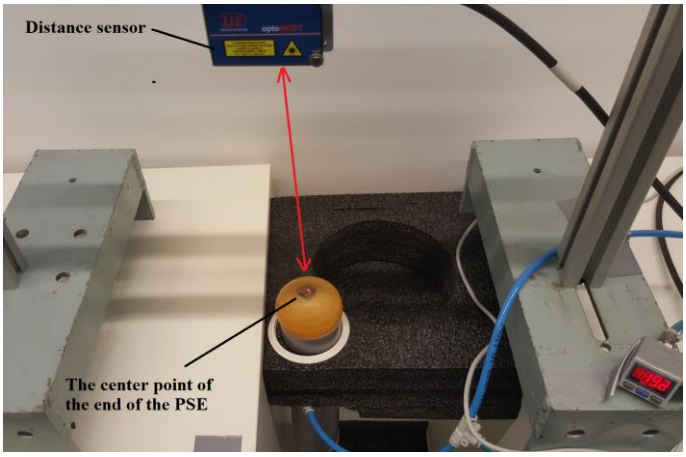

Figure 3.10.Setup of the experiment

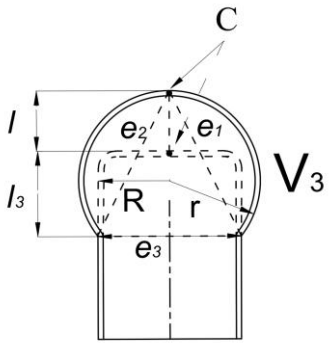

Figure 3.11. Scheme of deformed volume V_3

Based on the scheme Fig 3.11 the volume of a spherical cap V_3 with radius r and height h is given by the formula:

$$V_3 = V_3(h) = \pi(h)^2.\left(r - \frac{h}{3}\right) \tag{3.24}$$

where

$h = l + l_3$,

l_3 is the length of the tube corresponding to the volume V_3 (l_3 =0.02 m),

l is a displacement of the center point of the end of the tube and depends on pressure p_s which was found from experimental data by curve fitting procedure (Fig 3.12) where l is considered as a one-parameter polynomial function

$$l = \sum_{i=1}^{15} k_i p_s^i \tag{3.25}$$

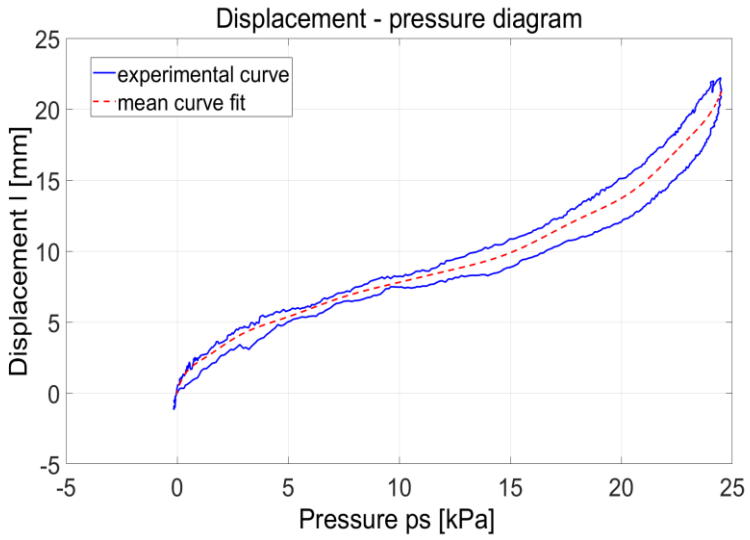

Figure 3.12. The relationship between the displacement of the center point of the end of the PSE (l) and internal pressure (p_s)

The radius of partial sphere r is given by the formula:

$$r = \frac{e_1 e_2}{\sqrt{(e_1 + e_2)^2 + e_3^2}} \tag{3.26}$$

where

$$e_1 = e_2 = \sqrt{\left(R^2 + h^2\right)}, \quad e_3 = 2R \tag{3.27}$$

Combining with (3.31), (3.32) and (3.33), we can rewrite equation (3.30) in the form:

$$V_3 = V_3(p_s) = \pi.\left(\sum_{i=1}^{15} k_i.p_s^i + l_3\right)^2.\left(\frac{\left(R^2 + \left(\sum_{i=1}^{15} k_i.p_s^i + l_3\right)^2\right)}{2\sqrt{2.R^2 + \left(\sum_{i=1}^{15} k_i.p_s^i + l_3\right)^2}} - \frac{\left(\sum_{i=1}^{15} k_i.p_s^i + l_3\right)}{3}\right) \quad (3.28)$$

After calculating the volume components the total volume of latex air spring is given by:

$$V_{ls} = V_{ls}(x, p_s) = V_1(x) + 2.V_2 + 2.V_3(p_s) - V_{foam} \quad (3.29)$$

The volume V_{foam} is determined experimentally by the difference between the volume of water before and after soaking the PU foam *(V_{foam} =0.15 l)*.

Table 2. The parameter of the latex tube

Parameter	Physical unit	Value
l_1	*[m]*	0.2
l_2	*[m]*	0.1
l_3	*[m]*	0.02
R	*[m]*	0.025
V_{foam}	*[l]*	0.15

The derivative of volume V_{ls} with respect to time is given by:

$$\dot{V}_{ls} = \dot{V}_1 + 2\dot{V}_2 + 2\dot{V}_3 - \dot{V}_{foam}, \quad (3.30)$$

The derivative of volume components in the equation (3.37) is expressed in the form:

$$\begin{aligned} \dot{V}_1 &= \frac{dV_1}{dx}.\dot{x} \\ \dot{V}_2 &= 0 \\ \dot{V}_3 &= \frac{dV_3}{dp_s}.\dot{p}_s \\ \dot{V}_{foam} &= 0 \end{aligned} \quad (3.31)$$

So we can rewrite (3.37) in the form:

$$\dot{V}_{ls} = \dot{V}_{ls}(x, \dot{x}, p_s, \dot{p}_s) = \frac{dV_1(x)}{dx}.\dot{x} + \frac{dV_3(p_s)}{dp_s}.\dot{p}_s, \quad (3.32)$$

From (3.28), (3.36) and (3.39) we see that:

$$\dot{p}_s = \frac{\kappa.q_s.R_{gas}.T - \kappa.p_s.\left(\frac{dV_1(x)}{dx}.\dot{x} + \frac{dV_3(p_s)}{dp_s}.\dot{p}_s\right)}{V_{ls}(x, p_s)}$$

So we have:

$$\dot{p}_s = \frac{\kappa.q_s.R_{gas}.T - \kappa.p_s.\frac{dV_1(x)}{dx}.\dot{x}}{V_{ls}(x, p_s) + \kappa.p_s.\frac{dV_3(p_s)}{dp_s}} \tag{3.33}$$

3.1.3. Numerical calculation

The mathematical model describing the mechanical subsystem derived in section 3.1.2 comprises equations from (3.16) to (3.40). This system of equations is made up by first-order differential equations. For the purpose of using Matlab software, it is useful to transform this system of equations into matrix form. So we write

$$\begin{aligned}
&\dot{X}_1 = X_2 \\
&\dot{X}_2 = g - \frac{F_{foam}(X_1)}{m} - \frac{F_p(X_1, X_6)}{m} \\
&\dot{X}_i = \left(\frac{1}{c_{i-2}} F_{dc}(X_1, X_i)\right)^{\frac{1}{n_{i-2}}}.\mathrm{sgn}\left(F_{dc}(X_1, X_i)\right) + \dot{z} \\
&i = 3...5 \\
&\dot{X}_6 = \frac{\kappa.q_s.R_{gas}.T - \kappa.X_6.\frac{dV_1(X_1)}{dX_1}(X_1).X_2}{V_{ls}(X_1, X_6) + \kappa.X_6.\frac{dV_3(X_6)}{dX_6}}
\end{aligned} \tag{3.34}$$

Then the system of equations describing mechanical subsystem in matrix form is

$$\dot{\mathbf{X}} = \mathbf{F}(\mathbf{X}), \tag{3.35}$$

where

$$\mathbf{X} = \begin{bmatrix} X_1 \\ X_2 \\ X_3 \\ X_4 \\ X_5 \\ X_6 \end{bmatrix} = \begin{bmatrix} x \\ \dot{x} \\ x_{d1} \\ x_{d2} \\ x_{d3} \\ p_s \end{bmatrix} \tag{3.36}$$

and

$$\mathbf{F}(\mathbf{X}) = \begin{bmatrix} F_1(\mathbf{X}) \\ F_2(\mathbf{X}) \\ F_3(\mathbf{X}) \\ F_4(\mathbf{X}) \\ F_5(\mathbf{X}) \\ F_6(\mathbf{X}) \end{bmatrix} = \begin{bmatrix} X_2 \\ g - \frac{F_{foam}(X_1)}{m} - \frac{F_p(X_1, X_6)}{m} \\ \left(\frac{1}{c_1}.F_{dc}(X_1, X_3)\right)^{\frac{1}{n_1}}.\text{sgn}\left(F_{dc}(X_1, X_3)\right) + \dot{z} \\ \left(\frac{1}{c_2}.F_{dc}(X_1, X_4)\right)^{\frac{1}{n_2}}.\text{sgn}\left(F_{dc}(X_1, X_4)\right) + \dot{z} \\ \left(\frac{1}{c_3}.F_{dc}(X_1, X_5)\right)^{\frac{1}{n_3}}.\text{sgn}\left(F_{dc}(X_1, X_5)\right) + \dot{z} \\ \frac{\kappa.q_s.R_{gas}.T - \kappa.X_6.\frac{dV_1(X_1)}{dX_1}(X_1).X_2}{V_{ls}(X_1, X_6) + \kappa.X_6.\frac{dV_3(X_6)}{dX_6}} \end{bmatrix}. \tag{3.37}$$

The predefined functions of excitation $z, \dot{z}, \ddot{z}$ are continuous in an interval of time. The variable q_s is calculated when the system of equations (3.2), (3.3),(3.4), (3.5), (3.8), (3.9),(3.10), (3.13), (3.14) and (3.15) describing the function of electro-pneumatic control subsystem is being solved.

The system of equations derived above makes up the mathematical model of the electro-pneumatic mechanical system. The numerical method is used to solve the system of equations which includes equations describing the mechanical subsystem (3.34) and equations describing the electro-pneumatic control subsystem. The solution of this system of equations results in describing system response and system characteristics as kinematics of mass ($x, \dot{x}, \ddot{x}$), pressure inside the PSE (p_s) in case of mechanical subsystem, the flow rate (q_s,q_r,q_c, q_{s1},q_{s2}, q_{s3},q_{s4}), pressure (p_{cr},e,…), supplied

coil current of proportional valves i_j ($j=1,2$) in case of electro-pneumatic control subsystem and forces (F_{foam}, $F_{p,\ldots}$), volume change of PSE (ΔV_b), etc.

To solve the system of equations, the initial and boundary conditions were provided. The initial conditions are the values of the variables $x,\ x_{di}, \dot{x}, p_s, q_{si}\ (i=1...3), q_c, p_c, V_{ls}$ at initial time t=0, and boundary conditions are the values of the parameters $p_{cr1}, p_{cr2}, e_s, \Delta p_s$.

3.1.3.1. Calculation of the response of the original system

The examples below show the behavior of the original system when it works under static conditions (without excitation $z(t)$), and dynamic conditions (with excitation $z(t)$) for both modes of operation (constant stiffness and constant pressure).

In the constant stiffness mode the pressure inside the PSE (p_s) is set to chosen desired pressure p_d at the initial time. In the constant pressure mode the electro-pneumatic feedback circuit tries to keep the pressure p_s equal to desired pressure p_d for all the time of the loading process. For both modes mentioned we can additionally use an automatic change of desired pressure p_d with a predefined time course. In this time the harmonic and triangle waveforms are implemented as templates in the control software.

In our case the simulation process takes 102 seconds in total. At the initial time (1), in Fig. 3.13, the foam block is loaded by mass m=10 kg which simulates the sitting down of the passenger. After a very short period of transition process, at the time (2) equal to 1 s, the desired pressure p_d is set to 10 kPa. Then the system works in constant pressure mode under static condition ($z(t)=0$) for 10 seconds. After that, at the time (3), the desired pressure p_d starts to be driven by harmonic template mode: $p_d = 10 + 10.\sin(2\pi.0{,}1.t)\ \ kPa$ for 30 seconds. After that the system works in constant pressure mode again but with the value of desired pressure set to 15 kPa (at the time (4)). In very short time of 1 s later, at the time (5), an external harmonic excitation ($z(t)$) is applied as a source of vibration load for period of 30 s. Then the system is switched to constant stiffness mode while keeping the external harmonic excitation ($z(t)$) up to the end of the process at the time (6). Parameters of the PID controller were set to K_P=7, K_I=0, and K_D=1, sampling time was dt=0.05 s. The calculations were performed in Matlab software. The results of simulations are depicted in figures from Fig 3.13 to Fig 3.21 and comprises displacement $x(t)$, velocity $v(t)$ and acceleration $a(t)$ of mass m, resultant force (F_{sum}) acting on the mass and components of the resultant force (F_r,F_d,F_f,F_p), change of volume of the PSE (ΔV_{ls}), instantaneous pressure (p_s) inside the PSE, flow rate of compressed air through the PSE (q_s), pressure inside the reservoir (p_{cr}) and supplied coil current of the valves (i_1, i_2, i_3, i_4).

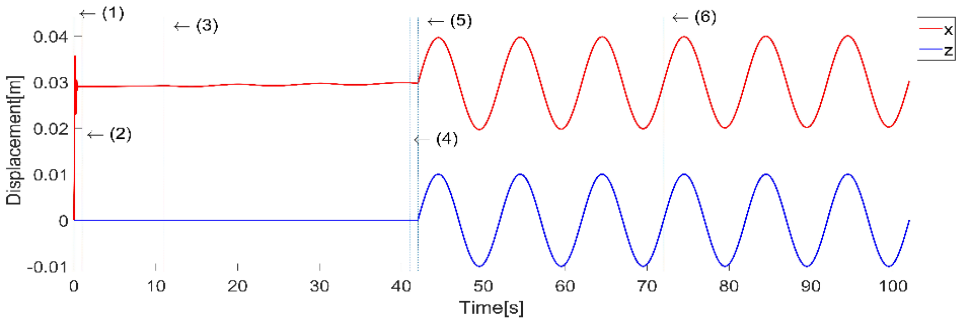

Figure 3.13. Displacement of mass x and diplacement excitation z

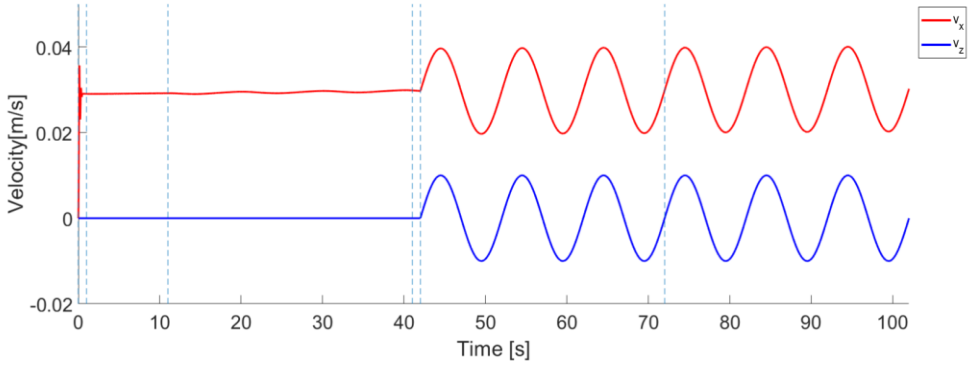

Figure 3.14. Velocity of mass v_x and velocity of excitation v_z

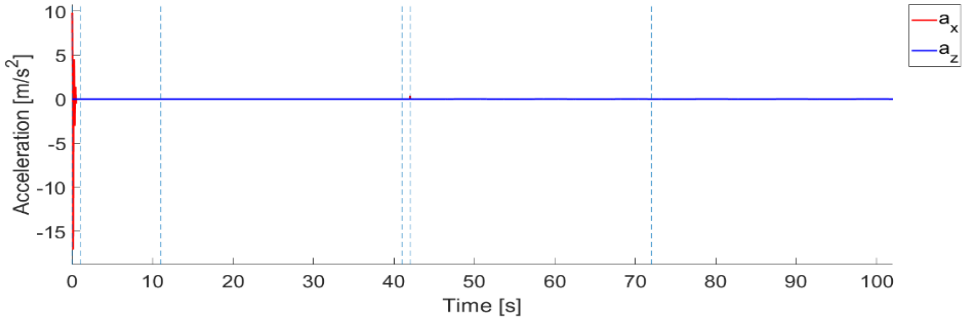

Figure 3.15. Acceleration of mass a_x and acceleration of excitation a_z

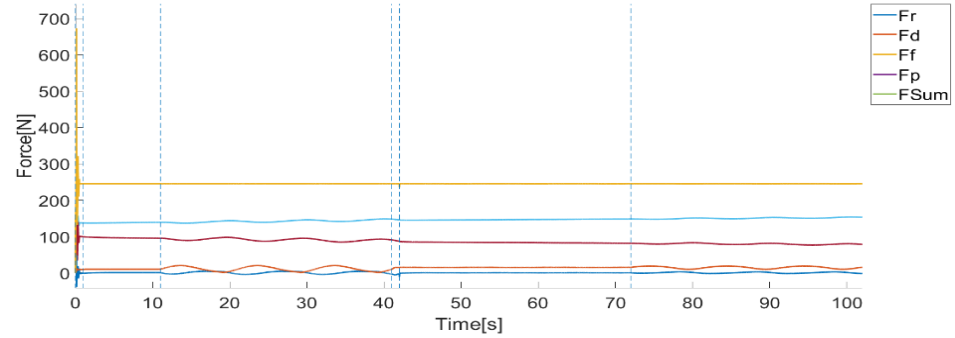

Figure 3.16. Forces

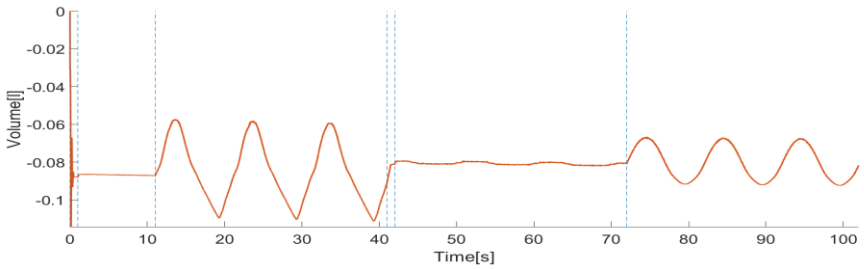

Figure 3.17. Volume change of latex air spring

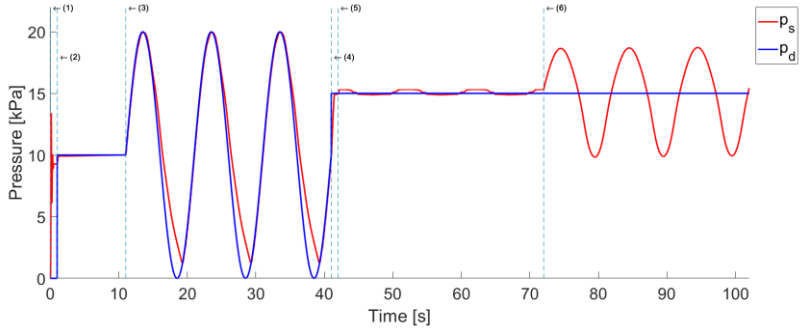

Figure 3.18. Pressure responce p_s and desired pressure p_d

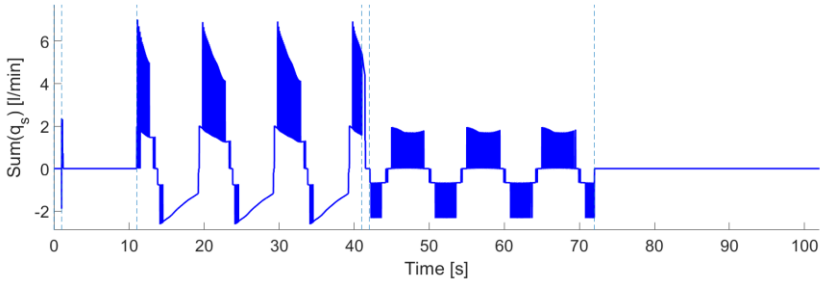

Figure 3.19. The flow rate q_s through the PSE

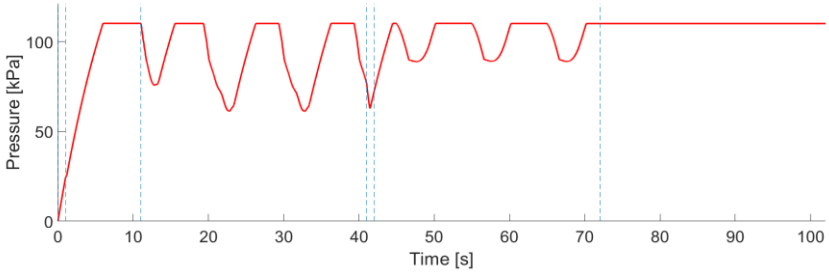

Figure 3.20. The pressure inside the reservoir p_{cr}

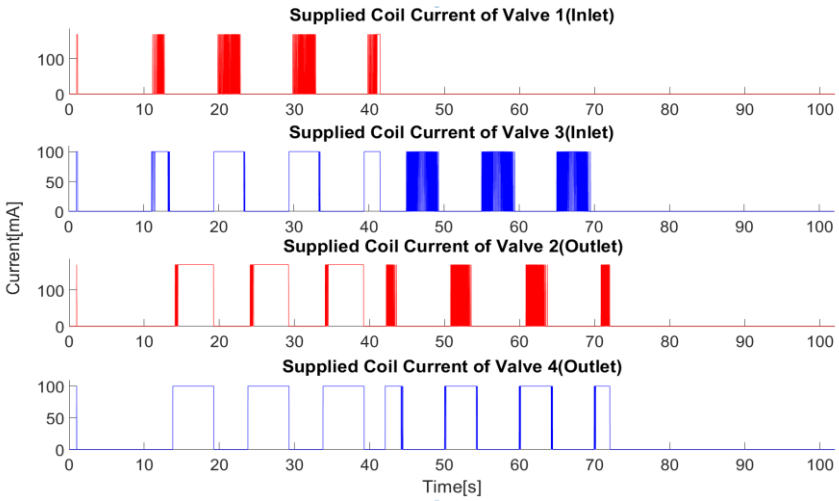

Figure 3.21. Supplied coil current of the valves V_1, V_2, V_3, V_4

3.1.3.2. Calculation of transmission of acceleration

The transmission of acceleration is an important property of efficiency of vibration isolation systems. This is a way how to evaluate the influence of the PSE under dynamic conditions. Generally it is possible to say that transmission of acceleration is calculated as a ratio of the amplitude of acceleration of mass, and amplitude of acceleration of excitation (Ax/Az) when excitation is a harmonic function. This way is suitable in cases when the system is excited by a signal with discrete change of frequency and especially in cases of linear systems. Another way is to use the signal with continual change of frequency which is advantageous for investigation of nonlinear systems. In such cases so called sweep sine functions are usually used. According to [18], the harmonic excitation function can be replaced by a sweep sine with variable frequency. Numerous human vibration studies conducted over the past several decades have shown that the human body is sensitive to low-frequency vibration below 10 Hz [17]. Based on this the range was set to 1 - 11 Hz. The amplitude of acceleration was set to constant value of 0.1 g. The time of the signal was 120 s so the variation of frequency was slow enough to sufficiently excite the system in resonance area.

The excitation function used for experiments under dynamic conditions is expressed in the form [18]:

$$z(t) = Z_a (t + t_0)^{2(1-n)} \sin\left(c(t + t_0)^n\right) \tag{3.38}$$

where

n is the exponent of excitation function (n=2)

f_{start} is start frequency,

f_{stop} is the stop frequency,

T is the total time of the excitation signal,

g is the gravitation acceleration

and the other parameters are calculated as follows:

$$c = \pi . \frac{f_{stop} - f_{start}}{T} \quad \left[1/s^2\right] \tag{3.39}$$

$$t_0 = \left(\frac{2\pi f_0}{nc}\right)^{\frac{1}{n-1}} \quad [s] \tag{3.40}$$

$$Z_a = \frac{0.1g}{n^2 c^2} \quad \left[m/s^2\right] \tag{3.41}$$

The kinematic characteristics of an excitation signal are shown in Fig 3.22, Fig 3.23 and Fig 3.24 when $f_{start} = 1\ Hz$, $f_{stop} = 11\ Hz, T = 32s$

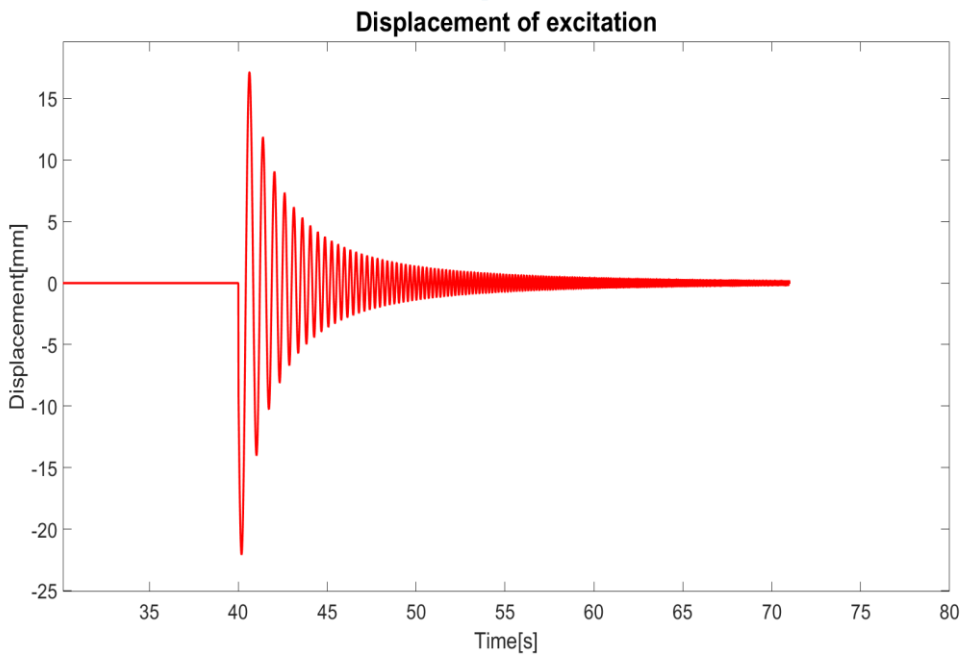

Figure 3.22.Displacement of excitation signal

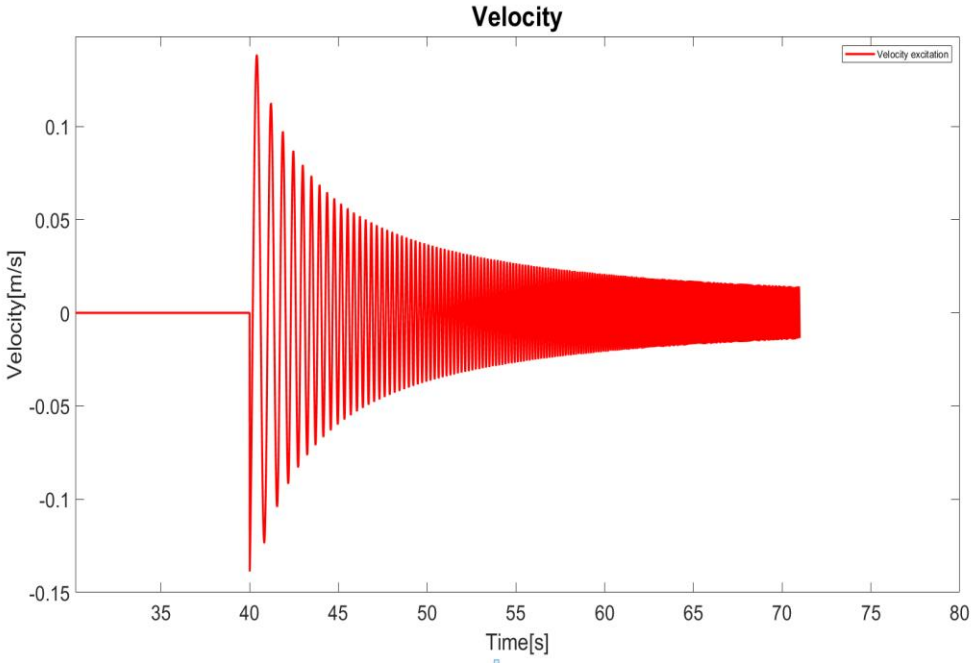

Figure 3.23.Velocity of excitation signal

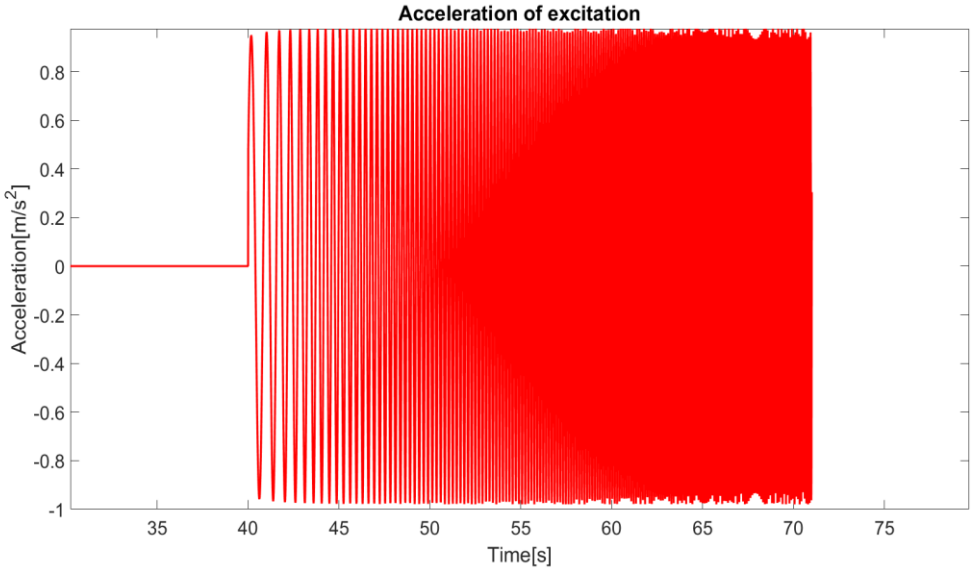

Figure 3.24. Acceleration of excitation signal

The Fig 3.25 and Fig 3.26 show calculated results of the transmission of acceleration in case of constant pressure mode and constant stiffness mode of control operation being used. The transmission curves are shown in cases of desired pressure pd∈{0, 5, 10, 15, 20, 25} kPa in dependence on the frequency of excitation in the range [1, 11] Hz.

In another case we assume that the control system works ideally (pressure error *e=0*); then we can find the ideal transmission curves. The calculation of this case was carried out and the results are shown in Fig 3.27.

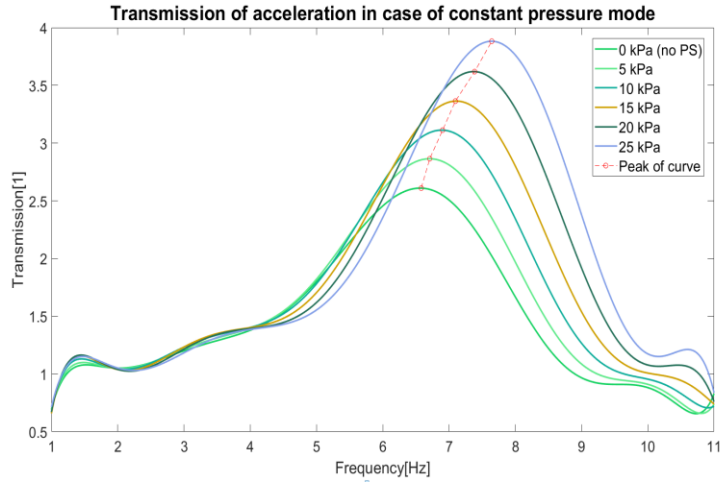

Figure 3.25.Transmission of acceleration - constant pressure mode

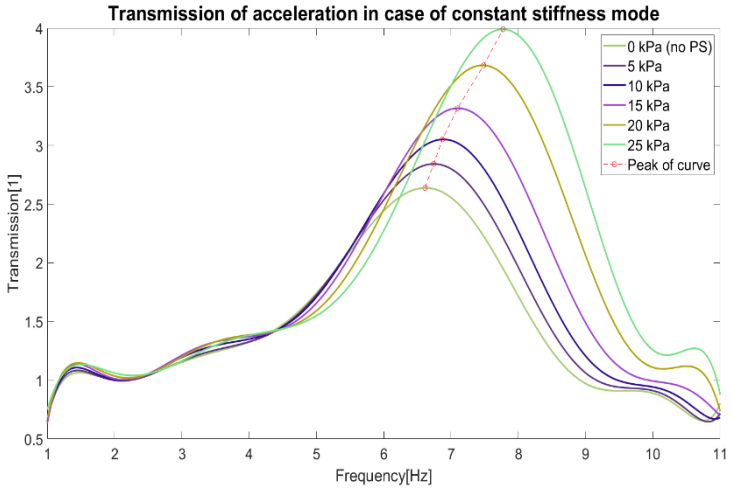

Figure 3.26.Transmission of acceleration - constant stiffness mode

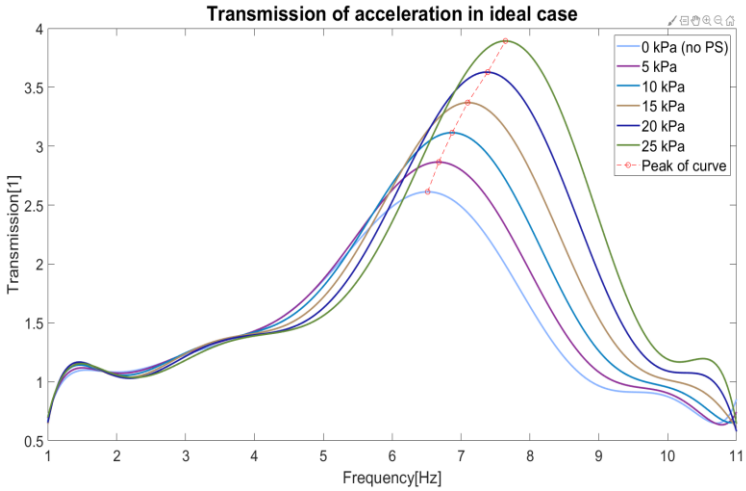

Figure 3.27. Transmission of acceleration in ideal case

3.1.4. Summary

The model of the original system consists of the model of foam block whose design is based on the article [15] and the model of a latex air spring and the model of electro-pneumatic control. Calculated results describe the behavior of the original system in detail when it works in different control modes (constant pressure and constant stiffness) under static or dynamic conditions.

The results show the capability of the original system to regulate the pressure inside the PSE under static conditions. Under dynamic conditions the function of the PSE and the electro-pneumatic control subsystem is evaluated through the transmission of acceleration. The results show that the transmission curves have a tendency to shift the peak position toward the higher frequency when the desired pressure increases in all control modes. The transmission-frequency diagram of all cases (constant pressure mode, constant stiffness mode and ideal case) are almost identical with same properties of shape of curve and position of peaks. Hence, the control modes have same influence on the transmission curves in every individual case of pressure inside the PSE. The peaks of transmission curves are located in the range of [6.5,8] Hz with peak values in the range [2.5, 4.0]. The change of pressure inside PSE in range [0, 25] kPa leads to the change of the transmission curves.

3.2. Mathematical model of the improved system

3.2.1. Introduction of the improved system

For the requirement of working faster and more precisely an improvement was applied. The improvement aims directly at enhancing the regulation of pressure inside the PSE. From experimental observations the relationship between change of pressure inside the PSE and its volume change is recognized. In this way the rate of change of internal pressure in a bigger PSE is lower than in a smaller PSE. Another factor that also influences the rate of change of pressure is the supplied flow rate of air to the PSE. Theoretically, the relationship between pressure, volume and the supplied flow rate is expressed by the formula (3.28) and is rewritten again in the equation below:

$$\dot{p}_s = \frac{\kappa . q_s . R_{gas} . T}{V_{ils}} - \kappa . p_s . \frac{\dot{V}_{ils}}{V_{ils}} \tag{3.42}$$

In equation (3.46) the volume of latex air spring V_{ls} of the original system is replaced by V_{ils} which is called the total volume of the improved latex air spring of the improved system.

Based on the above analysis a proposal for improvement was made. In this way the PSE was completely covered by tape. An additional latex tube is connected to the PSE (see Fig 3.28). It can be considered that the volume change is not caused by the PSE but by the additional latex tube

when compressed air is supplied. Therefore the volume change in case of improved PSE is much larger than in case of the original PSE and the regulation of pressure can be improved.

Figure 3.28.The additional latex tube connected to PSE

For increasing the flow rate of supplied compressed air the electro-pneumatic subsystem had to be modified. A vacuum pump generating output pressure (inside a reservoir R_2) less than 0 kPa is connected to the outlet valves. Another air compressor which creates higher inlet pressure (inside another reservoir R_1) is also used. The pressure sensor used for measuring the pressure inside the reservoir R_1 is replaced by an SMC PSE540A-R06 pressure sensor which can measure up to 1 MPa and another PSE543A-R06 pressure sensor is added for measuring vacuum pressure inside the reservoir R_2. The control circuit system also needed to be rebuilt. Control software that works in two control modes (constant pressure and constant stiffness) and displays the pressure characteristics of the improved system was created. The whole improved system was built as a mobile device in order to facilitate the experimental process (see Fig 3.29). The improved model is described in Fig 3.30.

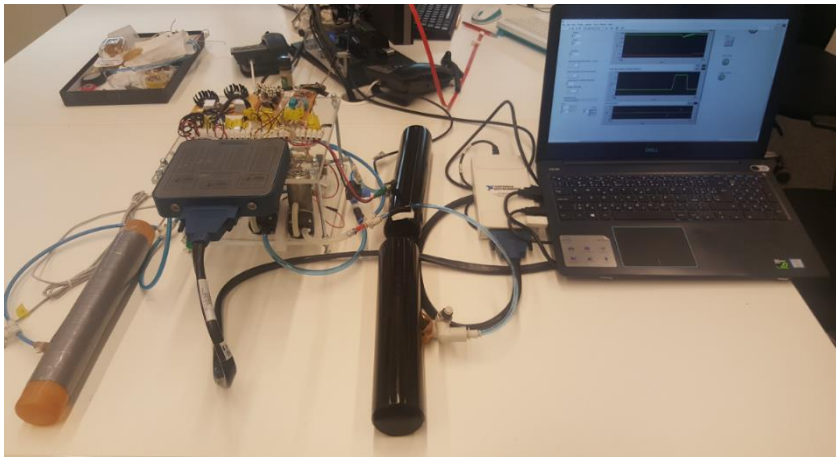

Figure 3.29. The real improved system

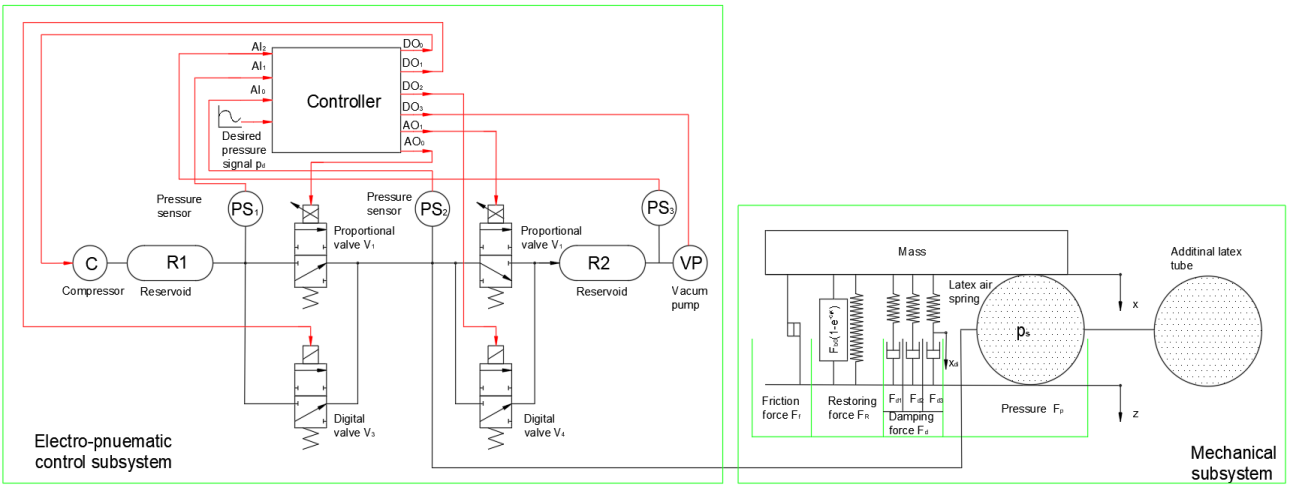

Figure 3.30. Detailed scheme of the improved system

The mathematical model of the improved system is based on the mathematical description of original system - applied changes in the system design are expressed by additional equations. The additional equations are introduced for every new component (the additional latex tube, the vacuum pump,…) to the system. Some parameter values are also updated in correspondence with newly replaced components.

3.2.2. Mathematical model of the vacuum pump

The vacuum pump VP is connected to the reservoir R_2 to create vacuum inside this reservoir R_2. The reservoir R_2 is connected to the outlet valve system (V_2 and V_4) thereby increasing the flow rate through the outlet valve system. The mathematical model of the vacuum pump can be built similarly to the model of the air compressor because of same operating principle. Fig 3.31 shows the scheme of the flow rates of compressed air from the PSE to the reservoir R_2 through the outlet valve system and from the reservoir to the vacuum pump.

Figure 3.31.The scheme of the process of releasing compressed air in the improved system

The equation of flow rate under the assumption of an ideal vacuum in reservoir is:

$$q_{vp} = C_f . \frac{dp_{vr}}{dt} \tag{3.43}$$

where

p_{vr} is the internal pressure of reservoir R_2,

q_{vp} is the flow rate from the reservoir R_2 to the vacuum pump,

C_f is the vacuum capacitance found experimentally and is given by (3.11).

The total flow rate through the reservoir is then given by:

$$q_{vr} = -q_{vp} + q_{s2} + q_{s4}, \tag{3.44}$$

where q_{s2}, q_{s4} are flow rates of valves V_2, V_4 respectively.

In this case q_{s2}, q_{s4} is calculated by (3.2) or (3.3) with $p_{upstream} = p_s$ and $p_{downstream} = p_{vr}$.

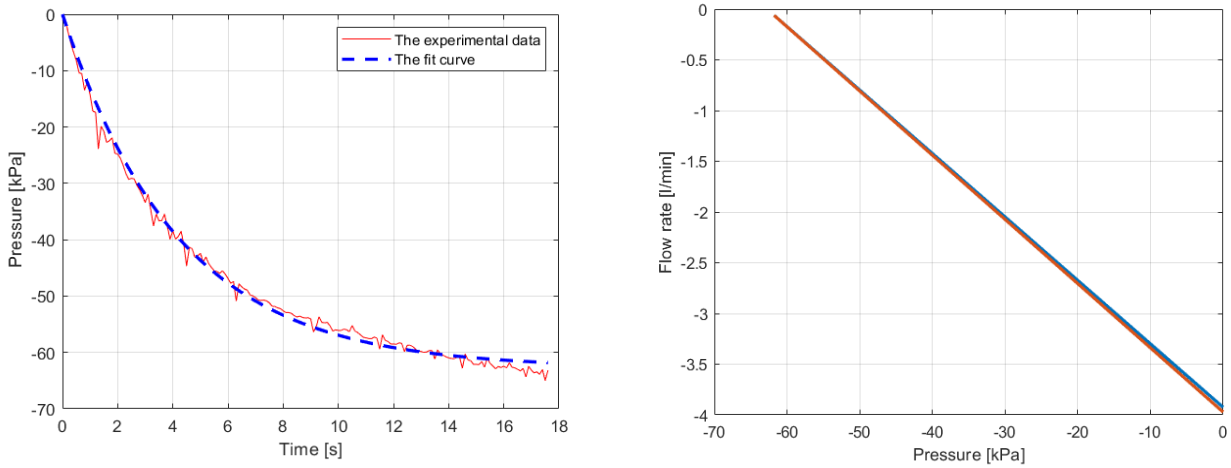

a) Pressure of vacuum pump – time diagram b) Flow rate – pressure diagram

Figure 3.32.The characteristics of the vacuum pump

When the vacuum pump works, the flow rate q_{vp} can be expressed in the form of a linear function of the pressure p_{r2} inside the reservoir R_2:

$$q_{vp} = a_2 \left(\frac{p_{vr} - p_{atm}}{b_2} \right), \tag{3.45}$$

The constants $a_2 = 0.23778$, $b_2 = -62.754$ are experimentally determined in correspondence with the results in Fig 3.32b.

Pressure p_{vr} is measured by sensor PS_3 and is kept in the interval [p_{vr1}, p_{vr2}] by the control system. Values p_{vr1}, p_{vr2} are set in control software as user-defined system parameters. The vacuum pump is switched on in case of $p_{vr}>p_{vr2}$ (*State*=ON) and switched off in case of $p_{vr}<p_{vr1}$ (*State*=OFF). The "*State*" is an internal variable that is automatically set by the controller. Normally the values of p_{vr1} and p_{vr2} are set to -60 kPa and -40 kPa respectively.

The function describing the flow from the reservoir to the vacuum pump is expressed by:

$$\begin{cases} q_{vp} = a_2\left(\dfrac{p_{vr}-p_{atm}}{b_2}\right) and\ State = ON\ \ if\ p_{vr} > p_{vr2} \\ q_{vp} = 0\ and\ State = OFF\ \ if\ p_{r2} < p_{vr1} \\ q_{vp} = a_2\left(\dfrac{p_{vr}-p_{atm}}{b_2}\right)\ if\ State = ON\ and\ \ p_{vr1} < p_{vr} < p_{vr2} \\ q_{vp} = 0\ if\ State = OFF\ and\ \ p_{vr1} < p_{vr} < p_{vr2} \end{cases} \tag{3.46}$$

The mathematical model of the compressor is updated with the values of p_{cr1} and p_{cr2} which are set to 190 kPa and 210 kPa respectively.

3.2.3. Mathematical model of the combination of the latex air spring and the additional latex tube

The additional latex tube is connected to the PSE as shown in Fig 3.28. The PSE is totally covered with tape so it can be assumed that change of the PSE volume caused by internal pressure is negligible and the total change of volume is completely caused by the change of volume of the additional latex tube. Therefore this section focuses on calculating the volume change of the additional latex tube.

According to above analysis we consider the volume of PSE being constant so we can use a simple calculation of its volume. The volume of the PSE is calculated in the way that is similar to the way used in the case of the original system and is given by:

$$V_{PSE} = V_1 + 2V_2 + 2V_3 - V_{foam} \tag{3.47}$$

in this case V_1,V_2,V_3 are calculated by:

$$V_1 = \pi R^2 l_1 \tag{3.48}$$

$$V_2 = \pi .R^2 .l_2 \tag{3.49}$$

$$V_3 = \pi .R^2 .l_3 \tag{3.50}$$

The total volume of latex air spring is rewritten into the form:

$$V_{PSE} = \pi.R^2.\left(l_1 + 2l_2 + 2l_3\right) - V_{foam} \tag{3.51}$$

Further on we are focusing on the calculation of the volume of the additional latex tube. The additional latex tube is designed in the way shown in Fig 3.33. It is filled with foam to reduce the volume that must be filled with compressed air. The volume of foam is the same as in the original PSE (V_{foam} *=0.15 l)*. We can see that its structure is similar to the structure of the original PSE.

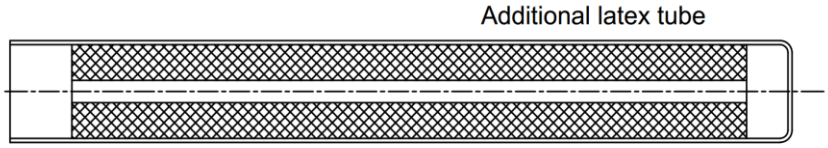

Figure 3.33.The scheme of the additional latex tube

It is assumed that unloaded latex tube with internal pressure 0 kPa has a cylindrical shape. With increasing pressure it deforms symmetrically due to its rotational symmetry. The change of volume of additional latex tube depends on pressure p_s and can be found out experimentally. The setup of the experiment is shown in Fig 3.34. At first the additional latex tube is filled with compressed air when the value of internal pressure reaches the value of desired pressure. Second, the additional latex tube is kept in stable position and its surface is scanned by a 3D scanner machine.

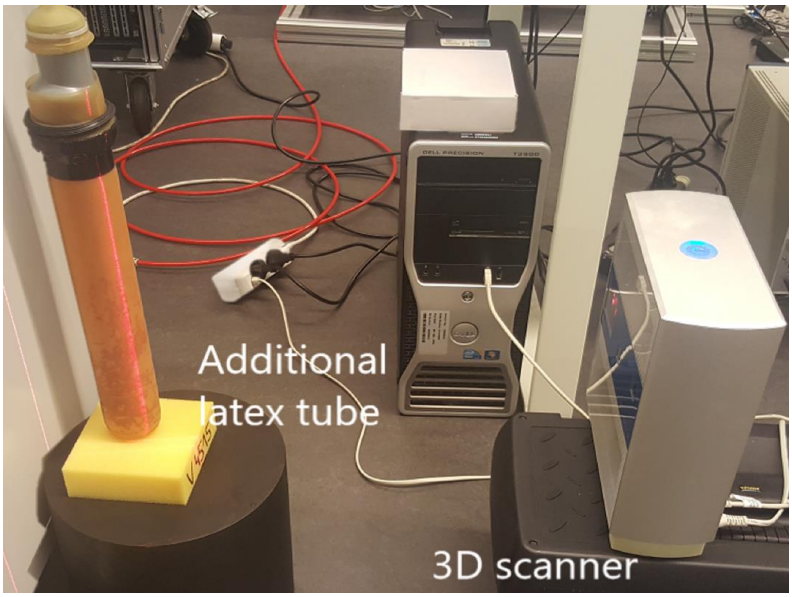

Figure 3.34.The setup of the experiment of the scanning of surface of the additional latex tube

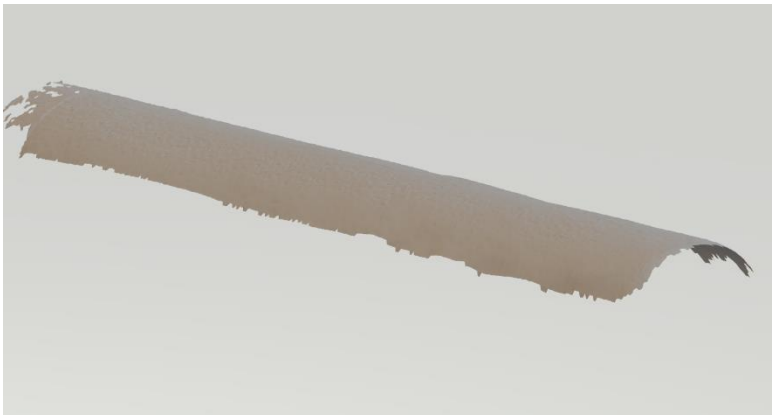

Figure 3.35. Example of scanned surface of the additional latex tube

The data obtained is represented by a cloud of points on the surface of the additional latex tube (see Fig 3.35) when the internal pressure changes in the range [0, 25] kPa with specific values of 0, 1, 2, ..., 25 kPa. The position of the center line and the area of the cross-section along the centerline are calculated. Then its volume can be calculated using integration techniques for a solid of revolution (see Fig 3.36).

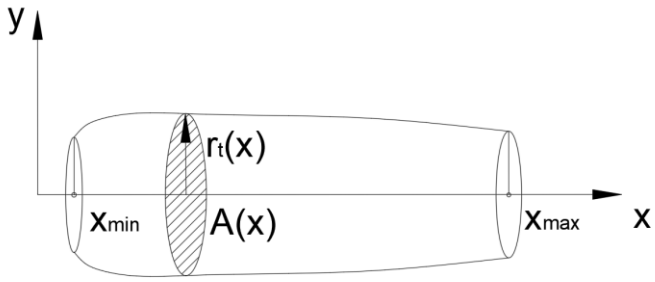

Figure 3.36. Scheme of the additional latex tube as a solid of revolution

The formula for the calculation of the volume of the additional latex tube is given by:

$$V_{add} = \int_{x_{\min}}^{x_{\max}} A(x)dx - V_{foam} \tag{3.52}$$

where *A(x)* is the cross-sectional area of the solid in accordance with the additional latex tube and is given by:

$$A(x) = \pi . r_t^2(x) \tag{3.53}$$

where *r*(*t*) is the radius of the cross-sectional area.

The calculation is programmed in Matlab software. The result is a set of volume values of the additional latex tube in dependence on pressure. Thus the volume (V_{add}) depending on internal pressure (p_s) can be given in form of a polynomial function (see Fig 3.37):

$$V_{add} = V_{add}(p_s) = k_0 + k_1(p_s - p_{atm}) + k_2(p_s - p_{atm})^2 + k_3(p_s - p_{atm})^3 + k_4(p_s - p_{atm})^4 - V_{foam} \tag{3.54}$$

By using Matlab a set of coefficients is obtained as shown below:

$k_0 = 8.512599267236148\text{e-}04$
$k_1 = 6.586794838689470\text{e-}09$
$k_2 = 4.111139460129753\text{e-}12$
$k_3 = -4.030675121010709\text{e-}16$
$k_4 = 1.163546770201630\text{e-}20$

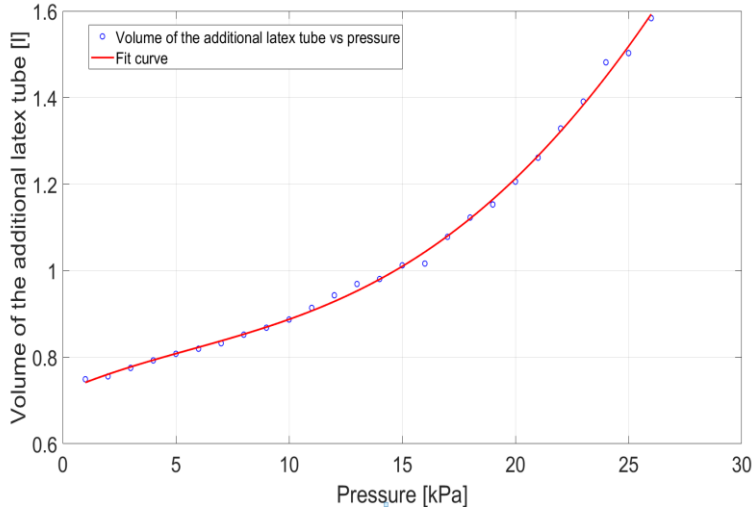

Figure 3.37. Volume-pressure diagram and the fit funtion

Finally the total volume of latex air spring in the case of the improved system can be given by:

$$V_{ils} = V_{ils}(p_s) = V_{PSE} + V_{add}(p_s) \tag{3.55}$$

Then the derivative of the total volume is:

$$\dot{V}_{ils} = \dot{V}_{PSE} + \dot{V}_{add} \tag{3.56}$$

From (3.55) and (3.57) we have the derivative of components of the total volume:

$$\dot{V}_{PSE} = 0 \tag{3.57}$$

$$\dot{V}_{add} = \frac{dV_{add}}{dp_s} \cdot \dot{p}_s$$

Thus, we get:

$$\dot{V}_{ils} = \dot{V}_{ils}\left(p_s, \dot{p}_s\right) = \frac{dV_{add}}{dp_s}.\dot{p}_s \tag{3.58}$$

In summary the mathematical model describing the improved system is given by first-order differential equations (3.34) with $V_{ls}(X_1,X_6)$ replaced by $V_{ils}(X_6)$ and by additional equations (3.44), (3.45) and (3.46) describing the improved electro-pneumatic subsystem

where

$$\mathbf{X} = \begin{bmatrix} X_1 \\ X_2 \\ X_3 \\ X_4 \\ X_5 \\ X_6 \end{bmatrix} = \begin{bmatrix} x \\ \dot{x} \\ x_{d1} \\ x_{d2} \\ x_{d3} \\ p_s \end{bmatrix}$$

Thus initial conditions for the system of equations of the improved system are the values of the variables $x,\ x_{di}, \dot{x}, p_s, q_{si}, q_c, p_c, V_{ils}$ at time t=0 and boundary conditions for the system equations are the values of the parameters $p_{cr1}, p_{cr2}, p_{vr1}, p_{vr2}, e_s, \Delta p_s$.

The comparison of the results of behavior of characteristics between the two systems is presented in the next section.

3.3. The comparison between the original system and the improved system

This section focuses on comparison of calculated results and experimental results to evaluate the influence of the improvement on the regulation of pressure inside the PSE and the transmission of acceleration. For the comparison, two system characteristics were used, the response time and the transmission of acceleration. The behavior of the original and the improved system is analyzed and evaluated numerically and experimentally. The function of pressure regulation is investigated under static conditions and the transmission of acceleration is performed under dynamic conditions.

3.3.1. The comparison of calculated results

3.3.1.1. Under the static conditions

This calculation regards the determination of pressure response inside the PSE without external load. The desired pressure is set in the form of a rectangular function which is given by:

$$p_d = \begin{cases} 0\,kPa, & \text{if } t<5 \\ 25\,kPa, & \text{if } 5 \le t<15 \\ 0\,kPa, & \text{if } t \ge 15 \end{cases}$$

In the case of the original system the inlet pressure is in the range [90,110] kPa and the outlet pressure is 0 kPa (atmospheric pressure). Meanwhile, in case of the improved system the inlet pressure is in the range [190, 210] kPa and the outlet pressure in the range [-40, -60] kPa. The pressure responses in both cases (original system and improved system) are shown in Fig 3.38.

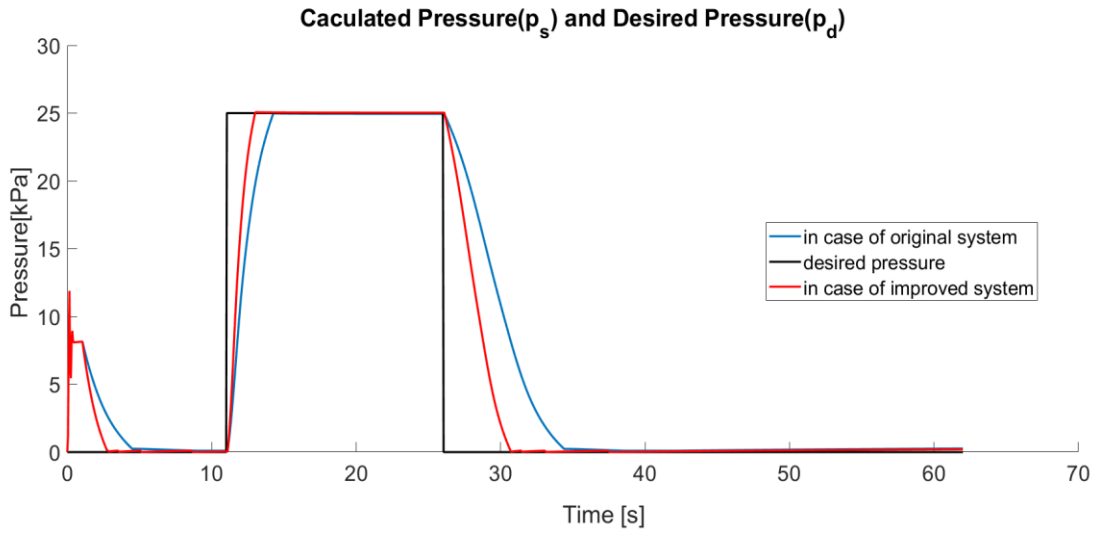

Figure 3.38. Pressure responses without external load

3.3.1.2. Under dynamic conditions

Under dynamic conditions there are two types of calculation. The first one is the calculation of pressure response inside the PSE under a periodic excitation function and the second one is for transmission of acceleration.

In the first type the loading mass is set to 10 kg, the excitation function is $z(t) = 10.\sin(2\pi ft)[mm]$ and the desired pressure is set to 15 kPa. The comparison of results is shown in Fig 3.39.

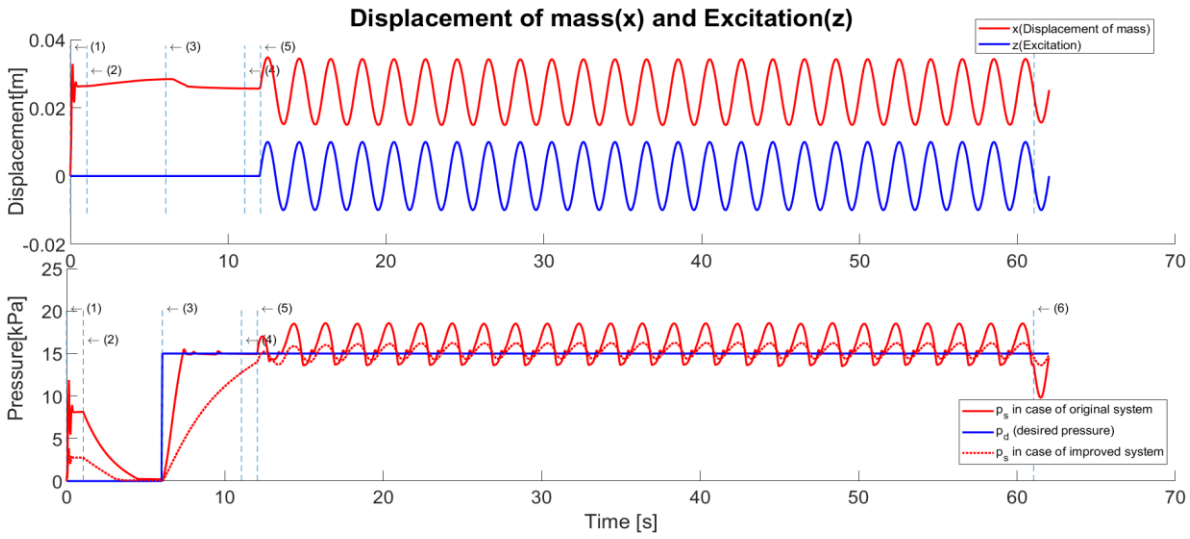

Figure 3.39. Comparison of pressure responses under periodic excitation

The calculation of transmission of acceleration was presented in section 3.1.3.2. The results in cases of the original system and the improved system are similar (see Fig 3.40). In this way, with a load of 10 kg, the behavior of transmission curves shows the shift of the peak position toward the higher frequency when the desired pressure increases and the peak value increases as well. However we can also see that the peak values of the transmission curves in the case of the improved system are slightly lower and appear at the smaller frequency than the peak values in case of the original system (except the case of p_d = 0 kPa). These peaks of transmission curves appear in the range of [6,8] Hz. Peak values are in range [2.5, 4.0].

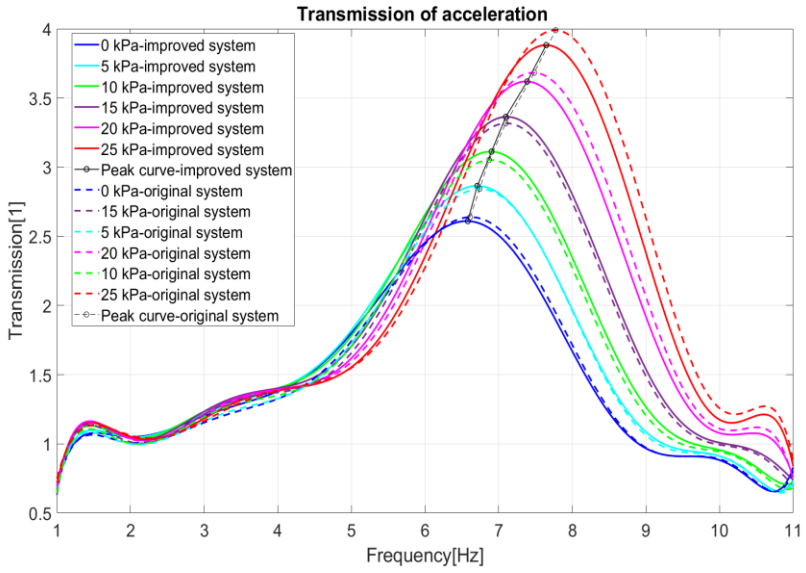

Figure 3.40. Comparison of transmission of acceleration

3.3.2. The comparison of the experimental results

It can be said that the original system differs from the improved system by the PSE and electro-pneumatic control subsystem. The original system comprises original PSE and original electro-pneumatic control subsystem while the improved system comprises improved PSE and improved electro-pneumatic control subsystem. The original PSE is the one that is not covered with tape at both ends while the improved one is the PSE that is fully covered with tape and the additional tube is connected to PSE. The original electro-pneumatic control subsystem is described in section 2.2 and the improved electro-pneumatic control subsystem is described in section 3.2.1. Experiments are carried out to verify the accuracy of the calculated results as well as the influence of the improvement on the regulation of pressure inside the PSE and on the transmission of acceleration.

3.3.2.1. Under static conditions

There are two types of experiments. The first one is the type of experiment for measurement of pressure response inside the PSE without external load. The second one is the type for measurement of pressure response inside the PSE with a dynamic external load.

In the first type of experiment the original PSE is connected to an electro-pneumatic control subsystem. For controlling of electro-pneumatic subsystem the Labview software is used. National Instruments hardware is used and connected to a laptop through USB cable. A Labview controller with a programmed user interface is created for setting control parameters and control pressure inside the PSE. The setup of experiment of the first type is shown in Fig 3.41. The original electro-pneumatic subsystem and the improved electro-pneumatic subsystem are used one by one with the same setting of desired pressure which is given by a rectangular function:

$$p_d = \begin{cases} 0\,kPa, & \text{if } t<4 \\ 25\,kPa, & \text{if } 4 \le t<13 \\ 0\,kPa, & \text{if } t \ge 13 \end{cases}$$

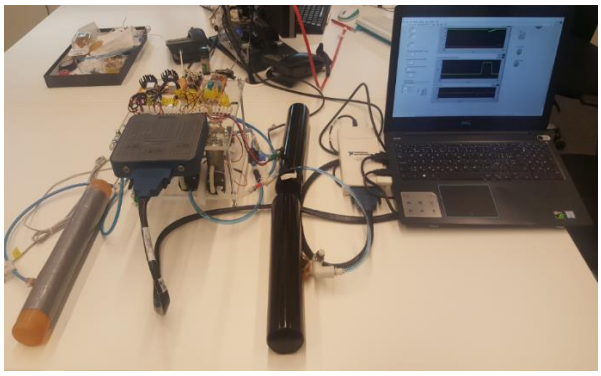

Figure 3.41. Setup of the experiment under static conditions without external load

The responses of pressure inside the PSE are measured by pressure sensors and are recorded by the Labview control software.

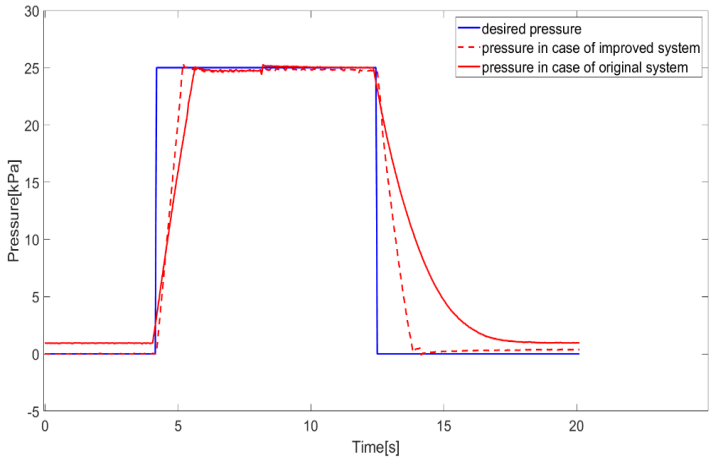

Figure 3.42. Experimental result of pressure responses

The results (see Fig 3.42.) show that the improved electro-pneumatic subsystem makes the pressure response faster with the pressure error smaller.

The second type of experiments is the measurement of pressure response in different control modes (constant pressure and constant stiffness) under static conditions, which means without external kinematic excitation of the lower platen, and under dynamic external load. These experiments are carried out by the Instron E3000 machine (shown in Fig 3.43).

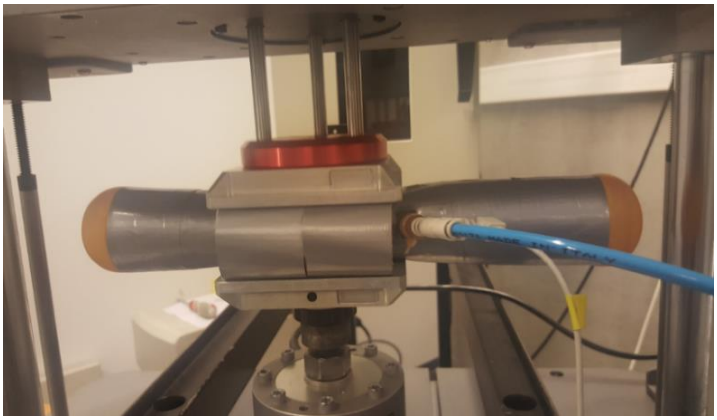

Figure 3.43. Setup of the experiment under static conditions with dynamic external load

The foam block with a PSE inserted in the middle is placed on a square compression platen (the base) and it is compressed by upper square platen. The motion of this upper platen is defined by

exciting function: $z(t) = 10.\sin(2\pi ft)[mm]$. Exciting frequency f is in range [0,3] Hz with values of (0.1, 0.3, 0.5, 0.7, 1, 1.5, 2, 2.5, 3) Hz (see Fig 3.44).

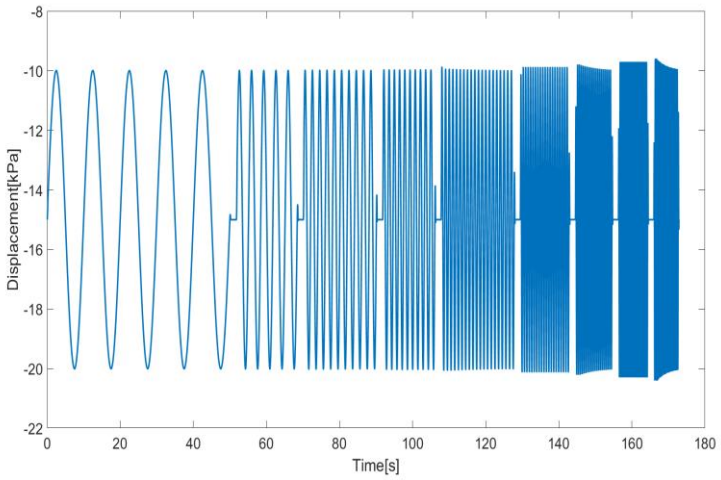

Figure 3.44. Motion of the upper square compression platen

The experiments with the original PSE and the original electro-pneumatic control subsystem are carried out first. Then other experiments are carried out with the replacement of the original PSE with the improved PSE or with the replacement of the original electro-pneumatic control subsystem with the improved electro-pneumatic control subsystem one by one. In this way the influence on the regulation of pressure inside the PSE is analyzed. Data is collected and subsequently processed by using Matlab software and the pressure error is evaluated ($e = p_s - p_d$ where p_d is desired pressure and p_s is measured pressure inside the PSE). Finally, we get the experimental results in form of pressure error in dependence on the exciting frequency as shown in figures below.In case of constant pressure mode the results are shown from Fig 3.45 to Fig 3.48.

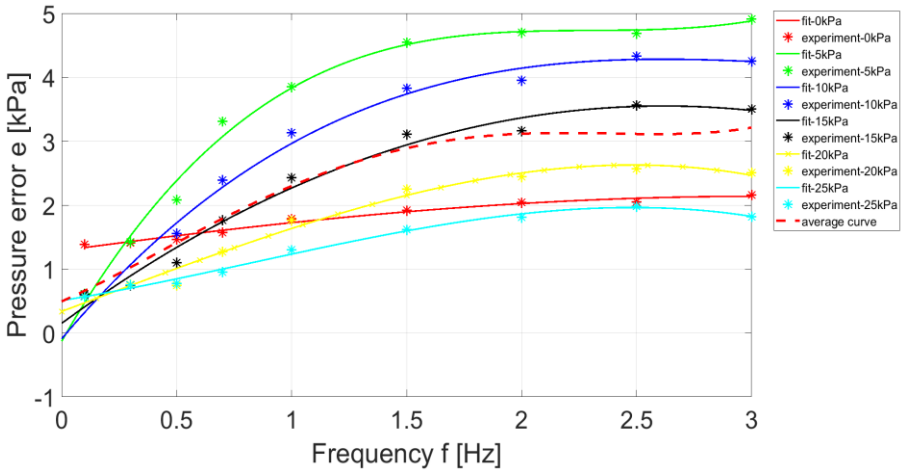

Figure 3.45. Original PSE - original control subsystem - constant pressure mode (case 1)

In case of measurement in constant pressure mode the results are shown from Fig 3.45 to Fig 3.48. Fig 3.45 shows the experimental results (case 1) in constant pressure mode when using the original PSE and the original electro-pneumatic control subsystem. When the desired pressure is set to 0 kPa, the values of the pressure error are equivalent for all values of exciting frequency in narrow range from 1.4 to 2.2 kPa. The increase of the value of the desired pressure in the range (0, 25] kPa causes the pressure error to decrease (excepting the case p_d=0 kPa) while increasing the value of the exciting frequency in the range [0,3] Hz causes the pressure error to increase.

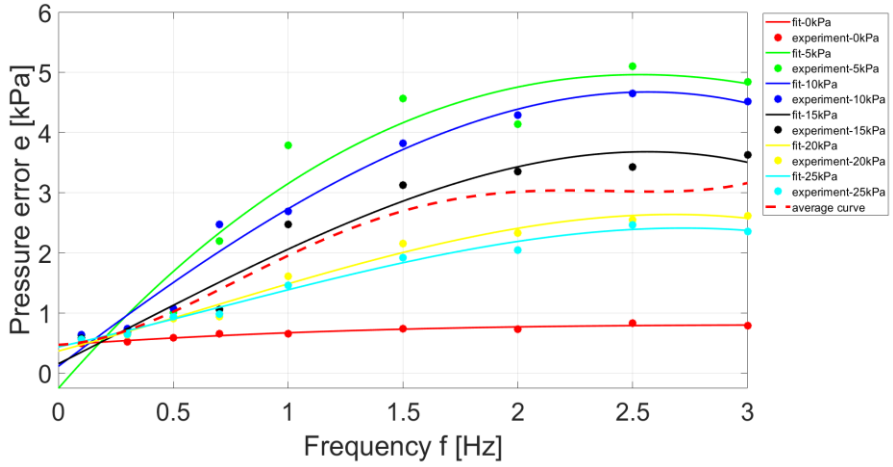

Figure 3.46. Original PSE - improved control subsystem - constant pressure mode (case 2)

Fig 3.46 shows the results (case 2) in constant pressure mode when using the original PSE and the improved electro-pneumatic control subsystem. There is a decrease of the pressure error (about the value of approximately 1 kPa) in case the value of the desired pressure is set to 0 kPa. In case the desired pressure value is greater than 0 kPa then the result of the pressure error seems to remain the same as when using the original electro-pneumatic control subsystem (see Fig 3.46).

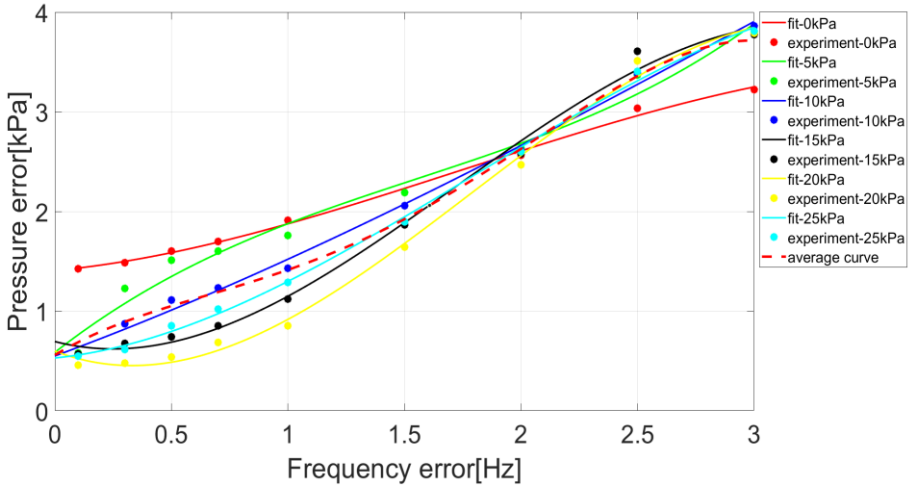

Figure 3.47. Improved PSE - original control subsystem - constant pressure mode (case 3)

Fig 3.47 shows the results (case 3) in constant pressure mode when using the improved PSE and the original electro-pneumatic control subsystem. The results show that the increase of value of exciting frequency in the range [0,3] Hz causes the pressure error to increase from 0.5 kPa to 3.8 kPa. In case the desired pressure is set to 0 kPa the pressure error changes in the range [1.5, 3.2] kPa. In case the desired pressure is set to a value greater than 0 kPa the pressure error changes in the range [0.5, 3.8] kPa. Increasing the value of the desired pressure in the range [0, 25] kPa just makes the tendency of pressure error to fluctuate around an average value at the same exciting frequency.

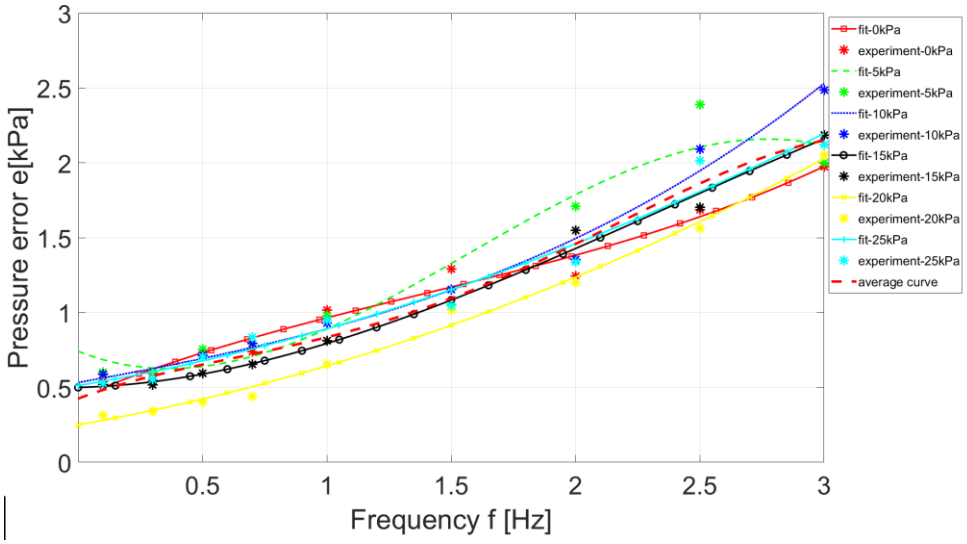

Figure 3.48. Improved PSE - improved control subsystem - constant pressure mode (case 4)

Fig 3.48 shows the results (case 4) in constant pressure mode when using the improved PSE and the improved electro-pneumatic control subsystem. The increase of value of exciting frequency in the range [0,3] Hz causes the pressure error to increase from 0.5 kPa to approximate 2 kPa. The increase of value of desired pressure in the range [0, 25] kPa causes the pressure error to fluctuate around an average value at the same exciting frequency.

The pressure error – frequency diagram in each of the cases above (presented from Fig 3.44 to Fig 3.48) is simplified by a couple of envelope curves (consists of upper envelope curve and lower envelope curve). Then these couples of envelope curves are gathered in Fig 3.49 to facilitate the comparison of the influence of components (original and improved PSE, original and improved electro-pneumatic control subsystem) on regulation of pressure inside the PSE, where:

the case 1 - OOC is a case of combination of the original PSE and original electro-pneumatic control subsystem (original system), the case 2 - OIC is a case of combination of the original PSE

and improved electro-pneumatic control subsystem, the case 3 - IOC is a case of combination of the improved PSE and original electro-pneumatic control subsystem, and the case 4 - IIC is a case of combination of the improved PSE and improved electro-pneumatic control subsystem (improved system).

From the Figure 3.49 we can see that:

The lower envelope curve in case 1 has values of pressure error in range [0.5, 1.8] kPa while the lower envelope curve in case 2 has values of pressure error in the range [0.5, 0.8] kPa. It confirms that improved electro-pneumatic control subsystem brings better regulation of pressure inside the PSE just for the value equal to 0 kPa in comparison with original control subsystem.

The upper envelope curve in case 1 has values of pressure error in the range [1.2, 4.7] kPa while the upper envelope curve in case 3 has value of pressure error in the range [1.0, 3.5] kPa. It proves that the improved PSE brings better regulation of pressure inside the PSE than the original PSE. The benefit of improved PSE is more obvious for higher values of pressure inside.

In case 4 the lower envelope curve has values of pressure error in the range [0.5, 1.5] kPa and the upper envelope has values of pressure error in the range [0.6, 2.3] kPa. It proves that the improved system brings much more better regulation of pressure inside the PSE than the original system when pressure inside the PSE change in the range [0, 25] kPa.

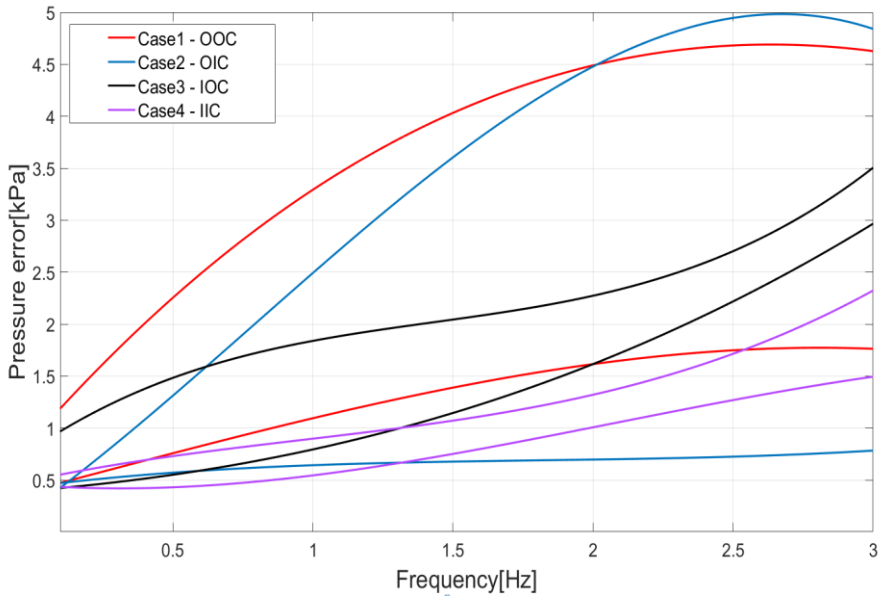

Figure 3.49. Envelope curves of pressure error – frequency relation in constant pressure mode

In case of constant stiffness mode both of the electro-pneumatic control subsystems (original and improved ones) fulfil the same function of closing all valves after the pressure inside the PSE

meets the desired pressure. Thus after closing the valves the pressure inside PSE is not regulated. But the external dynamic load still can cause the change of pressure inside the PSE. The maximum difference between the initial desired pressure and the instant pressure during the application of external dynamic load was measured and is presented in Fig. 3.50 and Fig 3.51. From this follows that these pressure change in the case of original PSE is higher then in the case of improved PSE. It is because the volume of the improved PSE is greater then the volume of the original PSE. The results in Fig 3.50 show that the pressure differences keep almost constant value for certain desired initial pressure setup and are independent on exciting frequency. In case the initial desired pressure is set to 0 kPa then the maximum pressure difference is approximately 4 kPa. In case the desired initial pressure is set to (5,10, 15, 20, 25) kPa the value of maximum pressure difference drops from 6 to 0.5 kPa.

The results in Fig 3.51 show that the use of improved PSE leads to a tendency of a slight increase of the pressure difference in every individual case of the initial desired pressure when increasing exciting frequency in the range [0, 3] Hz. In case the desired pressure is set to 0 kPa the maximum pressure difference increases from 2.5 kPa to 3.5 kPa. In case the initial desired pressure is set to 20 kPa the pressure error increases from approximate 0 kPa to 1.5 kPa.

The analysis above proves that the use of improved system leads to the faster pressure response in time domain under static conditions without external load. It leads also to the reduction of pressure error in exciting frequency domain under static conditions with dynamic external load. It indicates that the improvement enhances the regulation of pressure.

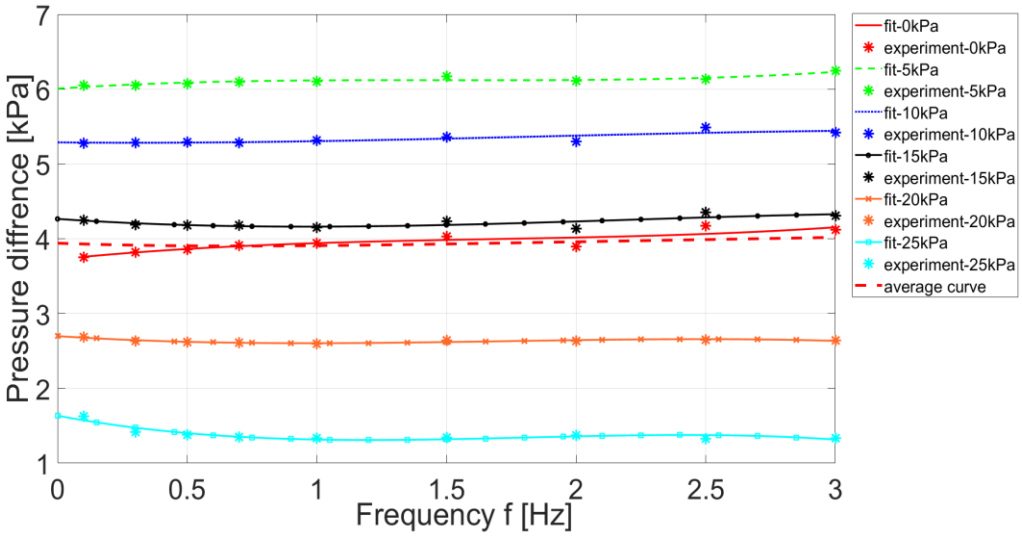

Figure 3.50. Original PSE - constant stiffness mode

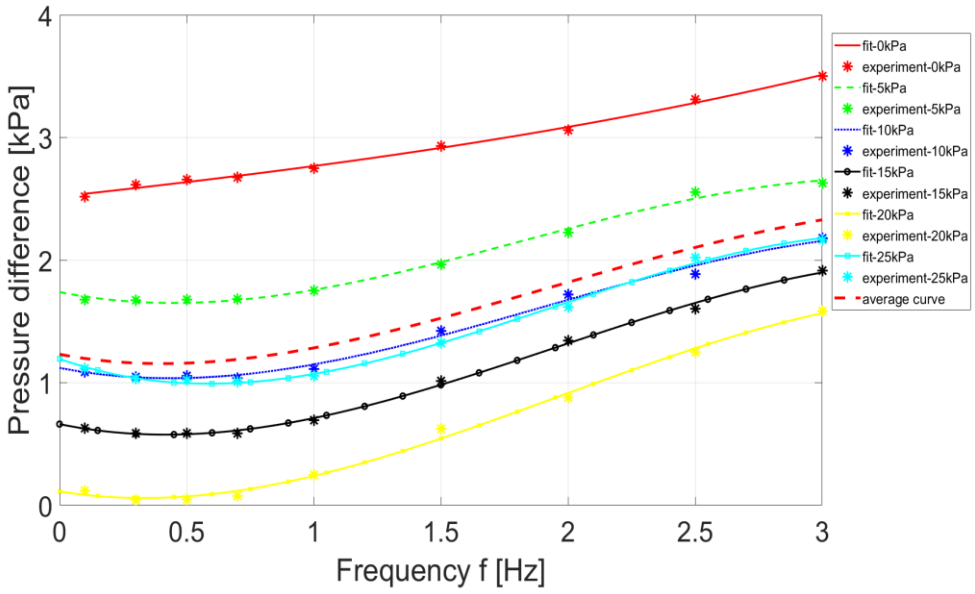

Figure 3.51. Improved PSE - constant stiffness mode

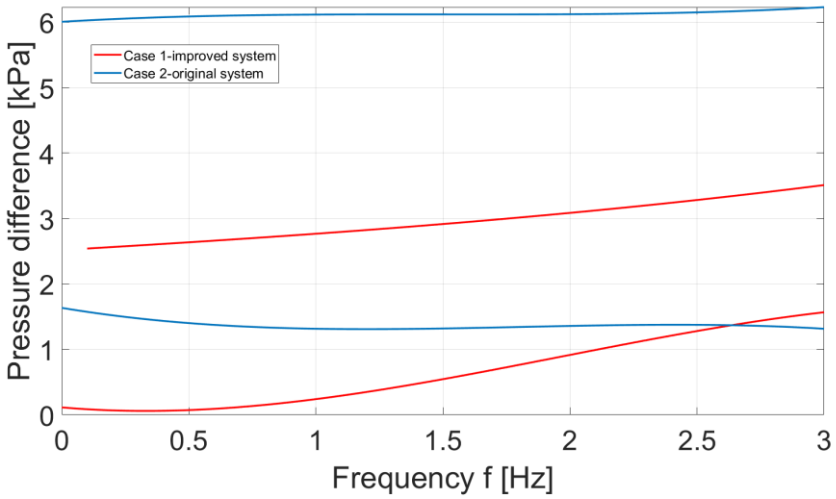

Figure 3.52. Envelope curves of pressure difference – frequency relation in constant stiffness mode

3.3.2.2. Under dynamic conditions

Under dynamic conditions there are two types of experiment. The first one is measurement of pressure response inside the PSE under harmonic excitation and the second one is experiment for calculation of transmission of acceleration.

The experiments are carried out with the machine Instron E3000. A loading mass (10 kg) is placed at the top of the foam block (100x100x50 mm^3) with a PSE inserted in the middle. The foam block is located in a cage attached to the upper movable platform of the machine (see Fig 3.53). The

motion of this cage determines the excitation of the system. Two accelerometers (acc1 and acc2) are attached to the cage and to the mass. This experiment is carried out with the original and improved systems.

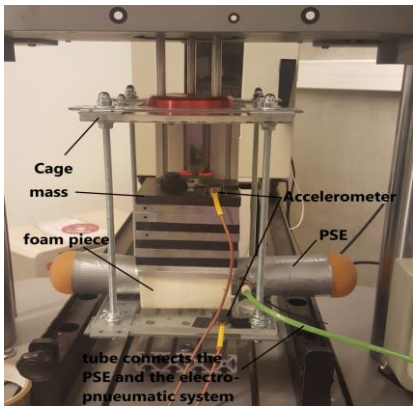

a) The setup in reality

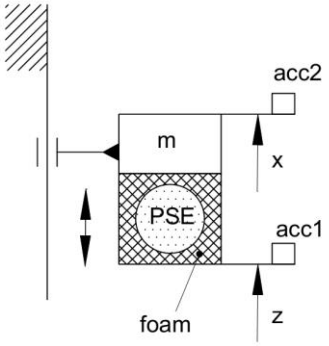

b) Scheme of experimental setup

Figure 3.53.Setup of the experiment performed under dynamic conditions

In the case of measurement of pressure response in the PSE under harmonic excitation with exciting frequency in the range [0,3] Hz the motion of the cage is given by a sine function:

$$z(t) = A\sin(2\pi . ft)\ [\text{mm}]$$

where

A is the exciting amplitude and f is the exciting frequency.

Fig 3.54 shows the pressure response in the case of using the original system and improved system under the excitation with A=10 m and f=0.1 Hz and the desired pressure set to 20 kPa. The results show a better quality of regulation of pressure when using the improved system.

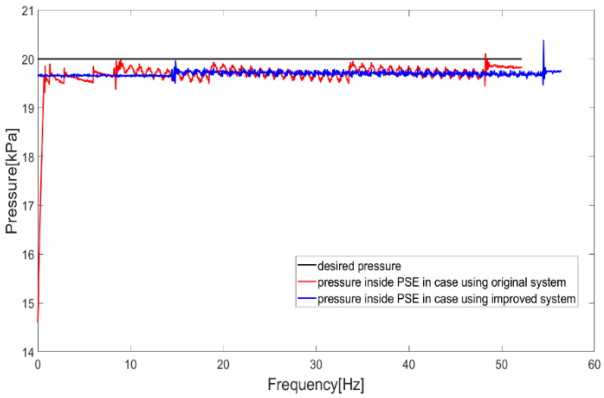

Figure 3.54. Experimental pressure response under excitation with frequency f=0.1 Hz and amplitude A=10 mm

The experiments were performed with exciting frequency *f* in range [0,3] Hz with values of 0.1, 0.3, 0.5, 0.7, 1, 1.5, 2, 2.5, 3 Hz. In the case of the constant pressure mode the data from results were used for presentation of the relationship of pressure error depending on the exciting frequency and desired pressure (see Fig 3.55 and Fig 3.56). From these figures we can recognize that replacement of the original system by the improved system causes the maximum value of the pressure error to decrease from 4 kPa to 2.6 kPa at 3 Hz of the exciting frequency.

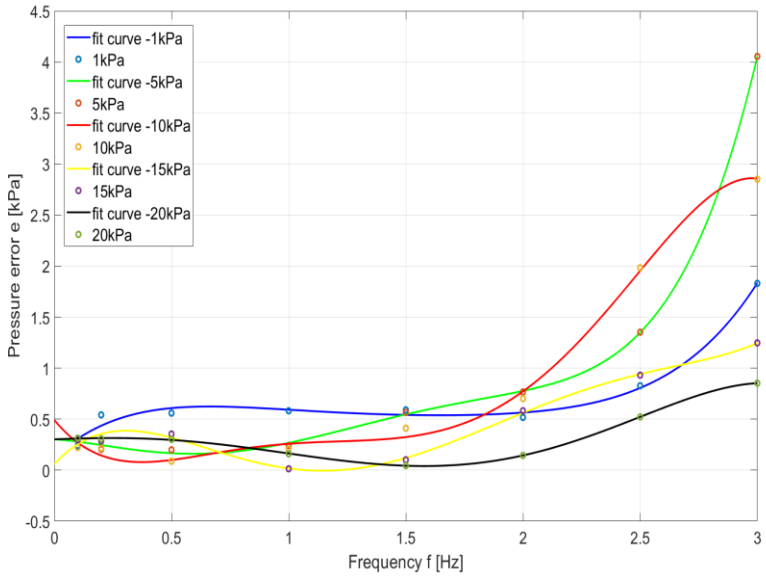

Figure 3.55. Pressure error - exciting frequency diagram in the case of using original system (constat pressure mode)

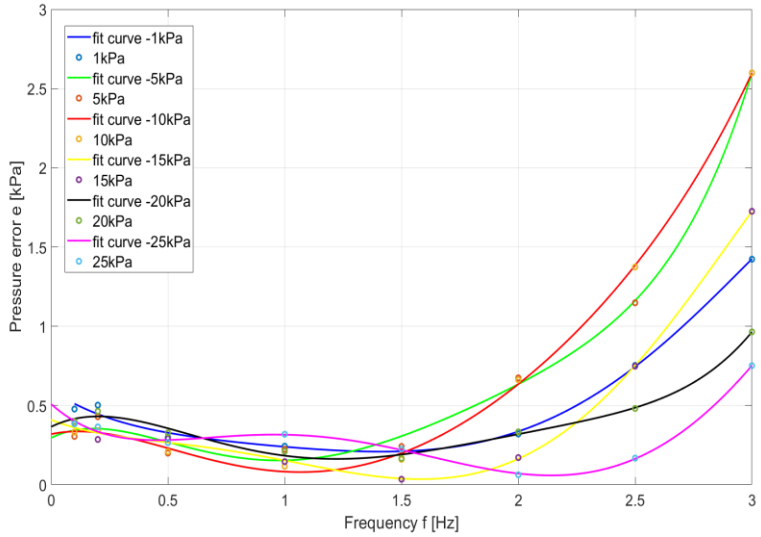

Figure 3.56. Pressure error - exciting frequency diagram in the case of using improved system (constant pressure mode)

In the case of calculation of transmission of acceleration the excitation function [18] is used for dynamic experiments in the form :

$$z(t) = Z_a (t + t_0)^{2(1-n)} \sin\left(c(t + t_0)^n\right)$$

with desired frequency changing in the range [1, 11] Hz and the constant acceleration amplitude of 0.1g. At the same time, frequency variation is slow enough to sufficiently excite response of the system close to the resonance frequency. The advantage of this function is the convenient calculation of the transmission of acceleration in the frequency range. The pressure inside the PSE is measured and recorded directly by the Labview program.

The transmission of acceleration is calculated as a ratio of output and input acceleration (acc2, acc1). The experimental results are shown from Fig 3.57 to Fig 3.60**.**

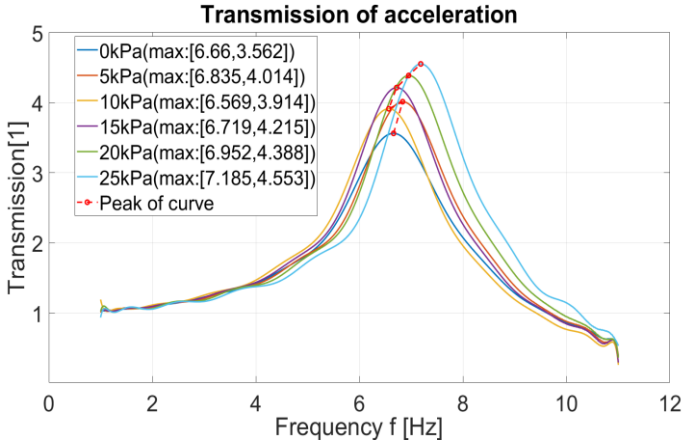

Figure 3.57. Original system - constant pressure mode

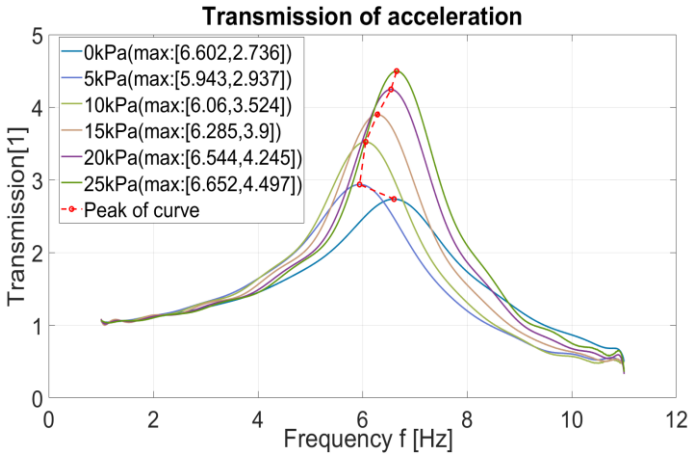

Figure 3.58. Original system - constant stiffness mode

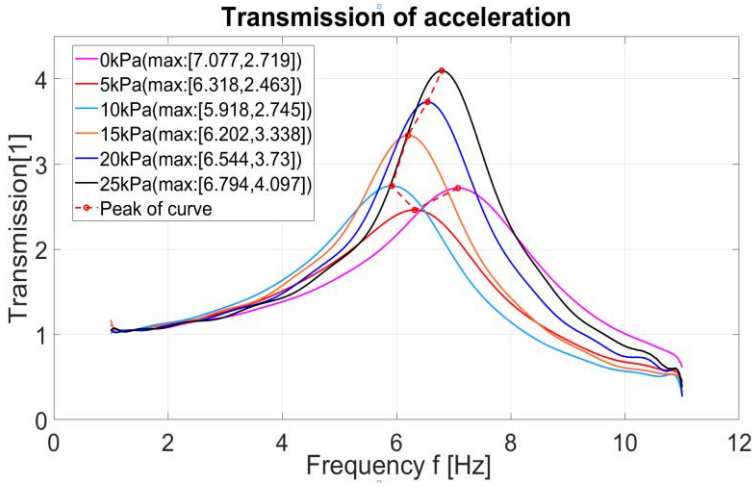

Figure 3.59. Improved system - constant pressure mode

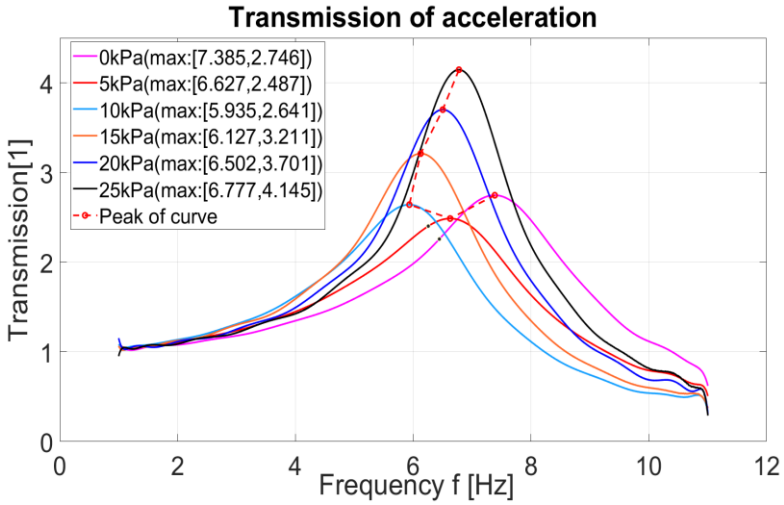

Figure 3.60. Improved system - constant stiffness mode

In the case of using the original system in constant pressure mode the transmission curve corresponding to the desired pressure 5 kPa has a peak higher than the transmission curve corresponding to the desired pressure 10 kPa (Fig 3.57). In case this system is working in constant stiffness mode the transmission curve corresponding to the desired pressure 0 kPa has a peak at a slightly further frequency than the transmission curve corresponding to the desired pressure 5 kPa (Fig 3.59). For the improved system this deviation also occurs in transmission lines of two cases where the desired pressure is 0 and 5 kPa respectively (Fig 3.58 and Fig 3.60). However, despite these irregularities the general trend can be observed: we can see that the behavior of transmission curves shows the shift of the peak position towards the higher frequency when the desired pressure increases and the peak value increases as well. With a load of 10 kg, these peaks are positioned in the range of [6,8] Hz. Peak values are in range [3.6, 4.6] for the original system in constant pressure mode and in range [2.4, 4.1] for the improved system in the same mode. Peak values are in range

[2.7, 4.5] for the original system in constant stiffness mode and in range [2.5, 4.1] for the improved system in the same mode. Thus the results show that the peak values of the transmission curves are smaller when the improved system is used.

3.4. Conclusion

The first part of this chapter presents a derivation of the simulation model of the original system and the improved system. Numerical calculation gives detailed results of behavior of characteristics of systems in chosen control modes (constant pressure, constant stiffness) under static conditions or dynamic conditions. The second part focuses on experiments which were made under the same or similar conditions as in case of numerical simulations. The results were used for comparison of original and improved system. Both systems were compared from the point of view of quality of pressure regulation and transmission of acceleration.

The results of calculations and experiments show that the improved system obviously brings positive effects. Under the static conditions the quality of regulation in constant pressure mode is assessed by pressure error. The pressure error is considered in the time domain (without external load) and in the frequency domain (with dynamic external load). The improved system in constant pressure mode always shows a higher regulation quality than the original system. Under the dynamic conditions the regulation quality is evaluated by transmission of acceleration. For both systems, original and improved ones, the transmission of acceleration shows the same tendency to shift the peak position toward the higher frequency when the desired pressure increases. This frequency shift is followed by simultaneous increase in peak value. However the improved system brings the reduction of peak values. This is an important implication of improvement considering the comfort of a sitting person.

4. Finite element analysis using MSC. Marc software

In this application the PSE is inserted into a car seat cushion to adjust the contact pressure distribution. The question is how the PSE influences the contact pressure distribution. In recent years the finite element method has emerged as a viable solution of this type of problem. For this purpose MSC.Marc software is used.

In this chapter a finite element model of interaction of a car seat cushion with the PSE inserted inside and a simplified model of the human body has been developed and used for investigation of the contact pressure distribution under static conditions.

Because the model consists of many parts with complex shapes and is made of materials with large deformations the finite element analysis of the system was broken down into several steps as follows:

- ✓ Determination of suitable constitutive model of materials.
- ✓ Building and analyzing the model of interaction of the mechanical subsystem with the load (presented in chapter 3).
- ✓ Building and analyzing a model of a car seat cushion with a PSE inserted inside in interaction with a simplified model of the human body.
- ✓ Comparison of simulation results and experimental results.

In terms of material properties the foam is the compressible and isotropic material, while latex and tape are kinds of incompressible and isotropic materials. Experiments are carried out to determine the stress-strain curve of the materials. These curves are obtained from bulge test of latex membrane, uniaxial tensile test of the tape and uniaxial compression test of foam.

4.1. Finite element model of latex tube

4.1.1. Bulge test of latex membrane

For the investigation of the properties of the latex membrane the bulge test was used. The plane-strain bulge test is a technique for measuring the mechanical properties of thin membranes. In this technique the relationship between stress and strain is determined from the pressure-deformation behavior of a spherical membrane. The first use of the bulge test for investigation of mechanical properties of the thin membrane was reported by Beams [20]. He developed models for a spherical cap geometry and derived equations for different initial boundary conditions. Later this lead to the development of simple expressions for calculation of stress and strain in bulged membranes.

Fig 4.1 shows the setup of the experiment. In this experiment a square piece of latex membrane was cut from a latex tube and fixed on a device with a circular window. The window and the latex membrane are sealed by screws and by additional latex sealing so that it is possible to pump or release compressed air to deform the latex membrane. One displacement sensor OptoNCDT 1402 is fixed just above the latex membrane and its laser beam is focused on the center of the circular window. This sensor is used for measuring the displacement of the top point of the spherical cap. The pressure of air supplied inside the spherical cap of the latex membrane is measured by a pressure sensor.

The spherical cap geometry is shown in Fig 4.2, where p_m is the applied pressure, t_m is the membrane thickness, h_m is the height of the spherical cap, r_m is the radius of the spherical cap, R_w is the radius of the circular window.

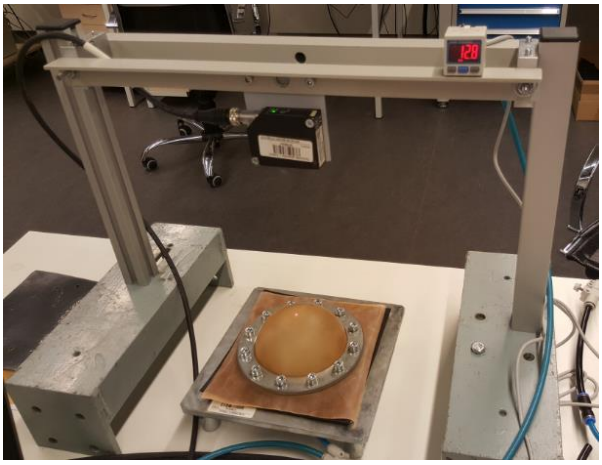

Figure 4.1. Experimental setup of the bulge test

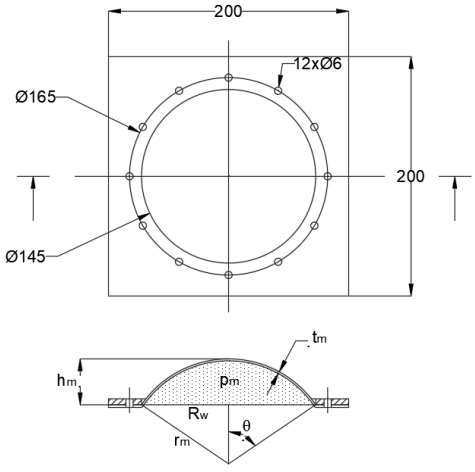

Figure 4.2. Spherical cap geometry and dimensions of the circular window

In accordance with [21] the stress σ_m in the spherical cap of the latex membrane can be expressed by the formula:

$$\sigma_m = \frac{p_m r_m}{2t_m} \tag{4.1}$$

The thickness t_m is given by equation [20]:

$$t_m = t_{m0}\lambda_3 = \frac{t_{m0}}{\lambda^2} \tag{4.2}$$

where t_{m0} is the initial thickness of the membrane.

From the geometry of the deformed membrane the radius r_m and angle θ are presented by:

$$r_m = \frac{h_m}{2} + \frac{R_m^2}{2h_m} \tag{4.3}$$

$$\theta = \arcsin\left(\frac{R_m}{r_m}\right) \tag{4.4}$$

In this case the engineering strain λ is derived by:

$$\lambda = \frac{l_m}{l_{m0}} = \frac{r_m\theta}{r_{m0}\theta_0} \tag{4.5}$$

where

l_{m0} is the initial length, l_m is the instantaneous length of the meridian curve of the deformed membrane, r_{m0}, θ_0 is the initial value of radius r_m and angle θ, respectively.

Spherical cap geometry is used for stress and strain calculation of the membrane.

From the experiment the obtained result is a relationship between deformation and pressure which is determined by $h_m=h_m(p_m)$.

There are two types of latex membranes with different thicknesses. The first type with thickness of 0.65 mm is used in latex tube in the original PSE. The second type 1.6 mm thick is used for the additional latex tube in the improved PSE.

The deformation–pressure response of the first type of latex is shown in Fig 4.3. It represents the curves the process of inflating (blue) and deflating (red). The data used for calculation of the strain –stress response is the average of the inflation path and the deflation path. Then the experimental strain-stress response is calculated and shown in Fig 4.4. This data is used as the input for the

experimental data fit function in the MSC.Marc software. This function generates a fit engineering stress-strain curve and coefficients of chosen constitutive model (2-term Ogden model) automatically. Fig 4.5 shows the fit stress-strain curve (the red curve) and the experimental stress-strain curve (the blue curve).

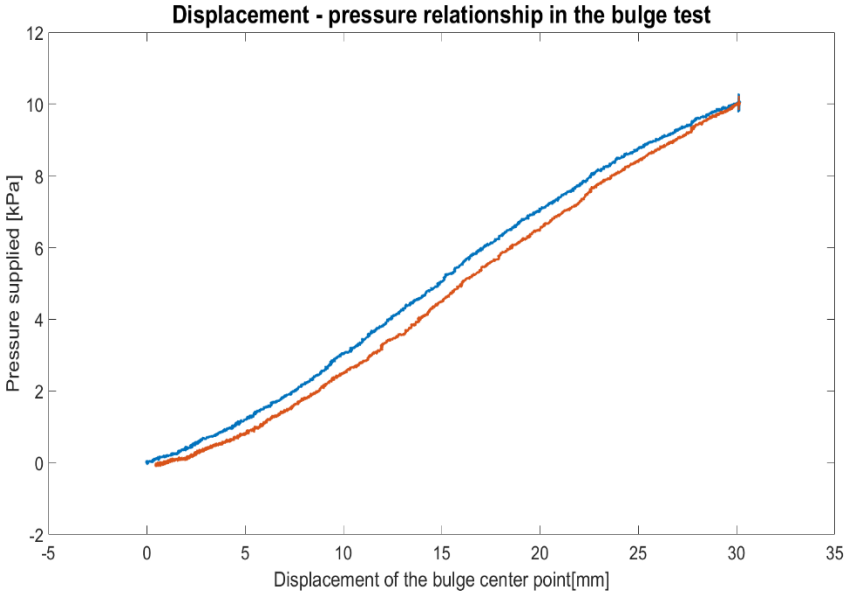

Figure 4.3. Deformation-pressure diagram of the bulge test in case of 0.65 mm thickness

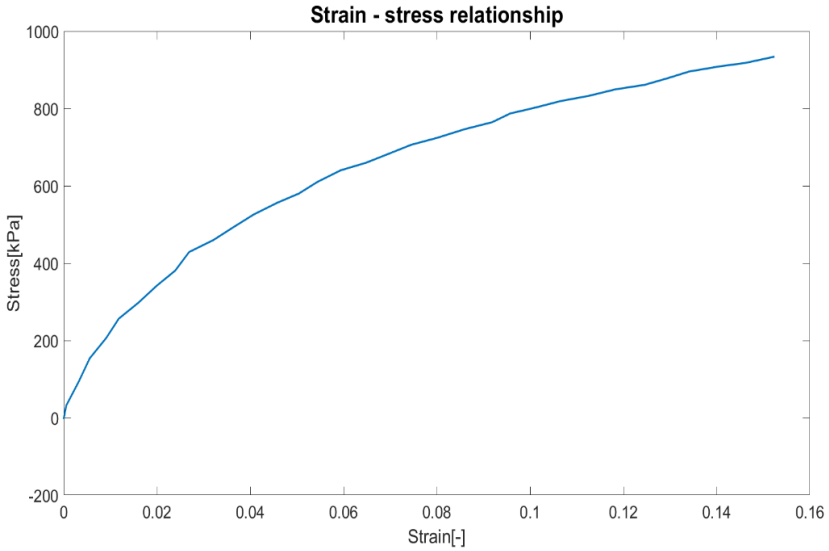

Figure 4.4. Strain-stress diagram of the bulge test in case of 0.6 mm thickness

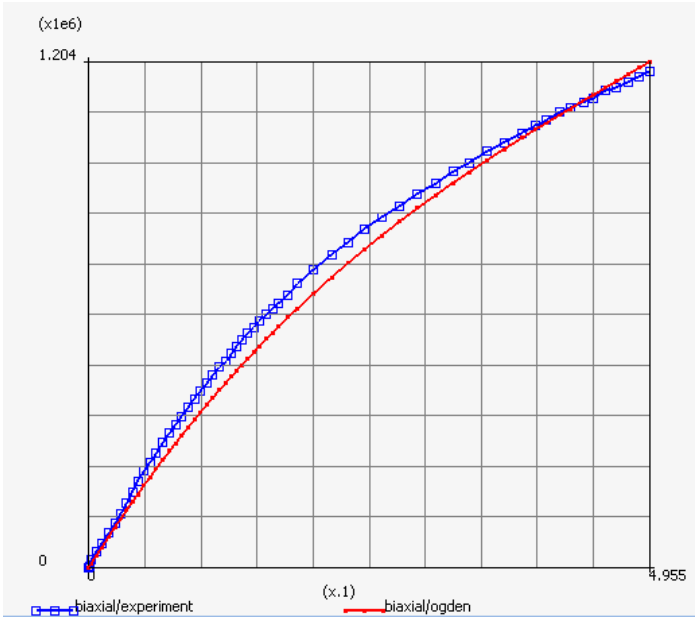

Figure 4.5. Experimental (blue) and fit stress-strain (red) curves of the latex membrane (thickness 0.65 mm)

Similarly we get results for the second type of latex. Fig 4.6, Fig 4.7 and Fig 4.8 show the deformation–pressure response, the experimental strain-stress response and the comparison between fit stress-strain curve (the red curve) and the experimental stress-strain curve (the green curve).

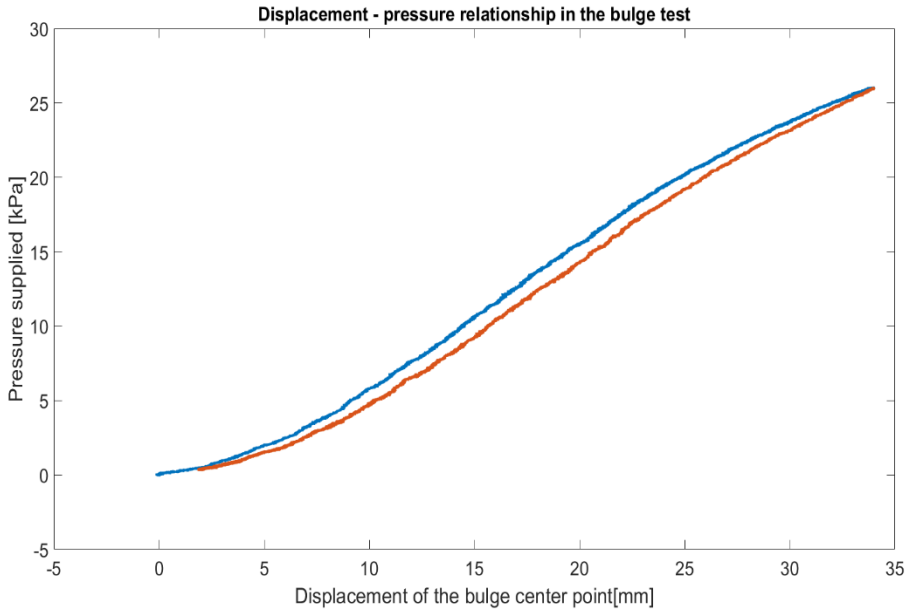

Figure 4.6. Deformation-pressure diagram of the bulge test of the latex membrane 1.65 mm thickness (inflating – blue, deflating - red)

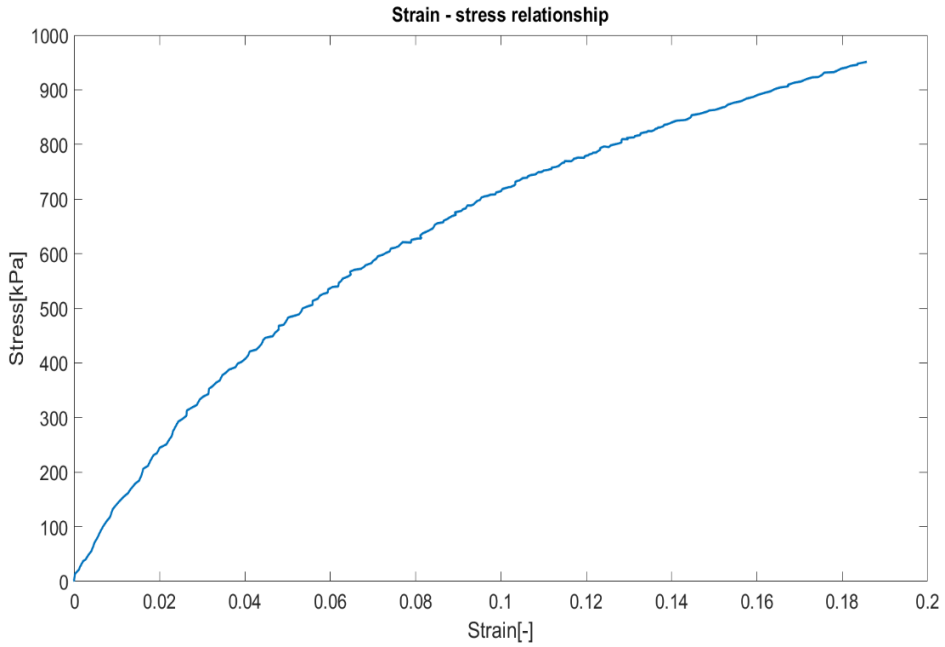

Figure 4.7. Strain-stress diagram of the latex membrane (thickness 1.65 mm)

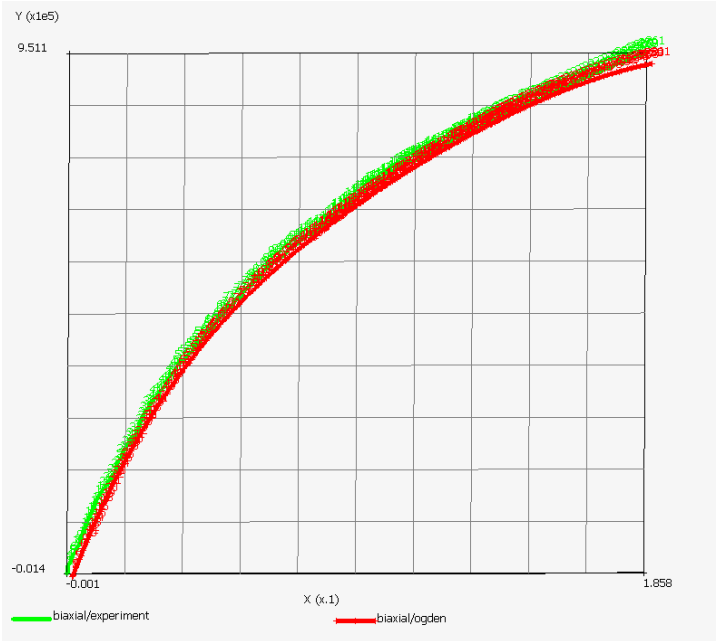

Figure 4.8. Experimental (green) and fit stress-strain (red) curves of the latex membrane (1.65 mm thickness)

4.1.2. Constitutive model

According to [22] the material model for latex can be defined by a stored energy function as hyperelastic material. Conventional hyperelastic material models such as the Ogden model work very well for latex. Ogden designed the energy function as a separable function of principal stretch in the generalized form:

$$W = \sum_{n=1}^{N} \frac{\mu_n}{\alpha_n}\left[\left(\lambda_1^{\alpha_n} + \lambda_2^{\alpha_n} + \lambda_3^{\alpha_n}\right) - 3\right] + 4,5K\left(J^{\frac{1}{3}} - 1\right)^2 \qquad (4.6)$$

where

μ_n and α_n are material constants, *K* is the initial bulk modulus, *J* is the volumetric ratio, defined as $J = \lambda_1^2\lambda_2^2\lambda_3^2$. Under consideration of incompressible material (*J=1*) and Ogden model selection for latex, we can use a 3-term formulation with engineering stress- engineering strain curve for biaxial mode with engineering strain $\lambda_1 = \lambda_2 = \lambda, \lambda_3 = \lambda^{-2}$ [23], thus:

$$W = \sum_{n=1}^{3} \frac{\mu_n}{\alpha_n}\left[\left(2\lambda^{\alpha_n} + \lambda^{-2\alpha_n}\right) - 3\right] \qquad (4.7)$$

According to [23], in the material fitting data option in MSC.Marc the biaxial deformation mode is selected. The software automatically calculates results as follows.

For the case of the latex membrane (thickness 0.65 mm) the set of coefficients is:

$\mu_1 = 1.21738\times10^8\ Pa$ $\mu_2 = 7.7123\times10^6 Pa$ $\mu_3 = 117.45\ Pa$

$\alpha_1 = 0.0110147$ $\alpha_2 = 0.0123274$ $\alpha_3 = 15.898$

K=3.5946×10^9

And for case of latex membrane (thickness 1.65 mm) the set of coefficients is:

$\mu_1 = 321385\,Pa$ $\mu_2 = 644492\,Pa$ $\mu_3 = 85164.5\ Pa$

$\alpha_1 =$ -6.69652 $\alpha_2 = 10.8952$ $\alpha_3 = 1.14959$

K=2.31789×10^{10}

4.1.3. Simulation results

The simulation of the bulge test of latex membrane (see Fig 4.9) is performed under the consideration of the same boundary and initial conditions as they were used in the bulge test. The simulation of deformation of latex tube loaded by internal pressure 25 kPa is shown in Fig 4.10.

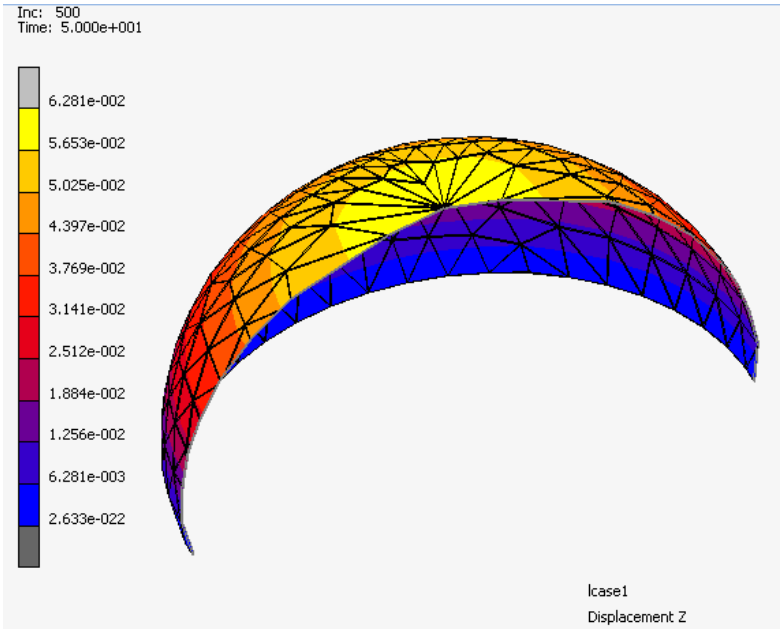

Figure 4.9. Simulation of the latex membrane in the bulge test (Displacement z [m])

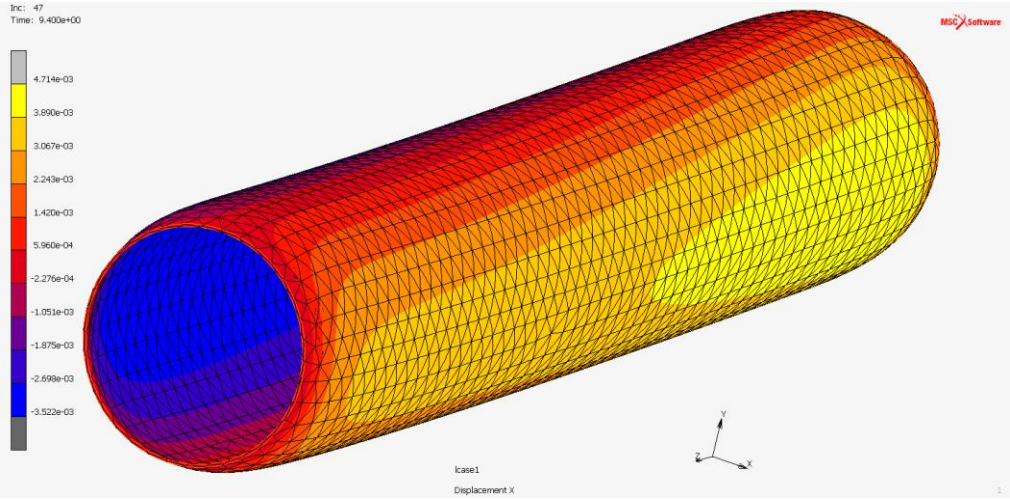

Figure 4.10. Simulation of the bulged latex tube at 25 kPa of internal pressure (Displacement x [m])

4.2. Finite element model of tape

4.2.1. Uniaxial tensile test of the tape

The specimen of the tape was 0.16 mm thick, 48 mm wide and 220 mm long. The uniaxial tensile test was carried out by Tira test 2810 machine shown in Fig 4.11. The force - tensile deformation response is shown in Fig 4.12. The comparison of fit stress-strain curve by using the experimental data fit function and the experimental stress-strain curve is shown in Fig 4.14.

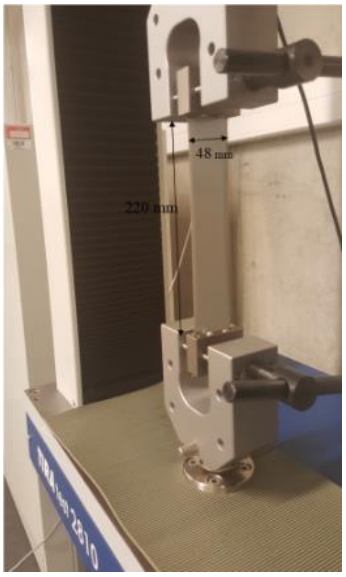

Figure 4.11. The setup of the tensile test

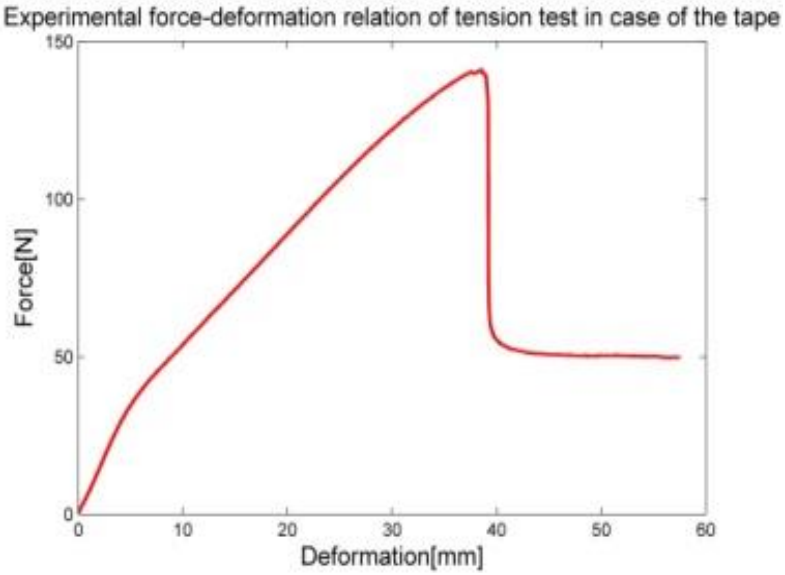

Figure 4.12. Force – deformation diagram of the tensile test of the tape

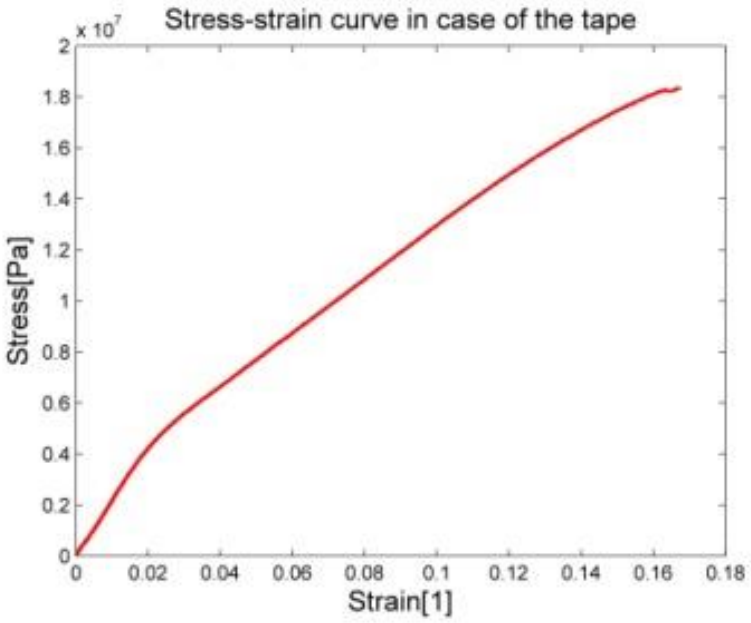

Figure 4.13. Stress-strain diagram of the tensile test of the tape

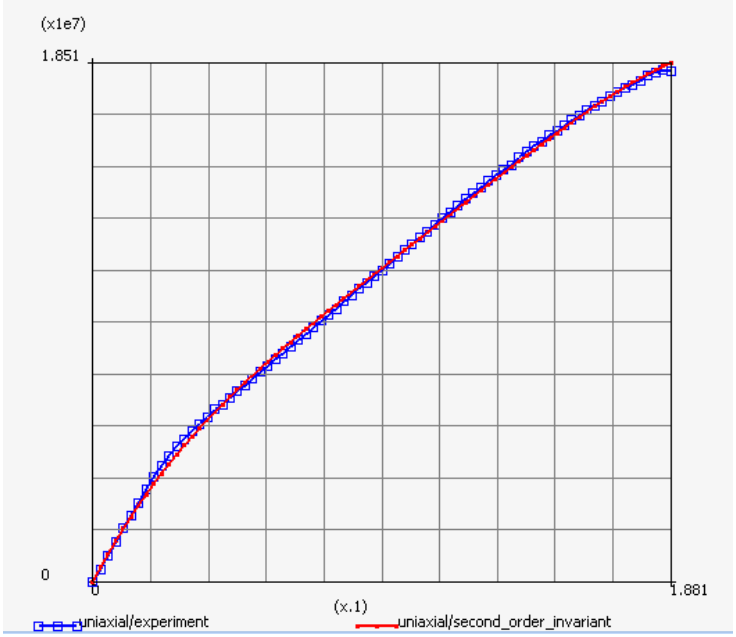

Figure 4.14. Experimental (blue) and fit stress-strain (red) curves of the tensile test of the tape

4.2.2. Constitutive model

The Mooney-Rivlin material model is used for the tape in form [23]:

$$W = C_{10}\left(I_1 - 3\right) + C_{01}\left(I_2 - 3\right) + C_{11}\left(I_1 - 3\right)\left(I_2 - 3\right) + C_{20}\left(I_1 - 3\right)^2 \tag{4.8}$$

For the case of uniaxial extension the engineering strains are $\lambda_1 = \lambda, \lambda_2 = \lambda_3 = \lambda^{-2}$ [22]. Hence:

$$I_1 = \lambda^2 + \frac{2}{\lambda} \qquad I_2 = 2\lambda + \frac{2}{\lambda^2} \tag{4.9}$$

The results obtained from material fitting data option are as follows:

C_{10} = -2.55107×10^8 C_{01} = 2.9003×10^8 C_{11} = 1.18362×10^8 C_{20} = -8.66098×10^8

4.2.3. Simulation result

The simulation of the tensile test of tape in MSC.Marc software is performed under the consideration of the same boundary and initial conditions as it was used for the experimental tensile test of the tape.

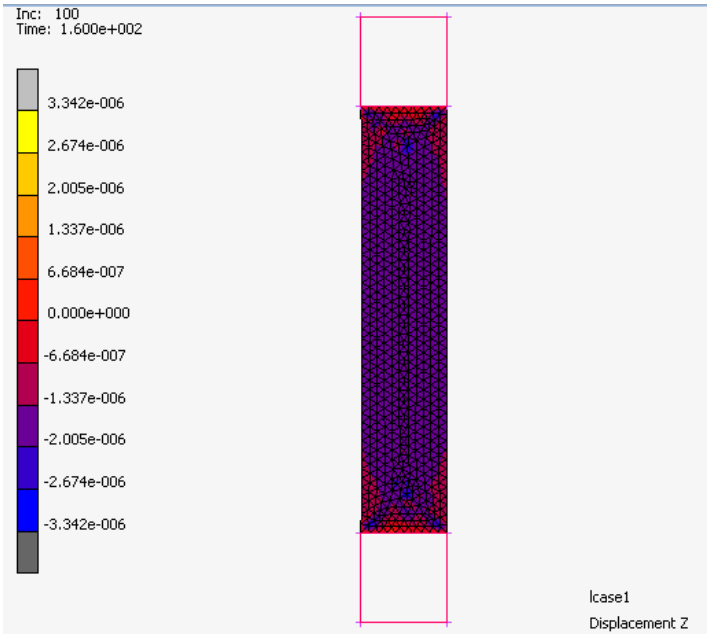

Figure 4.15. Simulated extension [m] of the tape in the tensile test

The results in Fig 4.16 show a good correspondence of experiment and simulation.

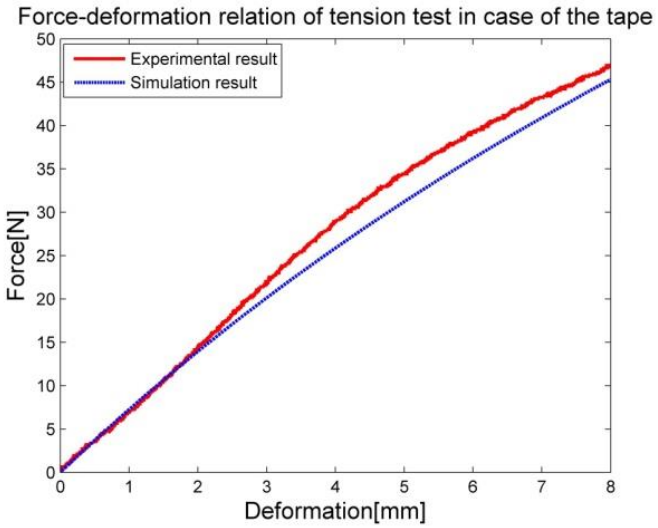

Figure 4.16. Simulated and experimental force-displacement diagram of the tensile test of the tape

4.3. Finite element model of foam

4.3.1. Uniaxial compression test of foam

The stress-strain behavior of foam in a state of uniaxial (one-dimensional) stress was obtained by a compression test. The strain energy function of finite hyperelasticity of compressible media is used to describe the elastic properties of open-cell soft foams. To determine the constitutive phenomenological material model the experimental data from a uniaxial compression test is used. The tested specimen was taken from a car seat cushioning of dimensions 100x100x80mm. The tests were conducted using an Instron loading machine. Fig 4.17 shows the experimental setup. The test was carried out under displacement control at a constant loading rate of 1 mm/min up to a given deformation of 60 mm.

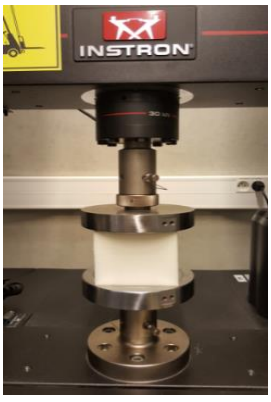

Figure 4.17. The experimental setup of the compression test of foam

The result of the compressible deformation-force relationship is shown in Fig 4.18.

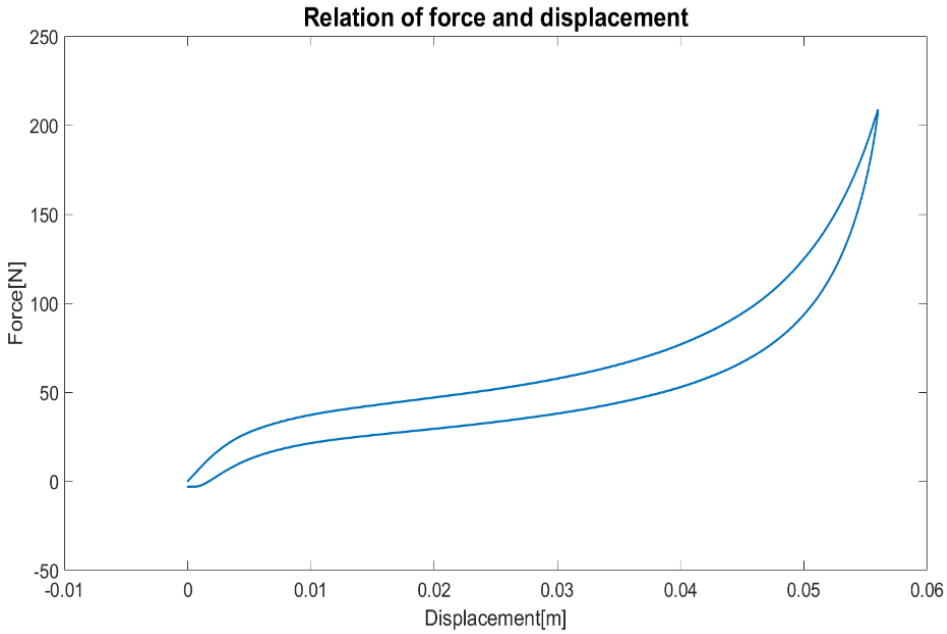

Figure 4.18. Deformation-force diagram of the compression test

The stress-strain data is calculated using Matlab software and is shown in Fig 4.19.

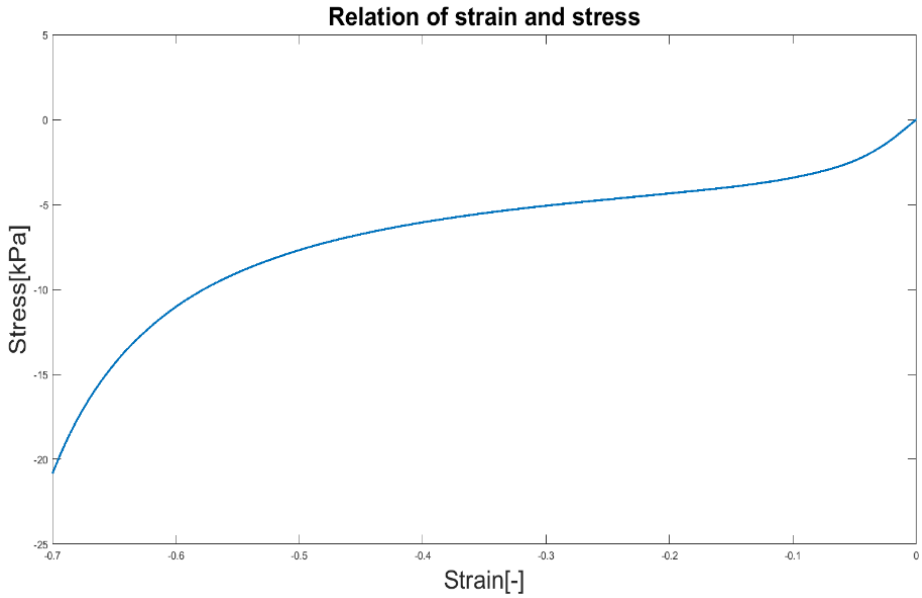

Figure 4.19. Stress-strain diagram of the foam

4.3.2. Constitutive model

In accordance with [24] the foam is considered as compressible material and the suitable material model is represented by function:

$$W = \sum_{n=1}^{N} \frac{\mu_n}{\alpha_n}\left[\left(\lambda_1^{\alpha_n} + \lambda_2^{\alpha_n} + \lambda_3^{\alpha_n}\right) - 3\right] + \sum_{n=1}^{N} \frac{\mu_n}{\alpha_n}\left(I - J^{\beta_n}\right) \tag{4.10}$$

where $\mu_n, \alpha_n \; and \; \beta_n$ are material constants. The second term of this function represents volumetric change, *J* is the Jacobian measuring dilatancy defined as the determinant of deformation gradient *f* ($f = \frac{\partial x}{\partial X}$, where *x* and *X* refer to the deformed and original coordinates of the body) with $\lambda_1 = 1, \lambda_2 = 1, \lambda_3 = \frac{L}{L_0}$. For this deformation state we have: $\lambda_1\lambda_2\lambda_3 = \frac{L}{L_0} = \frac{V}{V_0}$.

In the material fitting data option the uniaxial deformation mode was selected with the value of fictive Poison's ratio 0.01. The material model is Foam with 2 terms (*n*=2) with results obtained as follows:

$\mu_1 = 3.2 \times 10^6 \; Pa \quad \alpha_1 = 0.00157295 \quad \beta_1 = 1.19689 \times 10^{-5}$
$\mu_2 = 4058.48 \; Pa \quad \alpha_2 = 22.9999 \quad \beta_2 = 1.23469$

4.3.3. Viscoelastic properties

The response of viscoelasticity models depends on deformation and on rate of deformation. The behavior becomes time-dependent and typical phenomenon associated with this behavior is relaxation. Relaxation is the diminishing of stress at constant deformation level (Fig 4.20).

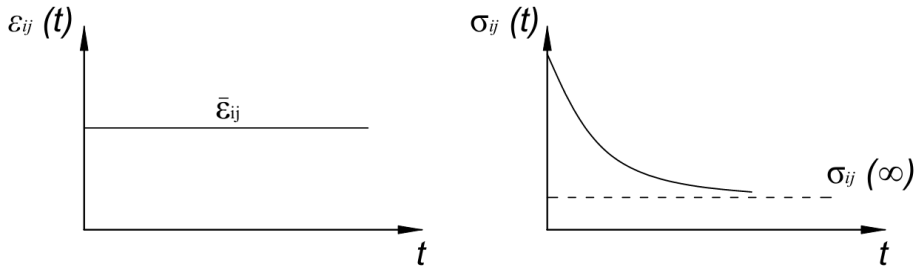

Figure 4.20. Relaxation behavior

To model a viscoelastic foam under an uniaxial stress deformation mode an experiment was carried out. Foam specimens of dimensions 100x100x80 mm were compressed and hold at a certain value of strain for a long time. Stress relaxation test data was obtained with 5%, 10%, 15%, 20%, 25%, …, 70% strain which was kept constant for time period of 1800 seconds. For the sake of completeness the sets of stress relaxation test data are shown in Fig 4.21.

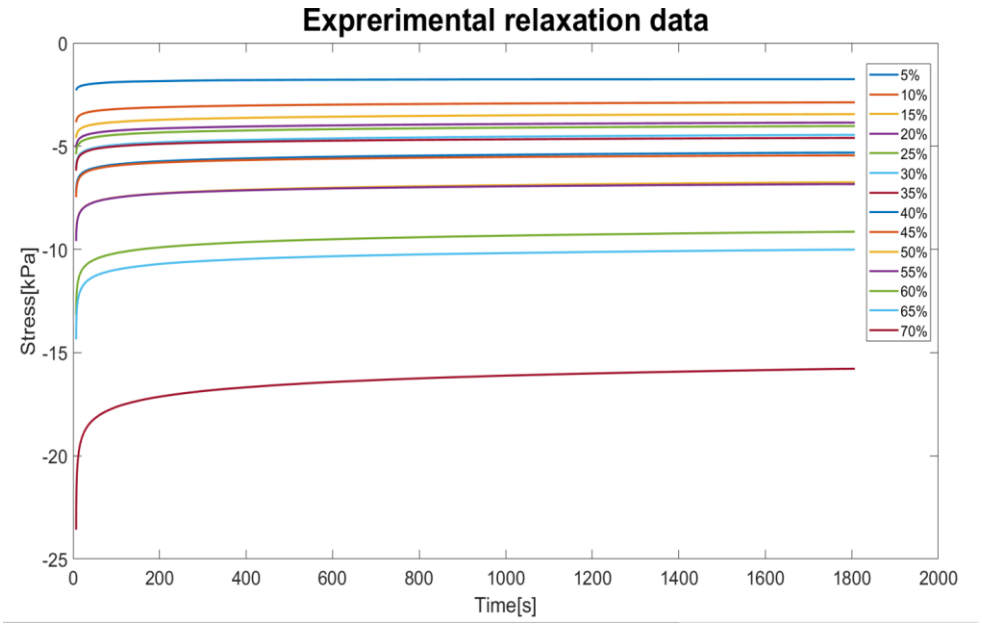

Figure 4.21. Relaxation data from the experiment

Using experimental data fit menu we found the coefficients and got the fit with the function order set to 9 of terms in the Prony series. Relaxation function of time domain Prony series is represented by:

$$S(t) = S^{(\infty)} + \sum_{k=1}^{N_D} S^{(k)} e^{-\frac{t}{\tau_k}} \tag{4.11}$$

where:

S(t) is the time dependent strain energy function,

$S^{(\infty)}$ is the infinity relaxation modulus,

N_D is the order of the Prony series,

τ_k is the relaxation time of Prony term k,

$S^{(k)}$ is the Prony coefficients.

The coefficients generated are shown below:

Term k	Relaxation time τ_k	Prony coefficients S^k
1	0.733073	0.0181693
2	0.799137	0.0725529
3	6.81538	0.0914753
4	10.2102	0.0695494
5	17.0064	0.00251894
6	251.667	0.0251244
7	8890.97	0.00165894
8	16063.3	0.14635
9	17171.8	0.000349927

4.3.4. Comparison of experimental result and simulation result

Result of experimental (green) and fit stress-strain (blue) curves of the compression test are shown in Fig 4.22.

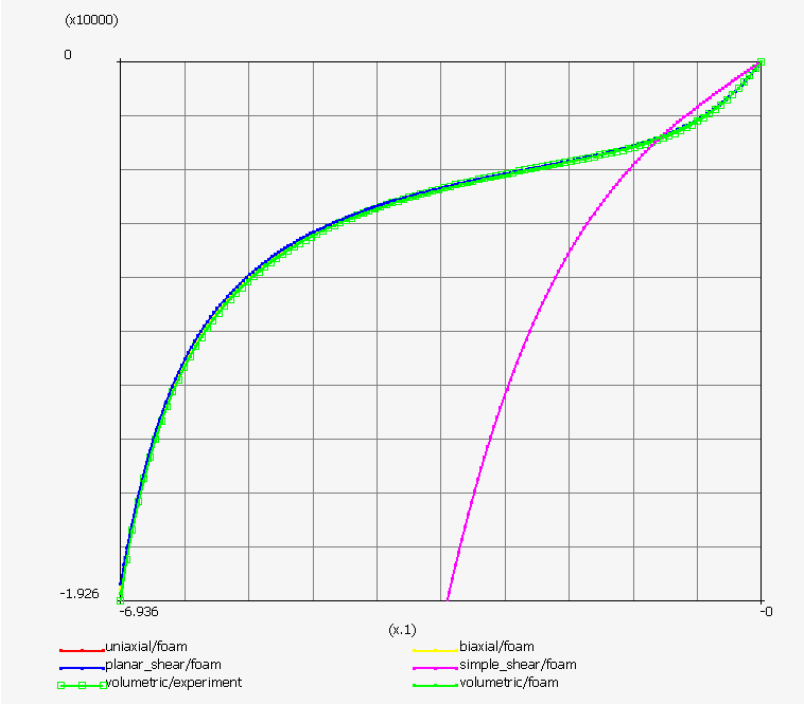

Figure 4.22. Experimental (green square) and fit (plain green) stress-strain curves of the compression test of foam

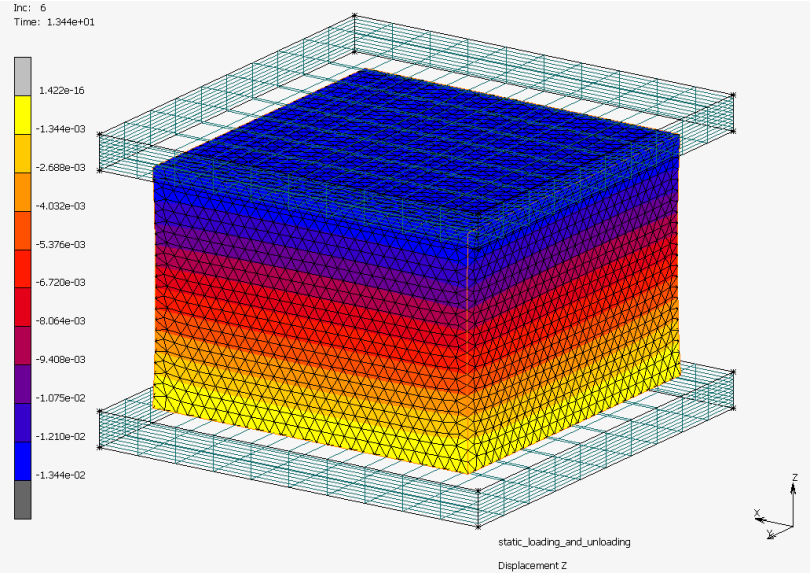

Figure 4.23. The simulation of compression test of foam in Marc (Displacement z [m])

The simulation is performed with the same boundary and initial conditions as they were used for experiments (see Fig 4.23). The results of force-displacement relationship in Fig 4.24 show acceptable correspondence of experiment and simulation.

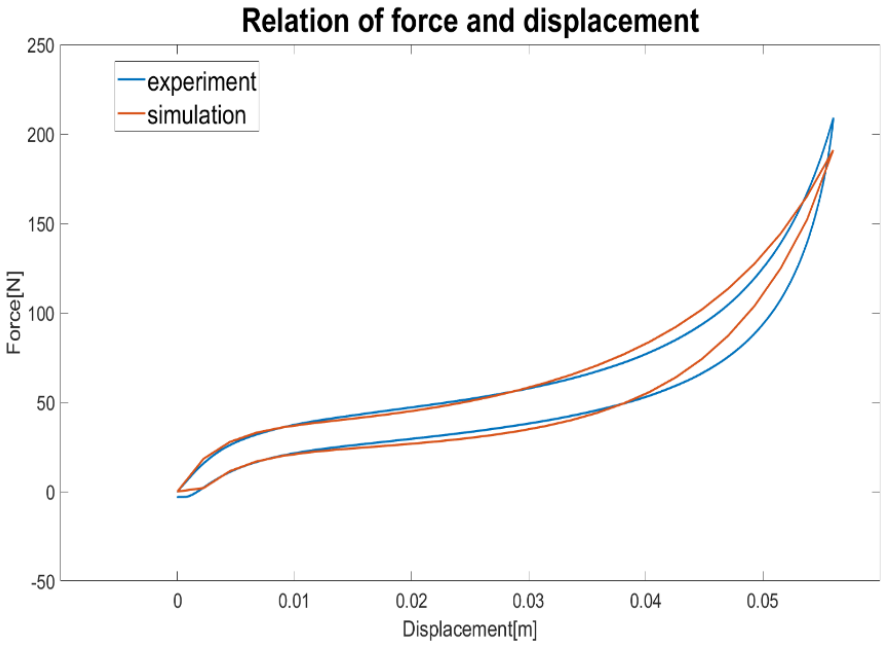

Figure 4.24. Force – displacement diagram from experiment and simulation

4.4. Finite element analysis of the models of compression test

4.4.1. Models of compression test

Two models were created. The first one corresponds to the model which is used in the compression test of a foam block with a PSE inserted inside under static conditions and presented in chapter 3, the second one corresponds to the model used in the car seat cushion.

The first model is used for the investigation of contact force between the model and load. The model consists of an original PSE and a foam block of 100x100x80 mm, as shown in Fig 4.25. The model is symmetrical so it is half-built to reduce computation time. The model is meshed using 11195 four-node tetrahedral elements and includes 4540 elements of the foam block, 994 elements of the tape cover layer, 4242 elements of the latex tube and 1470 elements of the foam. The material models previously verified in sections 4.1, 4.2 and 4.3 are used.

a) In reality b) In simulation

Figure 4.25. The first model used for the compression test

The second model comprises the foam brick which is cut out of a car seat cushion. It covers most of the PSE except its two free ends. The ends of the PSE are supported by a steel plate (see Fig 4.26). The steel plate is a part of construction and limits the inflation of the two ends of the PSE i at high pressure. The scheme of the model is shown in Fig 4.27. The foam brick is meshed using 19344 four-node tetrahedral elements and the steel plate is a solid body.

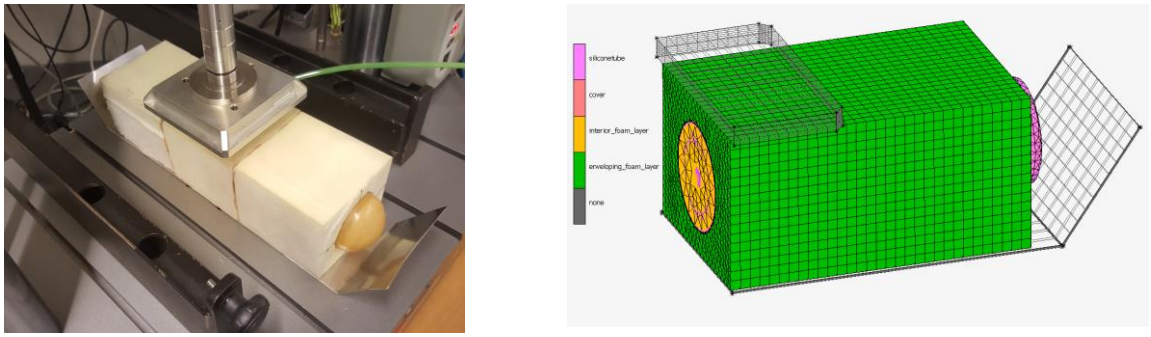

a) In reality b) In simulation

Figure 4.26. The second model used in the car seat cushion

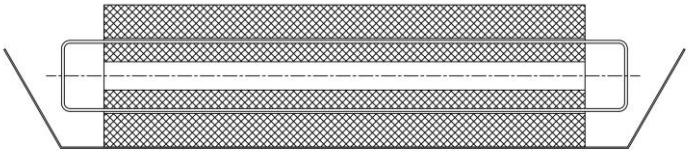

Figure 4.27. The scheme of the model used for car seat cushion

4.4.2. Contact friction problem

When the PSE is supplied with compressed air the latex tube stretches and bulges at both free ends and comes into contact with sloped parts of steel plate. For this purpose the friction coefficient between latex material of the spring and steel was experimentally investigated.

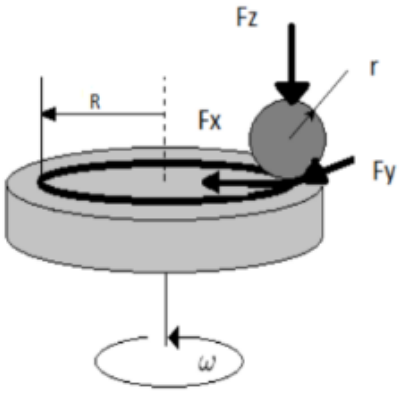

a) Principle of “ball on disc” tribometer

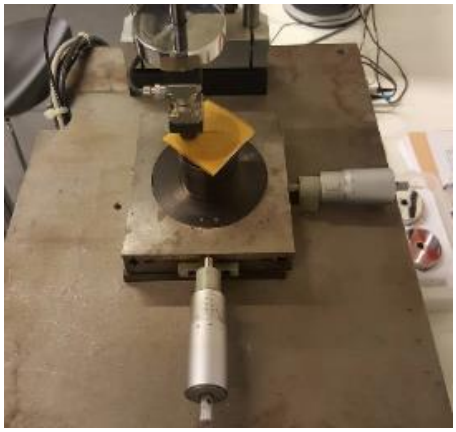

b) Experimental setup

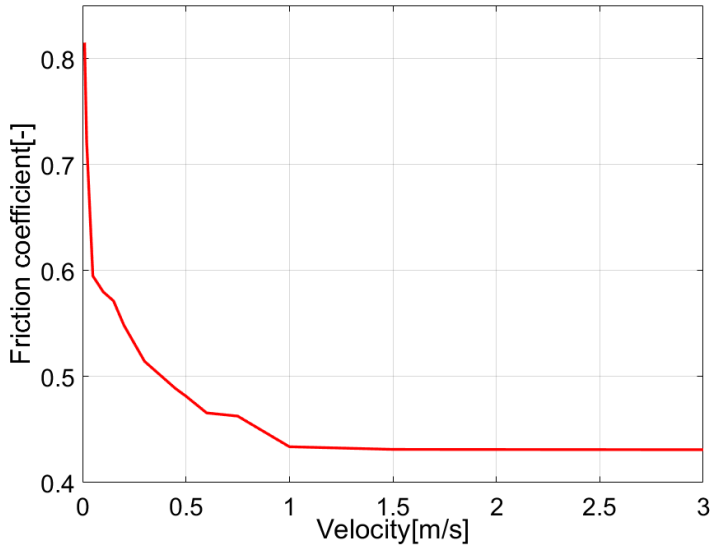

c) Dependence of friction coefficient on velocity

Figure 4.28. Determination of friction coefficient between steel and latex

According to [24] this experiment was carried out using a tribometer machine based on "ball on disc" principle as it is shown in Fig 4.28a and Fig 4.28b. The experiment was performed with a load F_z = 5 N and such combinations of the angular velocity of the disk ω_d and the radius R_d which ensure the range of tangential velocity from 0.01 m/s to 3 m/s. The radius of the steel ball was r_b = 3 mm. The measured value of the friction coefficient is presented in Fig 4.28c and shows obvious dependency on velocity up to 1 m/s. For higher velocity the friction coefficient keeps approximately constant value 0.43. For this simulation, the deformation speed of the latex membrane is considered very low so the chosen value of the friction coefficient between the latex tube and steel plate for the purpose of simulation is 0.8.

4.4.3. Simulation results and experimental results

The simulations were carried out for cases of internal pressure set to constant value 0 kPa, 5 kPa, 10 kPa, 15 kPa, 20 kPa and 25 kPa, respectively. In every case of internal pressure the external force is applied by the indentor which presses on the top of the foam block with displacement from 0 to 30mm. The indentor is located in the middle position concerning the longitudinal direction of the foam block. The course of displacement depending on time has a triangular shape with the rate of displacement of 2 mm/s.

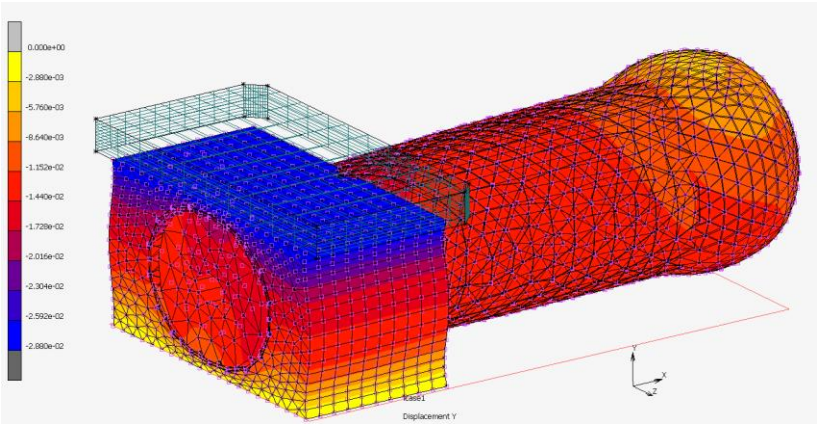

Figure 4.29. Simulation of model 1 with p_s = 20 kPa and displacement of the indentor at 30 mm (Displacement y [m])

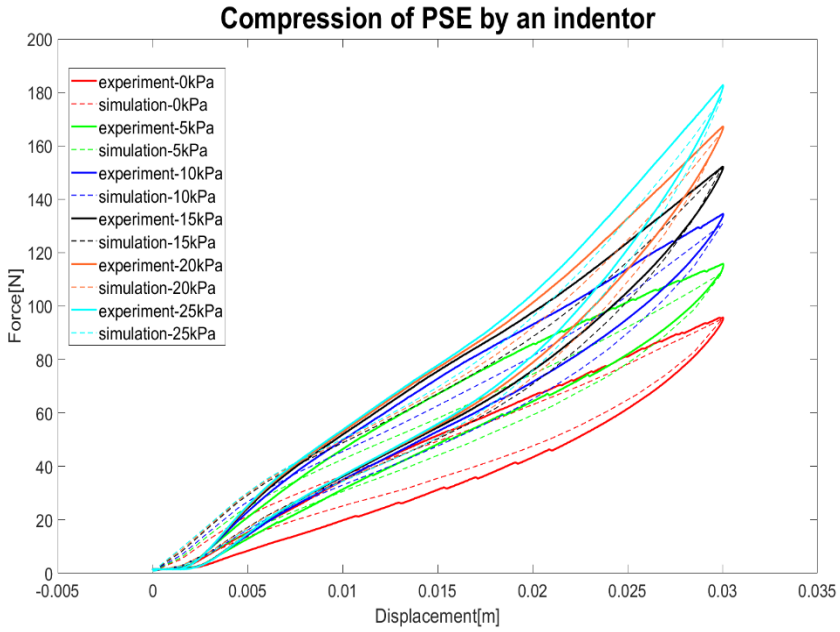

Figure 4.30. Force-displacement results of experiment and simulation (model 1)

Fig 4.29 shows the deformation in the first model of the compression test when internal pressure p_s is set to 20 kPa and displacement of the indentor is equal to 30 mm. The experimental results and simulation results of force-displacement relationship of loading and unloading process in the compression test when using constant pressure mode under static conditions are shown in Fig 4.30.

Fig 4.31 shows the deformation in the second model of the compression test when internal pressure p_s is set to 20 kPa and displacement of the indentor is equal to 10 mm. The experimental results and simulation results of force-displacement relationship are shown in Fig 4.32.

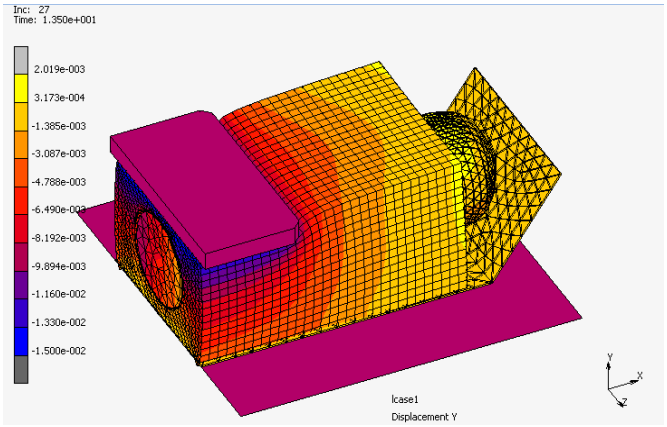

Figure 4.31. Simulation of model 2 with p_s = 20 kPa and displacement of the indentor at 10 mm (Displacement y [m])

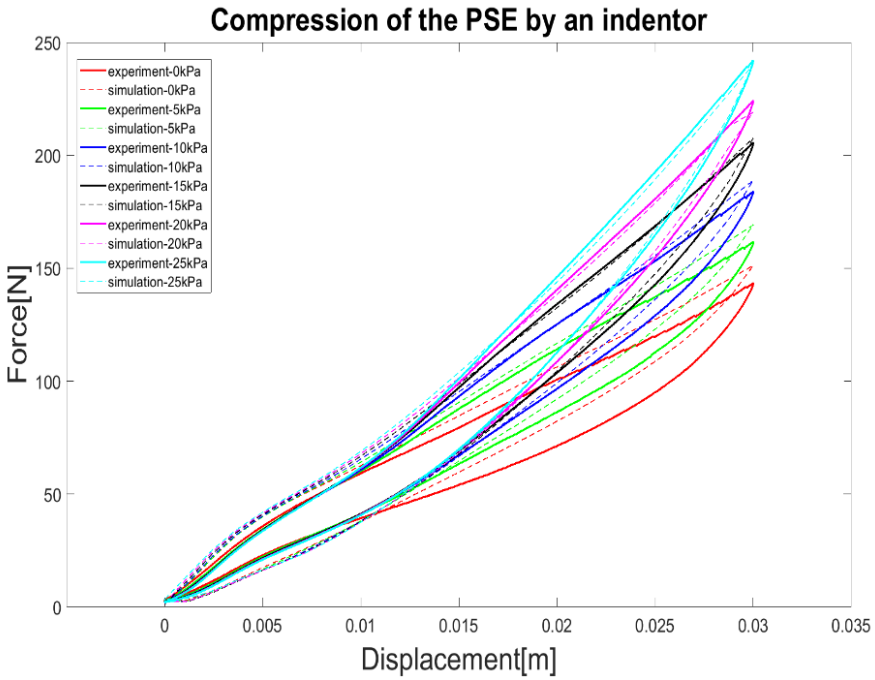

Figure 4.32. Force-displacement results of experiment and simulation (model 2)

4.5. Finite element analysis of a seat cushion with a simplified human body

This analysis is aimed at the objective of simulation of the distribution of contact pressure between a simplified human body and a car seat cushion with the PSE inserted inside in constant pressure mode under static conditions. Under the assumption that the model is symmetrical it is half-built for all components.

4.5.1. The complete model

The complete model is the model of interaction between a simplified human body and a seat cushion with the PSE inserted inside. First, a finite element model of the car seat cushion with a piece cut out to fit the foam brick was made. The cushion is shown in Fig 4.26. The 3D solid-geometrical model of the car seat cushion was developed using Inventor. Then the 3D model was imported to MSC.Marc and meshed with 288327 four-node tetrahedral elements (see Fig 4.33). The cushion is supported by a fixed square plane.

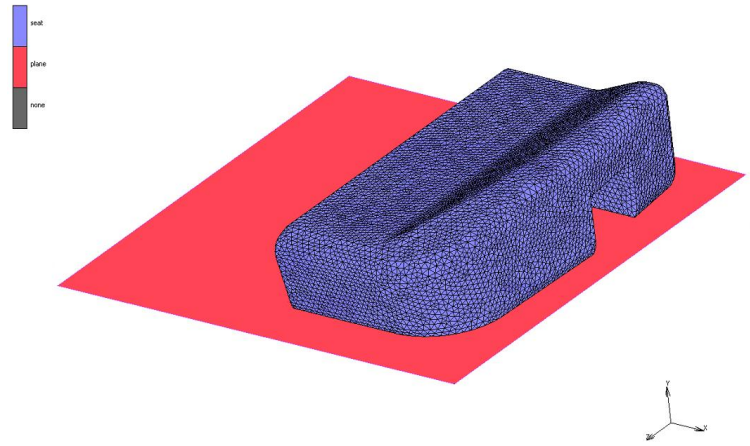

Figure 4.33. Geometry and mesh of the car seat cushion

The model of the foam brick with a PSE inserted inside is simplified by removal of the steel plate and the ends of PSE (see Fig 4.34). We assume that this simplification does not influence the distribution of pressure in contact zone between seat cushion and the human body. The model was meshed using four-node tetrahedral elements: 19344 elements of the foam block, 994 elements of the tape cover layer, 1380 elements of the latex tube and 1640 elements of the foam, which is inserted inside latex tube. The materials were modeled in the same way as in sections 4.1, 4.2 and 4.3.

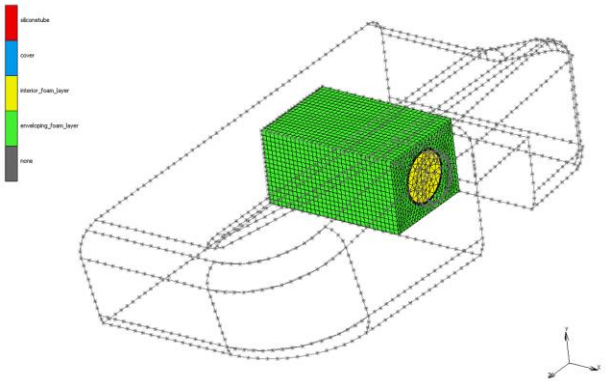

Figure 4.34. Geometry and mesh of the foam brick with a simplified PSE inserted inside

The model of the simplified human body is also created in simplified form. In this way the muscle layer of a half-build model consists a part of abdomen, waist and thigh. The bone part of the model includes half of sacrum, pelvis, and femur in according with [25]. The model of bones is meshed using four-node tetrahedral elements, which include 5769 elements of the femur, 5565 elements of the pelvis and 1982 elements of the sacrum (see Fig 4.35). With the assumption that these bones are solid the constitutive model of bones is chosen as steel but the mass density corresponds to bone and it is set in accordance with [26]. Thus the material of bones has the parameters:

Mass density: 2000 [kg/m^3] Young's Modulus: 2.1e+11[Pa] Poison's ratio: 0.3

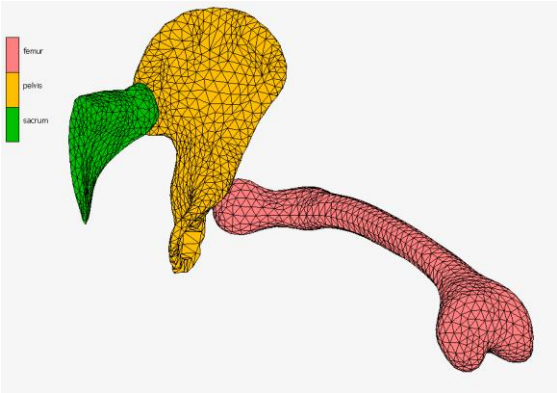

Figure 4.35. Geometry and mesh of bones

The original shape of muscles is based on standard proportions of the human body [26] while many simplifications were applied, e.g. thigh has a shape of a cylinder and abdomen part has a shape of an oval cylinder.

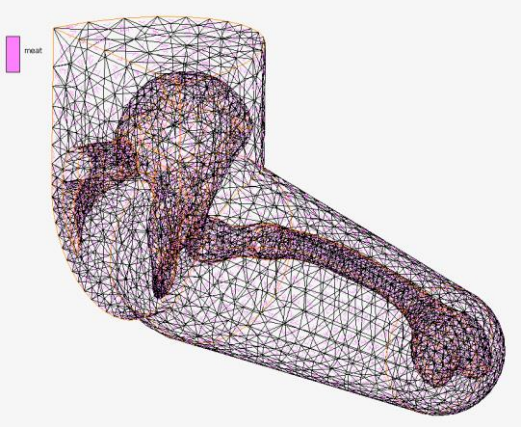

Figure 4.36. Geometry and mesh of the muscle layer (without bones)

The constitutive model of muscle tissue is based on the article [27]. Table 2 shows the values of parameters of the constitutive model of muscle tissue of calf and heel from the article [27].

Table 2. The parameters of the constitutive model of Ogden type of muscle tissue used in the article [27]

body part	$\mu[MPa]$	α	χ^2
calf	0.8335823E-02	0.7801210E+01	4.393327
heel	0.9195020E-02	0.2998462E+02	6.286381

Because the muscle tissue used in the complete model belongs to abdomen and thigh which are softer than calf and heel, the parameter values of the constitutive model are modified quantitatively. Specifically the constitutive model of muscle tissue of Ogden type is set to $\mu = 883.588[Pa]$, $\alpha = 1.8021$. In accordance with [27] the mass density of muscle tissue is set to 985 [kg/m^3].

In accordance with [28] the components are assembled into the model as shown in Fig 4.37.

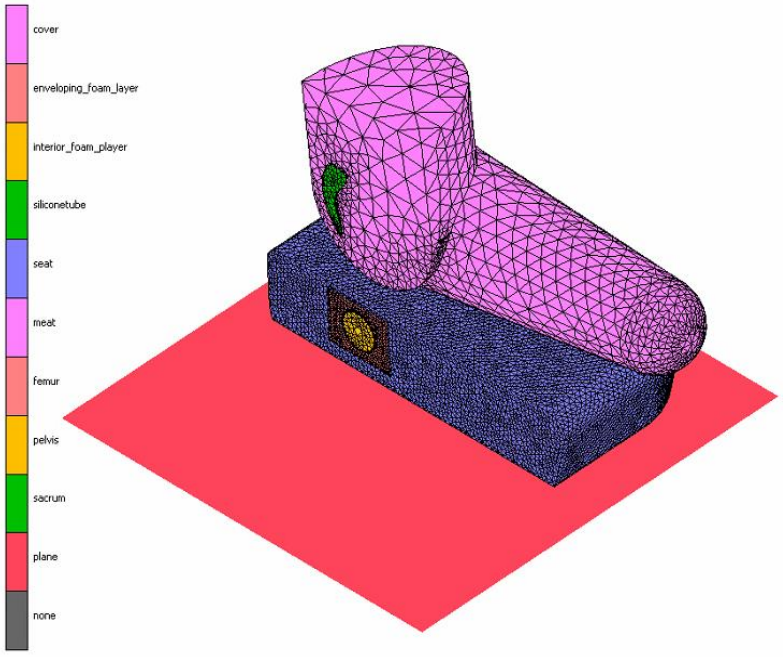

Figure 4.37. The complele model

A contact table was established for contact problem (see Table 3). This table consists of a list of entries representing components in the complete model. Each entry defines one pair of contact bodies which come into contact. Each contact table entry referes to a contact interaction. There are

two kinds of contact interaction: glue contact (G) and touch contact (T) which define the properties of the interaction between the two contact bodies.

Table 3. The contact table

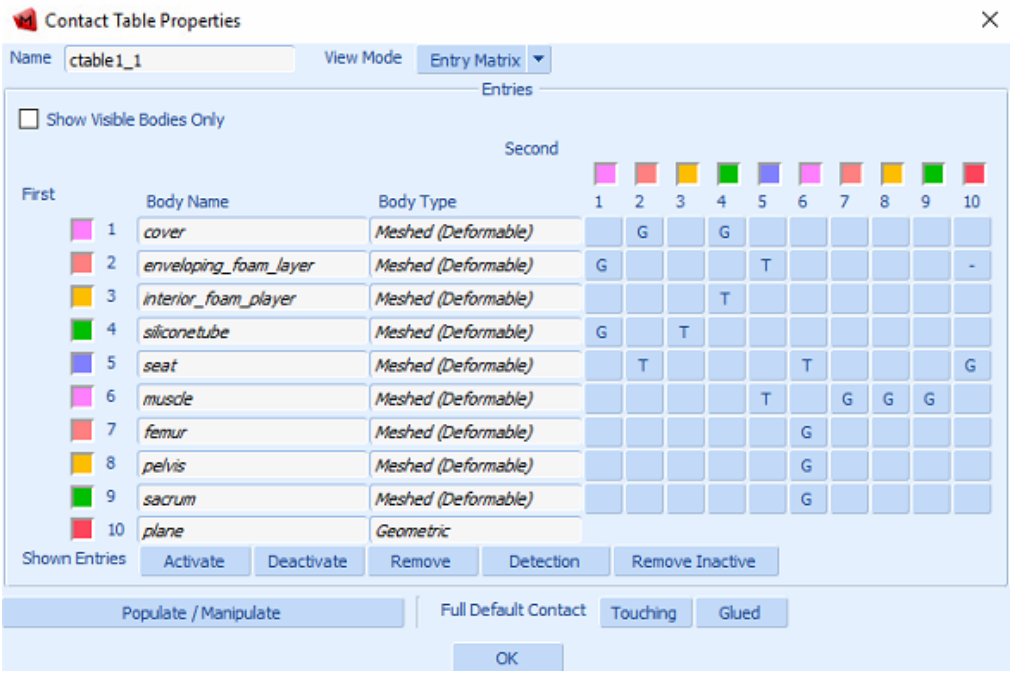

Now we determine the mass of the simplified human body in the complete model. With assumption that total mass of human is 75 kg and the height of human is 175 cm and based on a calculation of weight of parts of the human body [29] we have the results calculated in Table 4.

Table 4. The weight of parts of the human body

Total weigh : 75 kg	Height: 175 cm
Segment	**Weight** [kg]
Head	5.08
Hand	0.46
Forearm	1.20
Upper arm	2.04
Foot	1.03
Lower leg	3.24
Thigh	10.72
Upper part of body	11.9594
Middle part of body	12.3335
Lower part of body	8.39

Based on Table 5 the mass of simplified human body (half of lower part of body + thigh + bones) is set to 14 kg. The rest of the body, which is not included in the simplified model, represents the upper part and middle part of the body, two hands and head. The mass of the half of this rest of body is set at 18 kg.We assume that this weight can be represented and substituted by equivalent force (180 N) distributed on pelvis and sacrum (see Fig 4.38).

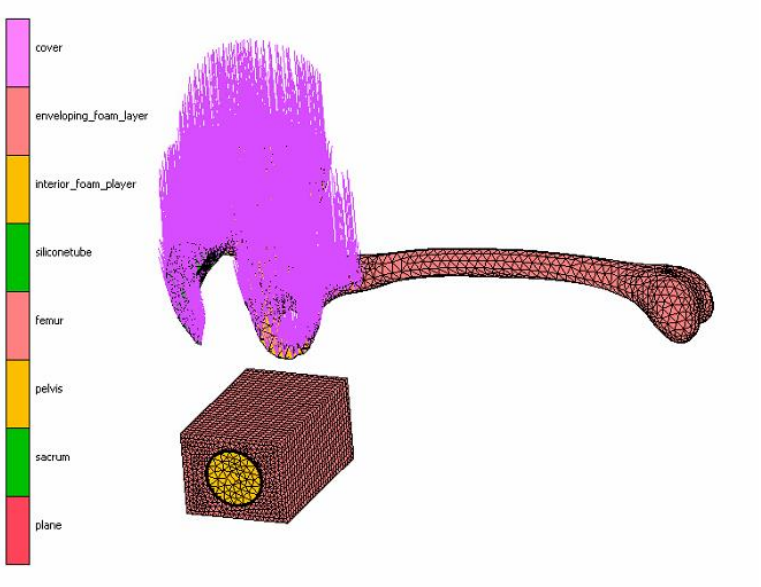

Figure 4.38. The equivalent force distributed on pelvis and sacrum

4.5.1.1. Simulation results and experimental result

To simulate the distribution of contact pressure between the human body and the seat cushion the internal pressure of the PSE that varies in the range [0, 25] kPa is designed as a time-dependent function:

$$p_s = \begin{cases} 0 & kPa \quad if\ 0 \le t < 5 \\ 5.(t-5)\ kPa & if\ 5 \le t < 10 \\ 25 & kPa \quad if\ 10 \le t \le 15 \end{cases} \tag{4.12}$$

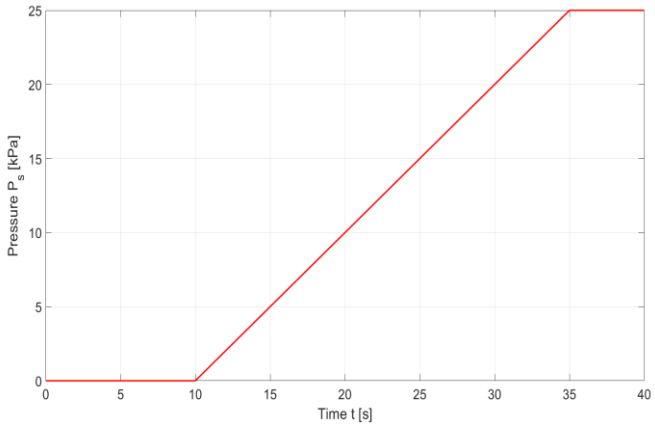

Figure 4.39. Designed internal pressure of the PSE

The results of simulated contact pressure distribution are shown in Fig 4.40 in the cases where the values of pressure p_s are 0 and 25 kPa, respectively. The simulation results show that increase of the pressure inside PSE from 0 to 25 kPa changes the distribution of contact pressure between the body and the car seat cushion. The value of a peak of the pressure increases from 15.84 kPa to 18.67 kPa.

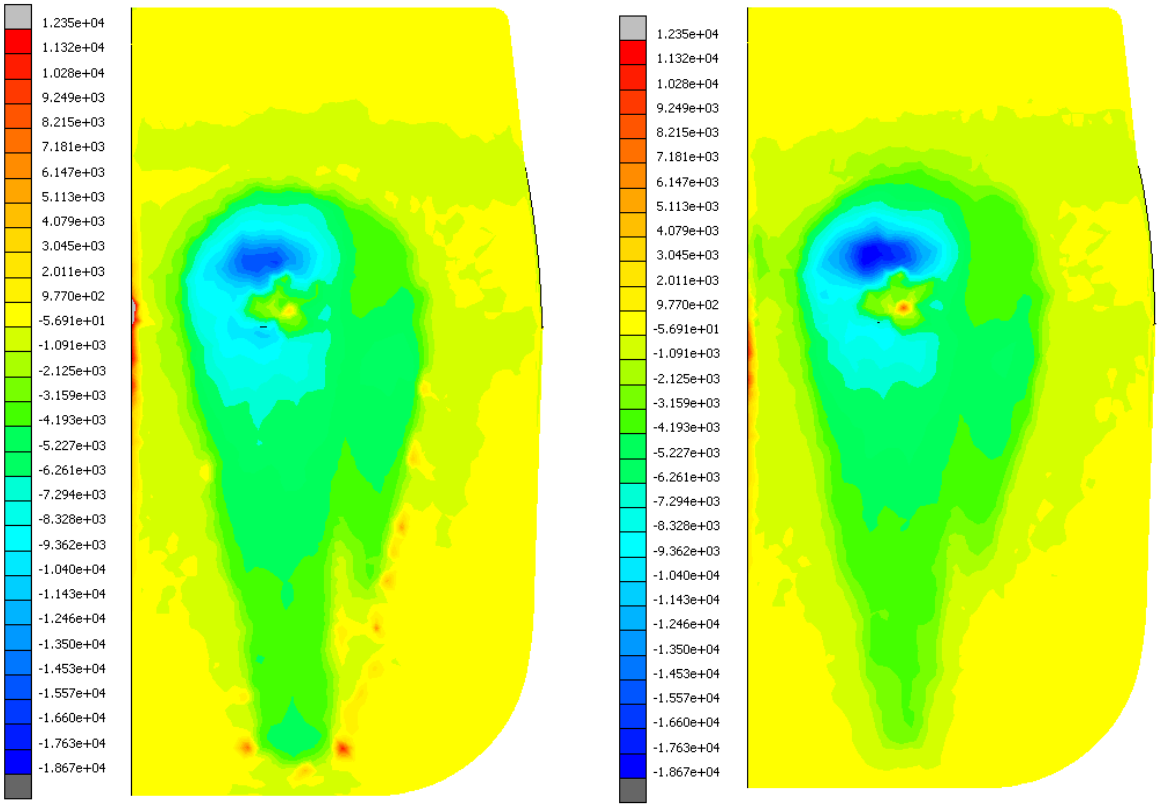

a) p_s=0 kPa b) p_s=25 kPa

Figure 4.40. Contact pressure distribution in simulation

An experiment was carried out to compare experimental data with simulation results. The person attending the experiment had a mass 75 kg and height 175 cm. This person was sitting in the car seat with a PSE inserted inside. Pressure inside the PSE was controlled by the electro-pneumatic control subsystem with the desired pressure varied in the range [0, 25] kPa. The distribution of contact pressure between the human body and the seat cushion was measured by an Xsensor pressure mapping system which covered the surface of the seat cushion.

Figure 4.41. Xsensor pressure mapping system

The experimental results show that increase of the pressure inside PSE from 0 to 25 kPa changes the distribution of contact pressure between the body and the car seat cushion with the peak value from 16.78 kPa to 19.36 kPa (see Fig 4.42).

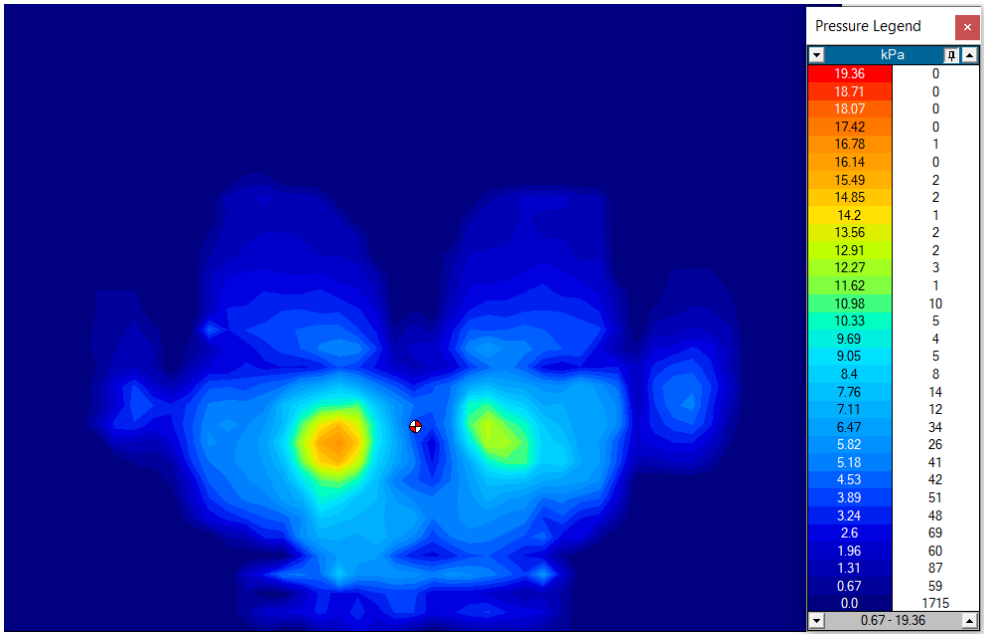

a) p_s=*0* kPa

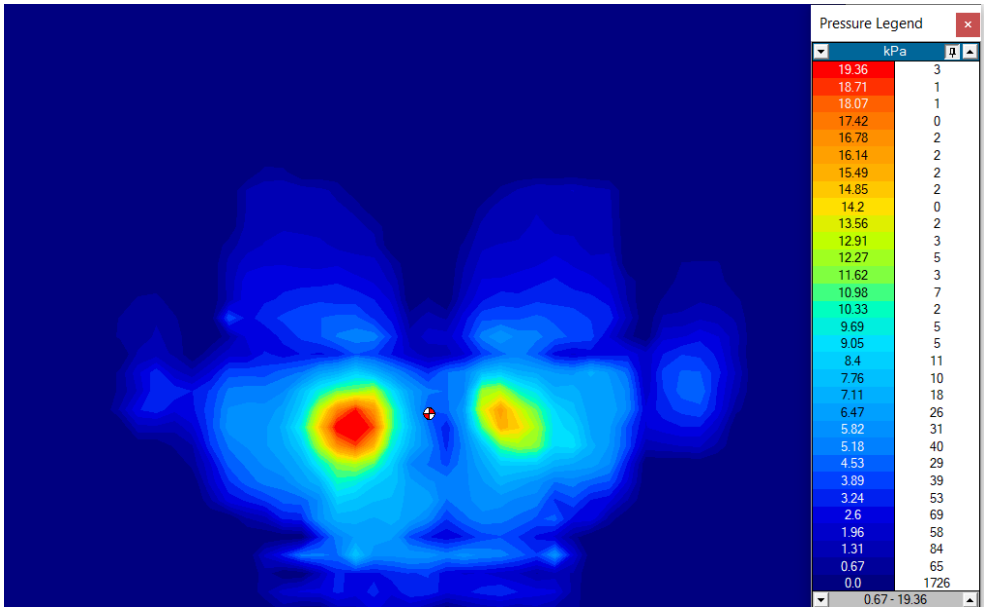

b) p_s=25 kPa

Figure 4.42. Contact pressure distribution in experiment

We can see that the simulation results and experimental results are in accordance (peak value from 15.84 kPa to 18.67 kPa for simulation results and from 16.78 kPa to 19.36 kPa for experimental results). The difference between peak values at 0 kPa and 25 kPa of pressure inside the PSE is about 3.5 kPa (about 20 %). These results confirm the influence of PSE on pressure distribution.

4.6. Conclusion

This chaper presents the study of the contact pressure distribution using finite element method. The FE model of compression test and the complete FE model were investigated and built step by step. At the beginning the suitable constitutive models of materials used for these models were determined and identified. Then these FE models were created in correspondence with reality. For compression test there are two FE models. The first one corresponds to the model which was used in the compression test in chapter 3, the second one corresponds to the model used for car seat cushion. The complete FE model is the model of interaction between simplified human body and seat cushion with the PSE inserted inside.

The behavior of the models were simulated and compared with the experimental results. The deformation of the PSE and seat cushion, contact force (in compression test) and contact pressure distribution (in the complete model) were investigated. Simulation results and experimental results show good correspondence of contact force – deformation relation (in compression test) and of the influence of the PSE on contact pressure distribution.

5. Summary

This thesis deals with the device which can be inserted inside car seat cushion and is capable of changing contact pressure between human body and the car seat cushion. The device includes the pneumatic spring element (denoted PSE) which is capable of changing contact pressure, and the electro-pneumatic control subsystem which controls pressure inside the PSE. My study focuses on investigation of the influence of this device on regulation of pressure inside the PSE. It also deals with the development of this device in order to investigate the posibility of faster and more precise work. The objectives of the studies presented in this thesis are:

- To model the influence of the device on the distribution of contact pressure between the human body and the car seat with PSE inserted inside.
- To investigate the influence of the device on the transmission of acceleration.

The studies are carried out using analytical calculation method and FEM in combination with experimental methods as they are presented in chapter 2, 3 and 4.

First, the structure and function of the car seat using the device which was made in the past is presented and analyzed carefully in chapter 2.

Second, the analytical and numerical calculations of simplified models that represent the interaction between the human body and the car seat cushion with the PSE inserted inside are presented in chapter 3. There are two simplified models, the first one is the original model and the second one is the improved model. The simplified model includes a mass which is in contact with a foam block with a PSE inserted in the middle. The difference between the original system and the improved system is in the PSE and the electro-pneumatic control subsystem. The calculated results give a detailed view of the behavior of the characteristics of the simplified models in two different control modes (constant pressure and constant stiffness) under static conditions and dynamic conditions. The aim of comparison of calculated results is to assess the influence of the improvement on the regulation of pressure inside the PSE and on the transmission of acceleration. The experiments made in accordance with the concept of numerical simulations are carried out to verify the calculated results and the influence of the device on the regulation of pressure inside the PSE and on the transmission of acceleration. The experimental results show good correspondence with the calculated results.

Last, the finite element method is used for simulation of contact pressure distribution in contact zone between the car seat cushion with a PSE inserted inside and a simplified human body. This work is done by using MSC. Marc software. The detailed study is presented in chapter 4. The constitutive models of all materials used in the model are defined. Materials used in the PSE and

the cushion comprise latex, tape and foam. The parameters of constitutive models of these materials are determined through optimisation-based curve-fitting techniques with stress–strain data from load-deformation tests of material samples. Then the finite element model of the interaction between the simplified human body and the car seat cushion under static conditions is built. This model is used for simulation cases when pressure inside the PSE is 0 kPa or 25 kPa. Pressure distribution in the contact zone of seat cushion is then evaluated.

The study in this thesis shows that the device, in the form of experimental model, is capable of influencing the transmission of acceleration. The device, implementend in the real car seat, is also capable of changing the contact pressure distribution.

6. References.

[1] El Falou, W., Duchene, J., Grabisch, M., Hewson, D., Langeron, Y., Lino, F: *Evaluation of driver discomfort during long-duration car driving,* Appl. Ergon. 34, 2449-2455, 2003.

[2] Wilkinson, R., Gray, R.: *Influences of duration of vertical vibration beyond the proposed ISO "fatigue-decreased proficiency" time, on the performance of various tasks.* AGARD Vib. Comb. Stresses Adv. Syst. 5, 18-51, 1975.

[3] Sandover, J.:*The fatigue approach to vibration and health: it is a practical and viable way of predicting the influences on people. J. sound Vib*. 215 (4), 699-721, 1998.

[4] Thomas, M., Lakis, A.A., Sassi, S.: *Adverse health influences of long-term wholebody random vibration exposure, recent research, development in sound and vibration*, Transw. Res. Netw. 2, 55-73, 2004.

[5] Lewis, C.H., Griffin, M.J.: *A review of the influences of vibration on visual acuity and continuous manual control. II: continuous manual control*, J. Sound Vib. 56 (3), 415-457, 1978.

[6] McLeod, R.W., Griffin, M.J.: *Review of the influences of translational whole-body vibration on continuous manual control performance*. J. Sound Vib. 133 (1), 55-115, 1989.

[7] Baik.S, Lee.J and Suh.J.: *A study on the characteristics of vibration in seat system*. SAE Paper 2003–01–1603, 2003.

[8] Tiemessen, IJ., Hulshof,CTJ. and Frings–Dresen, MHW.: *An overview of strategies to reduce whole–body vibration exposure on drivers: A systematic review*. International journal of industrial ergonomics 37, 245–256, 2007.

[9] Patten, W.N, Sha, S. and Mo, C.: *A vibration model of open celled polyurethane foam automotive seat cushions.* Journal of Sound and Vibration 217 (1), 145–161,1998.

[10] Ebe, K. and Griffin, MJ.: *Factors affecting static seat cushion comfort*. Ergonomics, 44, 901–921, 2001.

[11] David, C.: *Seat*, patent no. 303163, 2012.

[12] *Compact Proportional Solenoid Valve*. Series PVQ, SMC catalog.

[13] *Port Solenoid Valve. Series S070*, SMC catalog.

[14] Bohdan, T., Kulakowski, John, F., Gardner, J., Shearer L.: *Dynamic modeling and control of engineering systems*. Cambridge University Pressp. 219-243, 2007.

[15] Cirkl, D. and Hrus, T.: *Simulation Model of Polyurethane Foam for Uniaxial Dynamical Compression*. Vibroengineering PROCEDIA, vol 1, ISSN 2345-0533, 2013.

[16] Cirkl, D.: *Mechanical properties of polyurethane foam*. Ph.D Thesis, Technical University of Liberec, 2005.

[17] Griffin, M.J.: *Handbook of Human Vibration*. Academic Press, London, 1990.

[18] Sivcák, M.: *Dynamics of the vibration isolation system with more degrees of freedom*. Liberec: Technical University of Liberec, 2009.

[19] Belytschko, T., Kam Liu, W., Moran,B.: *Nonlinear Finite Elements for Continua and Structures,* 2014.

[20] Beams, J W.: *Mechanical properties of thin films of gold and silver*, Structure and properties of thin films: 183-192, 1995.

[21] Chung-Lin, W., Weileun, F., Ming-Chuen, Y.: *Measurement of Mechanical Properties of Thin Films Using Bulge Tes*, Department of Power Mechanical Engineering National Tsing Hua University Hsinchu, Taiwan, R.O.C.

[22].Gehard A.H.: *Nonlinear Solid Mechanics: A Continuum Approach for Engineering*, Technical University Graz, Austria, p.240-241.

[23]. Aidy A., Hosseini M. and Sahari B.B.: *A Review of Constitutive Models for Rubber-Like Materials*, American J. of Engineering and Applied Sciences 3: 232-239, 2010 ISSN 1941-7020.

[24]. *MAR103 Experimental Elastomer Analysis*.

[25] https://grabcad.com/library

[26] https://www.makingcomics.com/2014/01/19/standard-proportions-human-body/

[27] Mázik, L.: *Research on tribological behavior of rubber in dependency on its viscoelastic properties, Diploma thesis*, Technical University of Liberec, pp.32-41, 2010.

[28] *Correct sitting posture*: Driving, www.physiomed.co.uk

[29] https://ftvs.cuni.cz/FTVS-1376.html

[30]Jameson, Robert, J.: *Characterization of Bone Material Properties and Microstructure in Osteogenesis Imperfecta/Brittle Bone Disease*, 2014.

[31] Schrodt, Benderoth, M., Alizadehd M., Menger, J., Vogl, T., Silber, G.: *A Method to Characterize the Mechanical Behavior of Human Soft Tissue Using Finite Element Analysis*
[32] Hibbitt, Karlsson, Sorensen, *ABAQUS, Theory Manual, 6th Edition. Abacom Software GmbH,* 2000.

7. List of papers published by the author.

Main publications related to the thesis:

[1] Cirkl, D., TranXuan, T.: Simulation model of seat with implemented pneumatic spring, in Journal Vibroengineering PROCEDIA, Vol. 7, ISSN Print 2345-0533, ISSN Online 2538-8479 , 2016.

[2] TranXuan, T., Cirkl, D.,: Simulation model of seat with implemented pneumatic spring with consideration of variable pressure in air reservoir, 32nd COMPUTATIONAL MECHANICS Conference, 2016.

[3] TranXuan, T., Cirkl, D.,: *FEM model of pneumatic spring assembly*, in Journal Vibroengineering PROCEDIA, Vol. 13, ISSN Print 2345-0533, ISSN Online 2538-8479, 2017.

[4] TranXuan, T., Cirkl, D.,: *FEM model of pneumatic spring supported by a steel plate*, 33ndCOMPUTATIONAL MECHANICS Conference, 2017.

[5] TranXuan, T., Cirkl, D.,: *Modeling of dynamical behavior of pnuematic spring-mass system*, in Proceedings EM 2018, Paper #279, pp. 865–868, 2018.

[6] TranXuan, T., Cirkl, D.,: *The effect of system improvement on regulation of pressure inside pneumatic spring element and on transmission of acceleration*, , in Journal Vibroengineering PROCEDIA, Vol. 27, ISSN Print 2345-0533, ISSN Online 2538-8479, 2019.

Appendix A: Model of Polyurethane Foam for Uniaxial Dynamical Compression

Pores of PU foam create a typical material structure which is up to a certain degree able to resist to pressure loading due to its buckling strength. F_b is a force evoked by buckling strength of foam cells, c_b is a coefficient of the structure buckling strength.

$$F_b = F_{b0}.\left(1-e^{-c_b(x-z)}\right) \tag{A.1}$$

where

x-z is the relative displacement between the mass and the PU foam block.

After the initial cells crush with increasing compression, they come to contact between cell walls. Force characteristics of this phase are very similar to the course of force arising during compression of air in a closed vessel. This is described by progressive polytrophic function (3.20). S_p, p_p, h_p, n_p are constants of the model, where h_p means the vertical asymptote position.

$$F_{dp} = p_p.S_p.\left[\left(\frac{h_p}{h_p-(x-z)}\right)^{n_p}-\left(\frac{h_p}{h_p+(x-z)}\right)^{n_p}\right] \tag{A.2}$$

Damping of the matrix material is then described by Maxwell's viscoelastic components with nonlinear spring with polytropic characteristics (3.21) with constants S_{0i}, p_{0i}, h_i, n_{0i}, and nonlinear damper with constant of damping c_i and exponent n_i where $m=3$ is a number of used Maxwell's components.

$$F_{di} = F_{dc}\left(x, x_{di}\right) = p_{0i}.S_{0i}.\left[\left(\frac{h_i}{h_i-(x-x_{di})}\right)^{n_{0i}}-\left(\frac{h_i}{h_i+(x-x_{di})}\right)^{n_{0i}}\right] \tag{A.3}$$

$$F_{di} = c_i.\left|v_{di}\right|^{n_i}.\mathrm{sgn}\left(v_{di}\right), v_{di} = \dot{x}_{di}-\dot{z},\ i=1\ldots3 \tag{A.4}$$

Concerning the contact of cell-walls and struts of cells during compression and their mutual slipping, there is a logical assumption that also friction participates in PU foam damping. Friction is included in the model with a course of friction coefficient f_f defined in dependence on velocity $v=\dot{x}-\dot{z}$ by function arctan in combination with power function in equation (3.23)

$$f_f = \frac{2f_{f0}}{\pi}.\arctan\left(k_1.v\right)+k_2.\left|v\right|^{k_3}.\mathrm{sgn}\left(v\right) \tag{A.5}$$

The base value for friction force calculation is the sum of restoring force F_R and force of Maxwell's viscoelastic components F_{di}:

$$F_{Rd} = F_R + \sum_{i=1}^{3} F_{di} \tag{A.7}$$

Friction force then is:

$$F_f = f_f . F_{Rd} \tag{A.8}$$

The parameter of PU foam model is shown in Table 5.

Table 5. The parameter of PU foam model

Force component	Parameter	Physical unit	Value		
F_b	F_{b0}	[N]	80		
	c_b	[N/m]	600		
F_{dp}	S_p	[m^2]	0.0095		
	p_p	[Pa]	100		
	n_p	[1]	6.2		
	h_p	[m]	0.06		
			i=1	i=2	i=3
F_{di}	S_{0i}	[m^2]	1.2	0.03	0.8
	p_{0i}	[Pa]	100		
	n_{0i}	[1]	3	3.5	2
	h_i	[m]	0.05	0.05	0.18
	c_i	[-]	50	300	300
	n_i	[1]	0.2	0.2	0.2
F_f	f_{f0}	[1]	0.05		
	k_1	[s/m]	5000		
	k_2	[-]	0.2		
	k_3	[1]	1		